UNIVERSITÉ DE MONTRÉAL

PRODUCTION OF CHEMICALS BY MICROWAVE THERMAL TREATMENT OF LIGNIN

SHERIF FARAG

DÉPARTEMENT DE GÉNIE CHIMIQUE

ÉCOLE POLYTECHNIQUE DE MONTRÉAL

THÉSE PRÉSENTÉE

EN VUE DE L'OBTENTION

DU DIPLÔME DE PHILOSOPHIAE DOCTOR

(GÉNIE CHIMIQUE)

DÉCEMBRE 2013

UNIVERSITÉ DE MONTRÉAL

ÉCOLE POLYTECHNIQUE DE MONTRÉAL

Cette thèse intitulée :

PRODUCTION OF CHEMICALS BY MICROWAVE THERMAL TREATMENT OF LIGNIN

présentée par : FARAG Sherif

en vue de l'obtention du diplôme de : Philosophiae Doctor

a été dûment acceptée par le jury d'examen constitué de :

M. STUART Paul, Ph.D., président

M. CHAOUKI Jamal, Ph.D., membre et directeur de recherche

M. AKYEL Cevdet, D.Sc.A., membre et codirecteur de recherche

M. SRINIVASAN Bala, Ph.D., membre

M. HAWARI Jalal, Ph.D., membre

DEDICATION

To my beloved family

ACKNOWLEDGMENTS

Thanks be to God for everything I have in my life.

I would never have been able to finish this dissertation without the guidance of my supervisors, help from my friends, and support from my parents and my wife.

First of all, I would like to sincerely thank my supervisor, Dr. Jamal Chaouki, for his guidance, encouragement, understanding, patience, and most importantly, his friendship during my Ph.D. His mentorship was paramount in finding the optimum methodology and achieving my objectives. He encouraged me to grow as an independent thinker, which improved not only my scientific thinking, but all aspects of my life.

For everything you have done for me, Dr. Jamal Chaouki, I thank you.

I would like to express my deep thanks to my co-supervisor, Dr. Cevdet Akyel, for his support, guidance, encouragement, and helpful suggestions regarding the all issues belonging to his field. I am also thankful to all my committee members for agreeing to be a member of the jury.

I would also like to thank Dr. Amr Sobhy, who was the first researcher in this field in Dr. Chaouki's group. He is a good friend and always willing to help and give excellent suggestions.

I would like to extend my thanks to all my colleagues and friends in Dr. Chaouki's group for sharing knowledge and ideas. I am thankful to Ms. Soumaya Benzennou, and Mr. Philippe Leclerc, for helping me to write the French section of this dissertation. Many thanks also to Dr. Levent Erdogan (Electrical Engineering Department, École Polytechnique de Montréal) for his assistance to measure the dielectric properties of the investigated materials.

Special thanks go to all secretaries and technical staff of the chemical engineering department; in particular, Ms. Martine Lamarche, Mr. Robert Delisle, Mr. Yazid Belkhir, Mr. Jean Huard, and Mr. Gino Robin, for their assistance.

I am grateful for the financial and technical support from Lignoworks NSERC Strategic Network (www.lignoworks.ca), and the Agricultural Biorefinery Innovation Network (ABIN).

I would never have accomplished this dissertation without the lovely life that I have with my family: my wife Mai Attia, and my kids Yara and Omer. I would like to express my deep thanks for their support, encouragement, patience, understanding, and unwavering love from my wife in good times and bad.

Finally, and most important, I would like to express my fervent thanks to my parents, for everything they have done for me. Indeed, they are the main reason behind all my successes. I also wish to extend my thanks to my sisters and brothers—and in particular, my older brother Nasser—for their love, support, and encouragement.

Sherif FARAG

École Polytechnique de Montréal

Fall 2013

RÉSUMÉ

Ce travail a pour but d'étudier le potentiel de convertir un des composants de la biomasse lignocellulosique, la lignine, en produits à valeur ajoutée en utilisant la pyrolyse assistée par microondes (MWP). Pour atteindre cet objectif, plusieurs étapes ont été franchies. Nous avons tout d'abord réussi à prédire les profils de température au sein d'un matériau exposé aux ondes électromagnétiques (EMW) à l'aide d'un modèle mathématique tridimensionnel. Ensuite, un TGA-microondes (MW-TGA) original a été développé et mis en œuvre pour l'étude cinétique. Subséquemment, une comparaison entre la pyrolyse assistée par microondes et conventionnelle a été réalisée. L'étude structurelle détaillée de la bio-huile produite via MWP de la lignine kraft a été discutée en troisième étape. Finalement, un modèle cinétique des produits de la MWP ainsi que des produits chimiques extraits de la lignine kraft a été mis en place.

Tout d'abord, un modèle mathématique tridimensionnel a été présenté pour simuler le profil de température à l'intérieur d'un matériau exposé aux ondes électromagnétiques à 2.45 GHz. Les applications de COMSOL-Multiphysics ont permis de simuler le profil de température transitoire pour la pinède, le carbone, le Pyrex et des combinaisons de ces matériaux sous différentes conditions. Les résultats prédits ont été comparés aux données expérimentales pour la validation du modèle. Cette étude nous a permis de conclure que le chauffage microondes (MWH) induit à une distribution non-uniforme de la température dûment à la longueur de pénétration (D_p) et à la perte surfacique de chaleur. Toutefois, le gradient de température peut être minimisé significativement si l'on réduit les dimensions du matériau exposé à deux fois la D_p et l'on place un bon isolant thermique à sa surface. Le positionnement des matériaux avec forte/faible capacité de convertir la radiation microonde en chaleur pourrait favoriser des zones chaudes/froides désirées à l'intérieur du matériau chauffé, ce qui permet un profil spécifique de température. En outre, l'addition de matériaux de forte capacité de convertir les microondes en chaleur à la charge permet d'atteindre des températures beaucoup plus importantes comparées au cas du matériau seul exposé à la même puissance et temps de chauffage. Les discussions présentées dans cette étude visent à améliorer l'état de l'art par rapport aux profils de température dans un matériau

composite soumis au chauffage microondes ainsi qu'à développer une approche pour influencer/contrôler ces profils de température selon la sélection des matériaux.

L'objectif principal de la deuxième étape est d'étudier la cinétique de la MWP versus la pyrolyse conventionnelle (CP). Pour ce faire, un MW-TGA original a été construit et équipé d'un thermomètre novateur. Ce thermomètre est exempt des désavantages des thermomètres traditionnels dans le cas du MWH. Ainsi, le travail expérimental impliquant la MWP et la CP de la sciure de bois a été accompli. Des programmes MATLAB® ont été développés pour estimer les paramètres cinétiques, à savoir l'énergie d'activation, le facteur pré-exponentiel ainsi que l'ordre de la réaction (E_a, k_o, et n, respectivement). Nous avons essentiellement conclu de ce travail que la MWP a une vitesse de réaction plus importante que celle de la CP. Ceci peut s'expliquer par le fait que les EMW oscillantes ont engendré un mouvement chaotique plus aigu des molécules ce qui influence le paramètre k_o. Malgré cet effet remarquable sur ce k_o, l'énergie d'activation demeure presque constante dans les deux cas. La possibilité de l'influence directe des ondes sur les liaisons intermoléculaires semble être ténue vu que la longueur des ondes est beaucoup plus grande que la distance intramoléculaire. Ce résultat est aussi puissant qu'il permettrait d'interpréter une grande majorité des effets du MWH reportés dans différentes réactions.

La troisième étape présente une analyse détaillée de la structure des huiles produites par MWP de la lignine kraft. L'effet de deux paramètres a été évalué : (1) l'ajout d'un bon convertisseur de microondes-en-chaleur (noir de carbone) entre 20 et 40 wt%, et (2) la puissance nominale des microondes entre 1.5 et 2.7 kW. Cinq combinaisons pour ces deux variables ont été choisies pour lesquelles la radiation microondes a été gardée pendant 800 s. Les températures finales atteintes, mesurées en tant que valeur moyenne spatiale, étaient 900, 980, 1065, 1150, et 1240 K. Les rendements en produits de pyrolyse, solides, gaz condensables, et gaz non-condensables ont été comparés pour les conditions opératoires étudiées. Les gaz condensables collectés ont été séparés selon une phase-huile, prédominée de produits chimiques, et une phase aqueuse contenant surtout de l'eau et ayant une densité moindre que la phase-huile. Les résultats obtenus montrent que l'augmentation de la vitesse de chauffe et de la température finale induit une augmentation du

rendement en produits liquides. Les produits identifiés dans les huiles par GC-MS étaient majoritairement aromatiques : gaïacols, phénols, and catéchols. Toutefois, autour de 60 wt% n'a pas pu être identifié par GC-MS d'où le recours à la spectroscopie RMN ^{31}P et ^{13}C offrant plus de détails sur la composition structurelle des huiles. Selon l'analyse RMN, 80% du carbone détecté dans la phase-huile était un carbone aromatique. Les groupes hydroxyliques aliphatiques perçus dans la matière première ont été éliminés significativement dans l'huile; ceci est attribué à la formation provisoire de la molécule d'eau pendant la MWP. La concentration en groupes hydroxyliques phénoliques C5 substitués/condensés a baissée en faveur des groupes gaïacol, p-hydroxyphenyl, et catéchol hydroxyle. Un cheminement de dégradation détaillé pour chacune de ces conversions a été suggéré. Une telle étude est essentielle à la compréhension du cheminement de dégradation ainsi qu'à la composition structurelle des huiles de pyrolyse.

La quatrième étape fait l'objet d'une étude cinétique pour la MWP de la lignine kraft en appliquant des modèles tridimensionnels. Pour atteindre cet objectif, le MW-TGA utilisé pour la deuxième étape a été modifié et utilisé. Les modifications apportées ont permis de séparer les gaz produits (condensables et non-condensables) en sept parties. Le matériau convertisseur de microondes-en-chaleur a été ajouté à 30 wt% de la masse totale et la puissance nominale était de 2.1 kW. Le premier modèle considère la conversion de la matière première en solide, gaz condensable et gaz non-condensable en considérant que chaque produit est un bloc individuel. Dans le second modèle, le liquide est séparé en huile, contenant que des produits chimiques et 0% d'eau, et en eau ne contenant aucun produit chimique. Les produits sont ainsi l'huile, l'eau, les gaz non-condensables et le solide. De plus amples recherches ont été réalisées dans le troisième modèle en analysant l'huile produite par GC-MS. L'huile est donc subdivisée en quatre catégories : (1) phénoliques, contenant tous les composés phénoliques identifiés, (2) aromatiques à haute masse moléculaire, comportant toutes les molécules lourdes et les produits non identifiés par GC-MS, (3) aromatiques monocyclique non-phénoliques et (4) aliphatiques. Par conséquent, le troisième modèle considère la pyrolyse de la lignine en sept produits : ceux cités précédemment plus l'eau, les gaz non-condensables et le solide. Les paramètres cinétiques de chaque modèle ont été estimés et appliqués pour prédire la distribution des produits pour chaque modèle. Finalement, les résultats prédits ont été comparés aux données expérimentales aux fins de validation.

ABSTRACT

This work investigates the potential of converting one of the lignocellulosic biomass components, lignin, into value-added bio-products using microwave pyrolysis (MWP). To achieve this objective, a multi-step process was devised and accomplished. First, temperature profiles within a material exposed to electromagnetic waves (EMW) were predicted using a three dimensional mathematical model. Second, an original microwave-thermo gravimetric analyzer (MW-TGA) was designed and built for kinetic purposes, and the kinetics of MWP were investigated in contrast to conventional pyrolysis (CP). Third, a detailed structural investigation of a bio-oil produced from of kraft lignin using MWP was discussed at various conditions. Finally, a kinetic modeling of the MWP products from kraft lignin was achieved quantitatively, as well as qualitatively.

In the first step, a three-dimensional mathematical model was created to simulate temperature profiles inside a material exposed to EMW at 2.45 GHz. COMSOL-Multiphysics applications were used to simulate transient temperature profiles of pinewood, carbon, Pyrex, and combinations of these materials under different conditions. The predicted results were compared against the experimental data in order to validate the presented model. The key conclusions of this study show that microwave heating (MWH) leads to non-uniform distribution of temperature due to material penetration depth (D_p) and surface heat loss. However, limiting the dimensions of the exposed material to twice the D_p and placing strong thermal insulation on the surface significantly minimize temperature gradients. The locations of materials which are strong or weak microwave-to-heat convertors can be manipulated to create desired hot or cold zones inside the heated material, which leads to specific temperature profiles. In addition, the homogenous mixing of a material strong microwave-to-heat converter with the payload exhibits a significant increase in temperature, compared to the virgin material exposed to the same power and heating time. This study aims at improving the understanding of temperature profiles within composite materials subjected to MWH, as well as developing approaches to influence/control temperature profiles through material selection.

The main objective of the second step was to investigate the kinetics of MWP in contrast to CP. To achieve this objective, an original MW-TGA was built and equipped with an innovative thermometer, which does not suffer from the traditional drawbacks, particularly in case of MWH. Subsequently, experimental work on MWP and CP of sawdust was conducted. MATLAB® program codes were employed to estimate the kinetic parameters, activation energy, pre-exponential factors, and reaction orders (E_a, k_o, and n, respectively). The key conclusions of this investigation indicate that MWP has a faster reaction rate than CP. This is a consequence of enhancing the molecular chaotic motion resulting from the oscillating EMW: the molecular mobility, which is represented by k_o. Even though this noticeable effect on k_o, the estimated value of E_a was almost the same in both cases, this might be a consequence of the tenuous possibility of direct hacking the molecule-bonds by applied EMW, since the wavelength of EMW is much longer than the intermolecular distance of the target material. This result is so significant that it can account for most of the effects observed in different reactions when MWH is applied.

The third step investigated a detailed structural and compositional analysis of a bio-oil produced from kraft lignin using MWP. The effects of two parameters were considered: (1) loading of a strong microwave-to-heat convertor (char), 20-40 wt%, and (2) microwave nominal setting power, 1.5-2.7 kW. Five combinations of these two variables were chosen and applied for 800s of MWH. The reached final temperatures, measured as mean values, were 900, 980, 1065, 1150, and 1240 K. The yields of the pyrolysis products, solid, condensable gas, and non-condensable gas were compared at the conditions under investigation. The collected condensable gas was separated into oil phase, which is mostly chemicals, and aqueous phase, which is mostly water and lower density than the oil phase. The obtained results showed that increases the heating rate leads to an increase in the yield of the liquid product. The identified chemical compounds in the oil phase using GC-MS were mostly aromatics: guaiacols, phenols, and catechols. Nonetheless, at 60 wt%, the oil phases could not be identified using GC-MS. Therefore, ^{31}P and ^{13}C NMR spectroscopy were used to provide further detailed structural information. Based on the NMR analyses, up to 80% of the detected carbon atoms in the oil phase were aromatic carbons. The detected aliphatic hydroxyl groups in the virgin material were significantly eliminated in the oil phase, and this was attributed to water forming in the interim of MWP. The decreased concentrations of C5 substituted/condensed phenolic hydroxyl groups after MWP were attributed

to an increase in the concentrations of guaiacyl, p-hydroxyphenyl, and catechol hydroxyl groups. Detailed degradation pathways for each of those conversions were suggested. Such an investigation is significant because it aims at improving the understanding of the degradation pathways of a lignin network, as well as the structure of the obtained bio-oil.

In the final step, a kinetic investigation of kraft lignin products made from MWP was accomplished by applying three different models. To achieve this objective, the MW-TGA that was built in the second step was modified and used in this step. The modifications done on the MW-TGA enable the distribution of vapor products (condensable and non-condensable) up to 7 parts in the interim of MWP. The applied conditions were 30 wt% of char and a microwave nominal power setting of 2.1 kW. The first model considered the virgin material converted into condensable gas, non-condensable gas, and remaining solid, taking into consideration each product as an individual lump. In the second model, the liquid product was separated into oil, which is entirely chemical and contains 0 wt% water, and water, which contains 0 wt% chemicals. Therefore, the lumps of the second model were oil, water, non-condensable gas, and solid. Further investigations were achieved in the third model by analysing the oil product using GC-MS. The oil product was partitioned into four groups: (1) phenolics group, which contains all the identified phenolic components, (2) heavy molecular weight components group, which contents all the heavy molecular weight and the undefined components using a GC-MS analyzer, (3) aromatics with a single ring (non-phenolics) group, and (4) aliphatics group. Hence, the third model considered lignin converted into seven products, the above four groups, plus water, non-condensable gas, and solid. The kinetic parameters of each model were estimated, and then applied to predict the yield of each product at the selected temperatures. Finally, the predicted results were compared against the experimental data, which showed a high capacity of the presented models to estimate product yields.

TABLE OF CONTENT

LISTE OF TABLES

LISTE OF FIGURES

LIST OF ABBREVIATIONS

A	Instantaneous yield of the aliphatic compounds
ASR-Non-Ph,	Instantaneous yield of the aromatic single ring and non phenolic compounds
C	Specific heat
D_p	Penetration depth
E_{rms}	Root mean square of the electrical field
E_a	Activation energy
f	Frequency
G	Transient yield of the non-condensable gas product
H_{rms}	Root mean square of the magnetic field
K	Thermal conductivity
k_0	Pre-exponential factor
L	Transient yield of the condensable gas product
m	Mass
n	Reaction rate
O	Instantaneous yield of the oil product
P	Power dissipated
p_c	Properties of carbon
Ph	Instantaneous yield of the phenolics group
p_m	Properties of new mixture
p_w	Properties of pinewood
R	The universal gas constant
S	Remaining solid yield
S_∞	Final solid fraction

T	Temperature
t	Time
V	Volume
W	Instantaneous yield of the water product
x	Decomposition fraction
β	Heating rate
ε^*	Complex permittivity
ε'	Dielectric constant
ε''	Electric loss factor
ε_0	Electric permittivity of free space
ε''_{eff}	Effective dielectric loss factor
μ_0	Magnetic permeability of free space
μ''_{eff}	Effective magnetic loss factor
$tan\delta$	Loss tangent
ω	Angular frequency
α	Attenuation factor
ρ	Density

CHAPTER 1 INTRODUCTION

1.1 Background

Forests are one the most significant of Canada's resources, covering more than 400 million hectares, approximately half of the total area of the country and 10 per cent of the earth's treed area (Benoit 2008). This potential has established the forest industry as one of the cornerstones of the Canadian economy. In 2006, this sector contributed 3% to Canada's total gross domestic product (GDP). In addition, it provided more than 300,000 jobs, and between 500,000 and 600,000 indirect jobs across the country (Benoit 2008). Recently, however, the forest industry has reached a crossroads as it has been facing unexpected challenges for the past few years. The most serious of these challenges are increasing the competition with low-cost sources of wood, and the decline North American demand. The production of value-added forest-based products, in addition to traditional products, is one of the main solutions that can be applied to ensure a sustainable future for the industry. Therefore, this project aims to investigate the potential for converting lignocellulosic biomass/biomass waste into a value-added bio-product. This product diversification can deal with the current challenges, address the growing list of environmental concerns, and take advantage of expected rapid increase in price and demand of petrochemical-based energy and products.

1.2 The Lignocellulosic Biomass Components

Lignocellulosic biomass is composed of three intertwined components: cellulose, hemicellulose, and lignin. The distribution of each component depends on many factors, such as the species, the environment in which it was grown, and the extraction technique. Generally, the dry weight basis of each is 35-45% cellulose, 25–30% hemicellulose, and 20–35% lignin (Zakzeski, Bruijnincx et al. 2010, de Wild, Huijgen et al. 2012, Mu, Ben et al. 2013). The key to distinguishing between these three components is chemical structure, which can also help determine resistance to decomposition. As shown in Figure 1-1, hemicellulose is rich in branches and it is weakest compared with the other two components. It decomposes at a temperature range of 220-315 ^{o}C

with a solid residue of 20 wt% at 900 ^{o}C. Cellulose consists of long polymers of glucose without branches; therefore, it is stronger than hemicellulose. It decomposes between 315 ^{o}C and 400 ^{o}C with 6.5 wt% of solid residue at 900 ^{o}C. Lignin mainly consists of aromatics with various branches, and the activity of the chemical bonds covers a wide range. Thus lignin is the strongest component compared to cellulose and hemicellulose; it decomposes over a temperature range of 100-900 ^{o}C with a solid residue of 45 wt% at 900 ^{o}C (Yang, Yan et al. 2007).

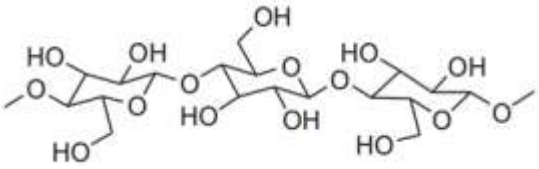

(A)

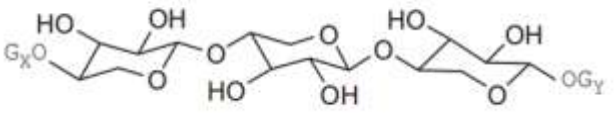

(B)

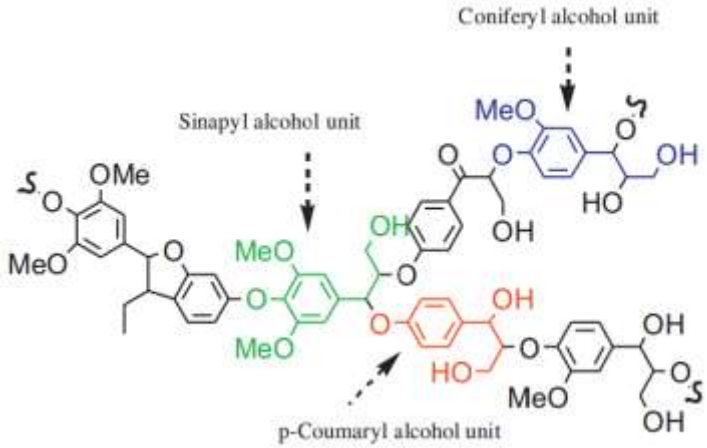

(C)

Figure 1-1: Schematic representation: (A) cellulose, (B) hemicellulose, and (C) lignin (Gu, Ma et al. 2013)

1.3 Lignin Structure

Lignin is found in between and within plant cells, filling the cellulose and hemicellulose, and acting as a glue to hold them together. Lignin is not just one type; rather, it is many, all with complex chemical structures. Generally speaking, lignin is a three-dimensional amorphous polymer and one of the most complex organic aromatic polymers in nature (Zakzeski, Bruijnincx et al. 2010, Kibet, Khachatryan et al. 2012, Mu, Ben et al. 2013). Still, the exact structure of a native lignin network is unknown. However, it is believed to be based upon three aromatic alcohols: p-coumaryl, coniferyl, and sinapyl, as depicted in Figure 1-2 (Zakzeski, Bruijnincx et al. 2010, de Wild, Huijgen et al. 2012, Kibet, Khachatryan et al. 2012).

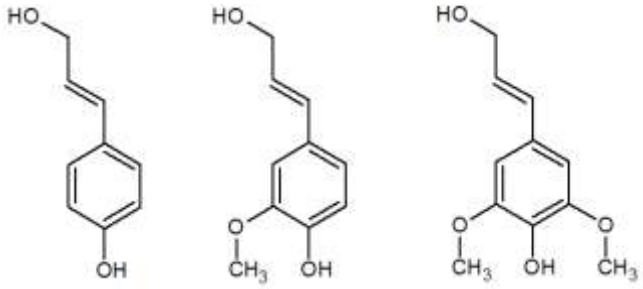

(A) (B) (C)

Figure 1-2: The three monolignols of a native lignin network: (A) coumaryl alcohol, (B) coniferyl alcohol, and (C) sinapyl alcohol

Although lignin is the only renewable resource among aromatics in nature, it has received less research attention than cellulose and hemicellulose (Ben and Ragauskas 2011, Mu, Ben et al. 2013). Furthermore, the annual production of lignin as a byproduct in the US paper industry is over 50 million tons, but only 2% of it is converted into bio-products, while the rest is combusted to recover energy (Ben and Ragauskas 2011). Accordingly, the production of value-added lignin-based products would valorize the material and deal with the waste issue. In addition, it will address the unexpected challenges faced by the Canadian forestry industry over the past few years.

1.4 Conversion of Biomass

Biomass can be converted into bio-products and/or energy using different routes, the most important being biochemical and thermochemical technologies. In the former, biological organisms and/or biological catalysts are used for the transformation. This can be effected through the application of different techniques such as fermentation, transesterification, and methane production in landfills. In the latter, heat and catalysts are employed using three main approaches, pyrolysis, gasification, and combustion, the key difference between them being the oxygen ratio: combustion is a complete oxidation, and gasification is a partial oxidization, whereas pyrolysis is a zero oxidation.

1.4.1 Pyrolysis of Biomass

Pyrolysis is a process of thermal decomposition of the chemical bonds of a target material, performed by heating the material in an inert environment. Thus it offers less pollution compared to the other thermochemical techniques, gasification and combustion. The decomposition temperature varies depending on the material, the type of pyrolysis process used, and a few other minor factors.

In general, pyrolysis produces three main products: (1) solid fraction, called “char,” consisting mostly of carbon. Char has many potential uses, such as solid fuel, feedstock for gasification, feedstock for activated carbon production, a soil additive, and others (Imam and Capareda 2012). (2) Condensable gas (bio-oil), which is a potential source for value-added chemicals and/or alternative fuel sources that could replace petrochemicals (Motasemi and Afzal 2013). Bio-oil contains hundreds of chemical components as a result of the breakdown a virgin material network. Figure 1-3 shows an example for a lignin network and some of the fragments produced in the liquid phase via pyrolysis. (3) Non-condensable gas, which is combustible, and can be used directly to produce heat. It can also be considered as feedstock to produce chemicals via further processes (de Wild, Huijgen et al. 2012).

The yield and quality of the pyrolysis products depend primarily on the applied conditions. For instance, in slow pyrolysis (T=550-950 K and t=450-550 s) the main product is solid, while in fast pyrolysis (T=850-1250 K and t=0.5-10 s) and flash pyrolysis (T=1050-1300 K and $t<0.5$ s), the main product is liquid (Motasemi and Afzal 2013). Furthermore, the feedstock characteristics, presence of a catalyst, design of the pyrolyser, and other conditions will affect the product quantity and/or quality as well. For example, the pyrolysis of sawdust pellets produced 58 wt% of condensable gas (Ren, Lei et al. 2012), whereas the pyrolysis of polystyrene plastic waste produced up to 80 wt% liquid (Karaduman 2002). In sum, controlling the pyrolysis conditions could lead to the desired product, both quantitatively and qualitatively.

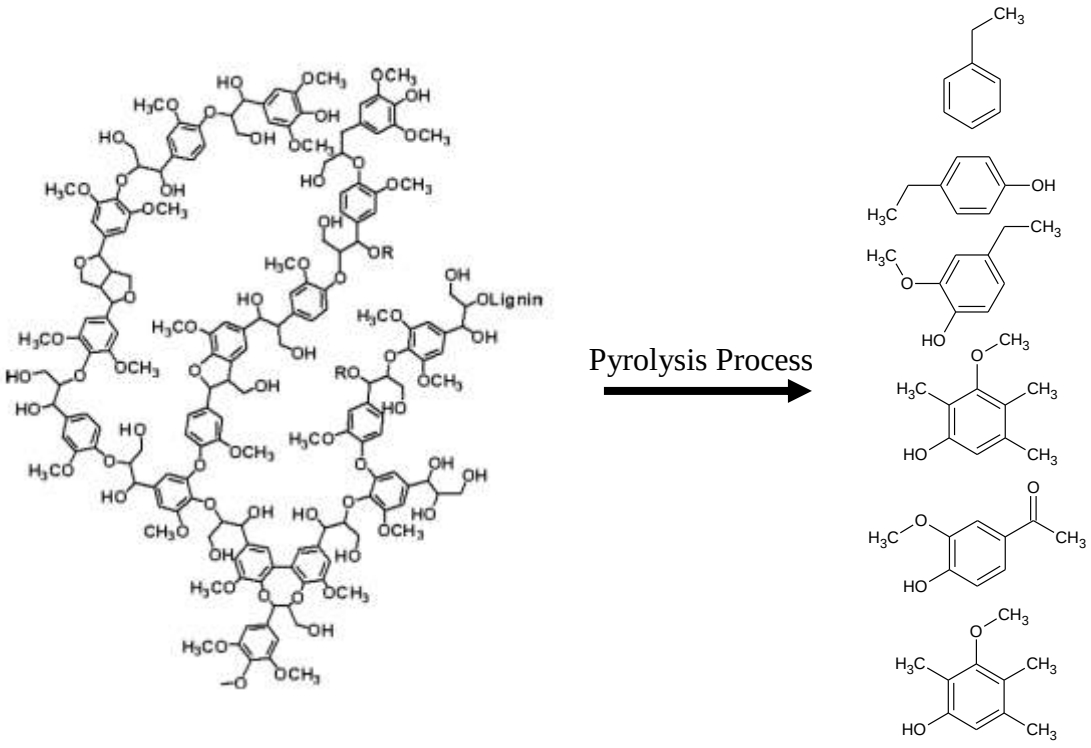

Figure 1-3: Pyrolysis of a lignin network and produced fragments in the liquid phase

The required heat energy in pyrolysis can be obtained via heat transfer from a heating source using any conventional heating (CH) technique. In this case, pyrolysis is called “conventional pyrolysis” (CP). Alternatively, it can be generated within the material itself using microwave

heating (MWH), which is called “microwave pyrolysis” (MWP). MWP is selected for application in this work, as it can produce more bio-chemicals, particularly liquids, than the other thermochemical techniques, gasification and combustion. Further information regarding MWH as well as MWP will be presented in the next chapters.

1.5 Microwave Heating Fundamentals

Microwave heating is one of the electromagnetic processes, which also include X-ray, infrared, visible light, etc.; each holds a specific frequency range and corresponding wavelength. As depicted in Figure 1-4, the selected frequencies of MWH range between 0.3 and 300 GHz, in order to prevent overlap with other applications (Jones, Lelyveld et al. 2002). In North America, 2.45 GHz is the allowed frequency for laboratory applications (Tang, Xia et al. 2008, Chiavaro, Barnaba et al. 2009, Mutyala, Fairbridge et al. 2010).

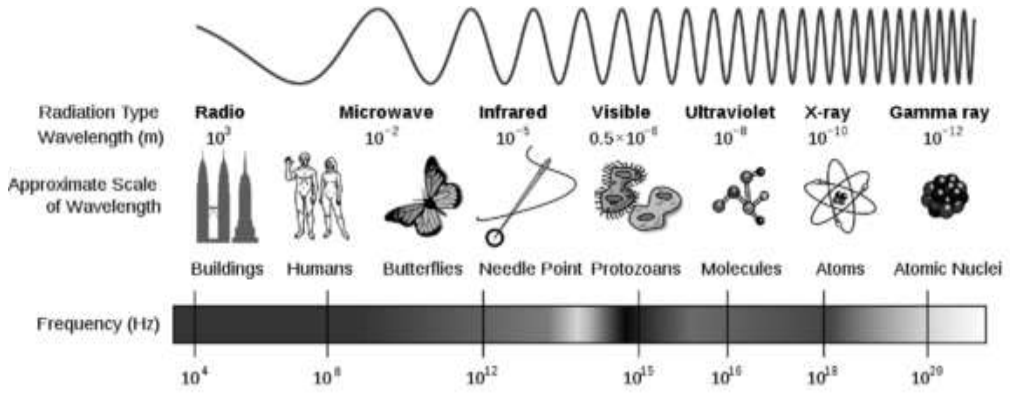

Figure 1-4: The electromagnetic spectrum (source: image courtesy of NASA)

Microwave heating is a mechanism of converting electromagnetic waves (EMW) into heat energy within a target material. This conversion occurs inside the whole or a part of the payload as it depends on the penetration limits of the applied EMW. Therefore, MWH is defined as “a volumetric energy conversion mechanism,” which is completely different than the superficial heat transfer of conventional heating. This mechanism depends mainly on the agitation of molecules of the exposed material in the presence of an alternating EMW. The molecules of the

exposed material form electric dipoles, which try to orient themselves to be in phase with the oscillating electric field, as depicted in Figure 1-5-A. This polarization is primarily responsible for generating heat energy inside the target material. On the other hand, as shown in Figure 1-5-B, free-moving ions are affected by the alternating field; however, this transformation is relatively small compared to that of the dipole oscillations.

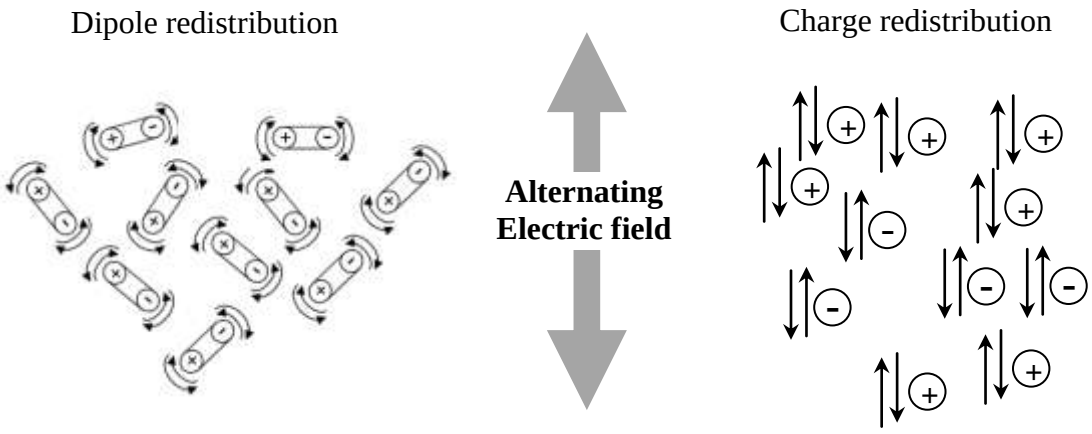

Figure 1-5: Molecular oscillations in present of an oscillating electromagnetic field

Since the agitation is restricted by the molecular interactions, the system temperature is increased. As known, temperature is a measure of average kinetic energy of particles in a body (Clark, Folz et al. 2000, Oloyede and Groombridge 2000, Durka, Gerven et al. 2009). Certainly, this agitation depends on the specifications of the applied EMW, as well as the characteristics of the exposed material. The most affected parameters are "dielectric constant" (ε'), which represents the amount of electric energy that can be stored within the heated material, and "loss factor" (ε''), which represents the ability of the heated material to dissipate microwave energy. The ratio between these two parameters is called "loss tangent" (*tan* δ), which is used to convert microwave energy to thermal energy within a material. Table 1.1 shows ε', ε'', and *tan* δ of selected materials; further information regarding the parameters governing MWH will be presented in Chapter 3.

Table 1.1: The dielectric properties of selected materials (Durka, Van Gerven et al. 2009)

Material	ε'	ε''	$tan\delta$
Vacuum	1.00	0	0
Air	1.0006	0	0
Water	80.4	9.89	0.123 (at 2.45GHz)
Methanol	32.6	21.48	0.659 (at 2.45 GHz)
Ethanol	24.3	22.86	0.941(at 2.45 GHz)
Glass	4.82	0.026	0.0054 (at 3 GHz)
Styrofoam	1.03	0.0001	0.0001 (at 3 GHz)
PTFE	2.08	0.0008	0.0004 (at 10 GHz)
Titanium oxide	50	0.25	0.005
Zirconium oxide	20	2	0.1
Zinc oxide	3	3	1.00
Magnesium oxide	9	0.0045	0.0005
Aluminum oxide	9	0.0063	0.0007

Microwave heating could be employed to avoid many issues and limitations associated with CH, such as temperature gradient inside and outside the heated material, and char layer formation in conventional pyrolysis. In addition, under controlled conditions, MWH can save more in energy consumption as well as enhance product quantity and quality, as reported in numerous publications (Lucchesi, Chemat et al. 2004, Karthikeyan, Balasubramanian et al. 2006, Budarin, Clark et al. 2009, Pan, Wu et al. 2009, Zhang and Zhao 2010, Paixão, Monteiro et al. 2011, Chandra Shekara, Jai Prakash et al. 2012). Variously sized and non-homogeneous feedstock is acceptable since MWH is a volumetric heating mechanism; however, penetration limits must be considered. As well, MWH is easily and rapidly initiated and terminated, which would increase production speed in different sectors. EMW only interacts with particular types of materials; thus, it can effectuate selective heating. This dramatically reduces the amount of heat energy needed to

achieve a particular end, which results in lower running costs and decreases the potential of thermal hazards. Furthermore, MWH allows for a higher level of control and more compact equipment, which can result in higher precision and safety, and magnetrons are available in a wide range of power outputs, which makes the process highly scalable. Last but not least, EMW can be generated and then guided to a target material anywhere, which makes the process highly flexible.

In contrast to the above advantages of MWH, EMW radiation presents an additional hazard in relation to thermal heating. The advantage of EMW only interacting with particular materials can be a problem in some cases, which makes the use of a microwave-receptor essential. The materials used in the construction of reactors are limited according to the ability to interact with EMW. The more sophisticated MWH apparatuses require an increase in the initial cost of the total system, which often leads to the choice of multiple smaller units rather than one large unit.

Recently, MWH has attracted a staggering amount of attention in scientific research, which is realized in the number of publications and patent applications over the last few years (See Figure 1-6). Although MWH has been proven as a powerful heating mechanism, especially in converting of biomass/waste into value-added products; it has not been industrialized yet (Motasemi and Afzal 2013). However, it has been established in a number of other applications, such as drying, extraction, separation, and reactivation (Oloyede and Groombridge 2000, Jones, Lelyveld et al. 2002).

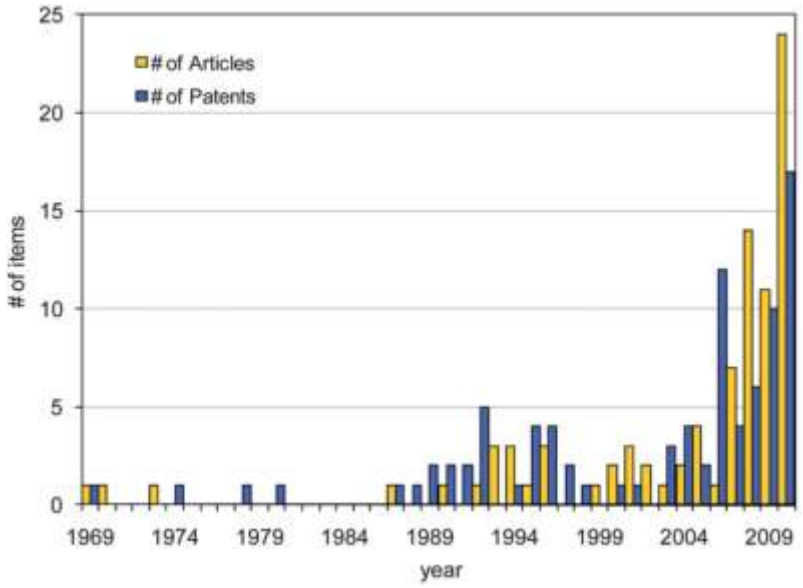

Figure 1-6: Evolution of scientific research in the area of MWP in 2010 as compared to previous years (Luque, Menendez et al. 2012)

1.6 Microwave-Assisted Pyrolysis

Employing MWH in pyrolysis would avert a number of issues/limitations associated with CH, the most important being char layer formation during CP. In CH, heat is transferred from a heating source to the outer surface of the heated material. Thus, surface temperature begins to rise, which results in heat transfer towards the core, primarily by thermal conduction. Once the temperature reaches the pyrolysis temperature, the heated material begins to decompose from the surface to the core. This forms a layer of char that grows in the same direction of the heat transfer, which behaves likewise a thermal insulator. This layer limits heat transfer through the heated material, which results in an outer surface hotter than the core, as shown in Figure 1-7-A. Consequently, volatile products would be affected quantitatively and/or qualitatively as a result of further thermal degradation during the flow out through this layer due to the pressure gradient at the pyrolysis zone. On the other hand, in MWH, EMW penetrate the entire heated material at almost the same time, limited only by penetration limits. Therefore, theoretically, MWH should lead to uniform temperature distribution within the heated material. However, in practice, it is likely to produce non-uniform temperature distribution, as the core is often hotter than the surface (Yang and Gunasekaran 2001, Cuccurullo, Berardi et al. 2002, Pandit and Prasad 2003,

Campañone and Zaritzky 2005, Rattanadecho 2006, Gunasekaran and Yang 2007, Ciacci, Galgano et al. 2010). This is a result of different factors, which will be discussed in Chapter 3. Accordingly, in MWP, the char layer formation grows in the direction opposite to that of CP, starting in the core and moving toward the outer surface, as depicted in Figure 1-7-B. In MWP, volatile products flow out through virgin material, i.e., through zones with a lower temperature, which preserves their chemical structure. Figure 1-8 shows a rubber stopper and a wood block heated in a microwave oven (MWO) then cut into two halves. The difference in colour between the surface and the core can shows the char layer formation experimentally. In conclusion, using electromagnetic irradiation rather than superficial heat transfer in pyrolysis would produce a better product different in terms of quality and quantity compared to traditional pyrolysis.

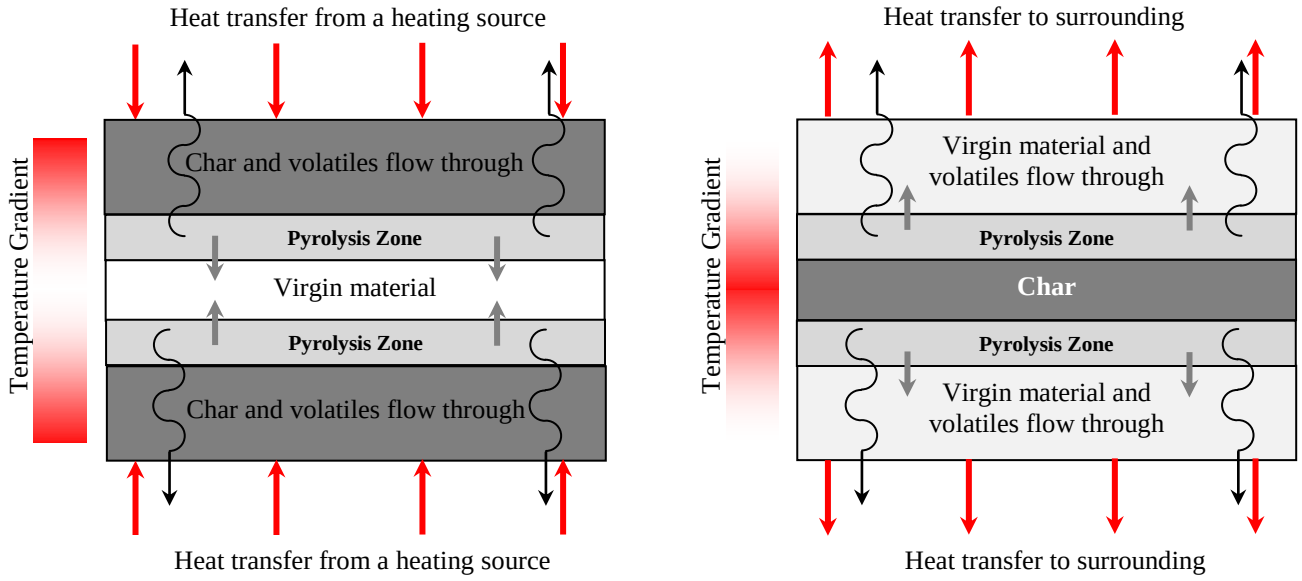

Figure 1-7: Schematic diagram of pyrolysis in one direction (A) CP and (B) MWP

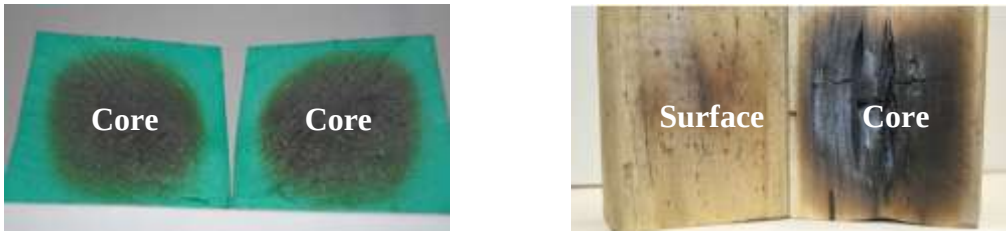

(A) (B)

Figure 1-8: Materials heated by MWH, (A) rubber stopper and (B) wood cube

1.7 Temperature Gradient in MWH

Although temperature gradient is a key factor in MWH, only a modest effort has been made to investigate this. For example, in brief, Ciacci, Galgano et al. (Ciacci, Galgano et al. 2010) simulated a MWP of a wood block, taking in to consideration heat and mass transfer. Campañone and Zaritzky (Campañone and Zaritzky 2005) predicted temperature profiles within different geometries: a sphere, an infinite cylinder, and a slab. Pandit and Prasad (Pandit and Prasad 2003) simulated temperature profiles within a potato, using finite element analysis. The key conclusion of those studies was that MWH leads to non-uniform temperature distribution and/or hot spots inside the heated material. The same conclusion was arrived at by Zhou, Puri et al. (Zhou, Puri et al. 1995), Rattanadecho (Rattanadecho 2006), Gunasekaran and Yang (Gunasekaran and Yang 2007), and Miura, Kaga et al. (Miura, Kaga et al. 2004). Further information regarding the examination of reviewing this aspect in the scientific literature will be presented in Chapter 3. In spite of the efforts made, the simulation of temperature profiles within materials exposed to EMW still needs further investigation. Approaches that can be employed to control in the reported observations are almost entirely absent. Furthermore, different scenarios required to investigate how to achieve a desired temperature profile. Therefore, a goal of this work is to investigate these missed points, which will be presented in Chapter 3.

1.8 Effect of MWH on Different Reactions

Indeed, in the scientific literature, extensive research has been reported on the effects of MWH on different reactions. This section summarizes the key conclusions of some of the publications

related to this work; in addition, a further literature review will be presented in Chapter 4. Zhang and Zhao (Zhang and Zhao 2010) studied the production of 5-hydroxymethylfurfural and furfural from corn stalk, rice straw, and pine wood in an ionic liquid, and reported that MWH increased product yield and decreased reaction time. Budarin, Clark et al. (Budarin, Clark et al. 2009) investigated the preparation of bio-oils using MWP on wheat straw; the oils produced were rich in aromatics compared to those produced using CP. Krzan and Zagar (Krzan and Zagar 2009) studied the liquefaction of wood with glycols using p-toluenesulfonic acid as a catalyst, applying MWH. The authors concluded that MWH decreases the liquefaction time and minimizes the loading of catalyst. Menéndez, Domínguez et al. (Menéndez, Domínguez et al. 2004) investigated MWP of four different types of wet sewage sludge, and MWP was found to achieve the reaction much faster than through by CP; in addition, it produced more non-condensable gas yield. Lucchesi, Chemat et al. (Lucchesi, Chemat et al. 2004) studied solvent-free microwave extraction of oil from basil, garden mint, and thyme. The authors reported that MWH achieved the reaction in less time compared to CH. In addition, a noticeable savings in energy consumption were achieved: 0.25 kWh compare to 4.5 kWh with CH. Similar results were reported by Paixão, Monteiro et al. (Paixão, Monteiro et al. 2011). Orozco, Ahmad et al. (Orozco, Ahmad et al. 2007) found that MWH increased the glucose yield of grass and cellulose in dilution of phosphoric acid and water. Furthermore, it has higher reaction rate at moderate temperatures. Karthikeyan, Balasubramanian et al. (Karthikeyan, Balasubramanian et al. 2006) realized that MWH completed extraction of polycyclic aromatic hydrocarbon from airborne particles within minutes, compared to hours using CH, and the obtained products were different in quality. Sithambaram, Nyutu et al. (Sithambaram, Nyutu et al. 2008) found that MWH enhanced conversion of K-OMS catalyzed oxidation of tetralin compared to CH: (52–88%) and (42–80%), respectively. A similar conclusion was arrived at by Chandra Shekara, Jai Prakash et al. (Chandra Shekara, Jai Prakash et al. 2012) in an investigation of the solventless acylation of p-cresol with different carboxylic acids over BEA zeolite. To conclude, MWH shows noticeable demonstrated effects on reaction rate, reaction temperature, energy consumption, catalyst loading, and other parameters.

Although extensive research has been reported on this aspect, few attempts have been made to find a scientific explanation for the observed effects. Few researchers have done a comparison between MWH and CH based using a kinetic study. Adnadjevic and Jovanovic (Adnadjevic and

Jovanovic 2012), Adnađević, Gigov et al. (Adnađević, Gigov et al. 2008), Fukushima, Kashimura et al. (Fukushima, Kashimura et al. 2013), Sun, Wang et al. (Sun, Wang et al. 2012) Chen, Wang et al. (Chen, Wang et al. 2013), Yan, Hu et al. (Yan, Hu et al. 2012), Adnadjević and Jovanović (Adnadjević and Jovanović 2012), and Li, Han et al. (Li, Han et al. 2013) reported that reaction activation energy (E_a) in the case of MWH is less than that of CH as a result of an effect related to applied EMW. In fact, this is a doubtful statement because the wavelength of applied EMW, 12.24 cm, is much longer than the intermolecular distance of the heated material. On the other hand, Mazo, Estenoz et al. (Mazo, Estenoz et al. 2012) and Yadav and Borkar (Yadav and Borkar 2006) have found that the E_a is the same for both cases, MWH and CH. Regarding the effect on the pre-exponential factor (k_o), Adnadjevic and Jovanovic (Adnadjevic and Jovanovic 2012), Adnađević, Gigov et al. (Adnađević, Gigov et al. 2008), and Mazo, Estenoz et al. (Mazo, Estenoz et al. 2012) reported that the k_o in MWH is lower than that of CH. Indeed, this statement is not acceptable based on the MWH mechanism, which mainly depends on the agitation of the molecules of the heated material, i.e., k_o should be higher in MWH than CH. On the contrary, Adnadjević and Jovanović (Adnadjević and Jovanović 2012), Li, Han et al. (Li, Han et al. 2013), Temur Ergan and Bayramoğlu (Temur Ergan and Bayramoğlu 2011), and Yadav and Borkar (Yadav and Borkar 2006) have found the opposite, that k_o in MWH is higher than that in CH. To sum up, even though significant effects have been discovered in different MWH reactions, little effort has been made to interpret these observations. In addition, many of the published conclusions are inconsistent with each other. Thus another aim of this project is to investigate this, which will be presented in Chapter 4.

1.9 Pyrolysis of Lignin and Products Investigation

As mention earlier, pyrolysis, combustion, and gasification are the three techniques of thermochemical technology. Each is employed for a specific purpose: combustion is used to generate heat energy, whereas gasification is used to produce synthesized gas. Pyrolysis is applied to produce bio-products in the form of solid, condensable gas, and non condensable gas. Pyrolysis liquid has received more interesting than solid and gas products in scientific research, as it has the potential to produce value-added bio-chemicals. In addition, it can be used as a fuel resource to replace petrochemical-based fuels. However, the complexity of crude liquid created

by pyrolysis makes further processes for upgrading, such as dehydration and separation, essential. This level of complexity is affected by the pyrolysis condition, the structure of virgin material, and many other conditions. For example, liquids obtained from the pyrolysis of lignin are more complex than those obtained from cellulose and hemicellulose. Accordingly, the characterization of pyrolysis liquids is limited by many factors, in addition to the basic issues regarding the limitations of analyzers. Thus, scientific publications that present detailed structural investigations of bio-oils are quite scarce.

The pyrolysis of lignin, using MWH or CH, has been investigated for the past two decades, but few studies have examined the liquid product qualitatively; the majority investigated it quantitatively. This section presents a brief literature review of this aspect; in addition, further reviews will be presented in Chapter 5 and Chapter 6. Zheng, Chen et al. (Zheng, Chen et al. 2013) investigated the fast pyrolysis of lignin under a catalytic reaction of $Mo_2N/\gamma\text{-}Al_2O_3$, using a pyrolysis-gas chromatography/mass spectrometry system (Py-GC-MS). Choi and Meier (Choi and Meier 2013) studied the pyrolysis of kraft lignin under effect of different temperatures and catalysts, using GC-MS/GC-FID to analyze the liquid product. Jiang, Nowakowski et al. (Jiang, Nowakowski et al. 2010) examined the temperature dependence of the composition of lignin pyrolysis products employing Pr-GC-MS. Lou, Wu et al. (Lou, Wu et al. 2010) investigated the effect of temperature and catalysts (sodium chloride, Permutite) on the pyrolysis of bamboo lignin, using Py-GC-MS. Zhang, Resende et al. (Zhang, Resende et al. 2012) studied the pyrolysis of three lignin types, prairie cord grass, aspen, and synthetic kraft lignin, using Py-GC-MS and TGA/FTIR. De Wild, Huijgen et al. (de Wild, Huijgen et al. 2012) investigated the pyrolysis of lignin from two different biomass sources using a fluidized bed reactor. In that work, the obtained condensable gas product was analyzed using GC-MS. Luo, Wang et al. 2012 (Luo, Wang et al. 2012) examined the thermal behaviour of organosolv lignin under the catalytic effect of zeolites using TGA-FTIR.

Most of the publications on this subject focus on investigating the liquid products from lignin pyrolysis employed GC-MS, TGA, and/or FT-IR analyses. However, these techniques are limited because of the complexity of the crude liquid, which results in many chemical compounds that

could not be identified. For instance, GC-MS cannot identify around 40 wt% of the cured oil, and using FT-IR for the quantitative analysis of a complex mixture is limited (Ben and Ragauskas 2011). Consequently, a full structural investigation of a bio-oil has not been achieved; in addition, scientific publications that present compositional analyses of bio-oils, particularly from lignin pyrolysis, are few in number. Therefore, the third aim of this project is the compositional analysis and structural investigation of a bio-oil from the MWP of lignin at various conditions, which will be presented in Chapter 5.

1.10 Pyrolysis Modeling

The pyrolysis of lignin has been investigated from different aspects, such as product distribution (Jiang, Nowakowski et al. 2010, Lou and Wu 2011), the presence of catalysis (Mullen and Boateng 2010, Rutkowski 2011), and kinetics (Ferdous, Dalai et al. 2002, Montané, Torné-Fernández et al. 2005, Mani, Murugan et al. 2008, Faravelli, Frassoldati et al. 2010, Jiang, Nowakowski et al. 2010, Janković 2011). Extensive studies have been conducted to model lignin pyrolysis using a single step global reaction. This model considers the virgin material as decomposed into volatiles and solid. However, it cannot distinguish between condensable and non-condensable products. Thus, an investigation of single/multi step parallel reactions is required, which can predict further outcomes.

$$\text{Virgin material} \longrightarrow y \text{ char} + (1\text{-}y) \text{ volatiles}$$

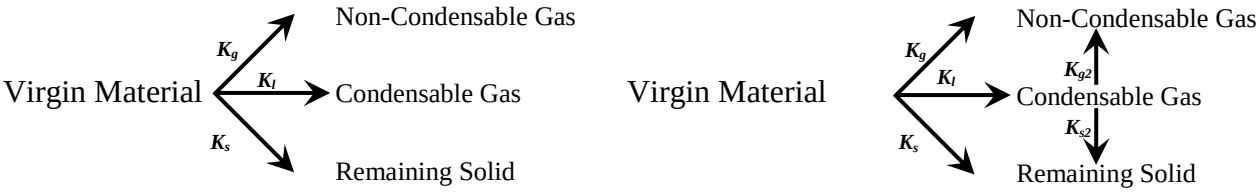

In spite of the extensive publications regarding this aspect, the kinetic modeling of individual pyrolysis products, both qualitative and quantitative, is scarce in the scientific literature. It may

be a consequence of particular failings of the experimental setup. As a result, most of the current pyrolysis models investigate only volatile products quantitatively, without modeling their chemical composition. As will be discussed in Chapter 5, qualitative investigation is so significant because it can distinguish between products with the same yield. Therefore, the fourth step in this work aims to investigate the kinetics of the pyrolysis products as well as the extracted chemicals from MWP of lignin, which will be presented in Chapter 5. Such investigations will lead to an improved understanding of the underlying processes, and provide needed information for the rational design and scaling-up the pyrolysis reactor.

CHAPTER 2 OBJECTIVES AND METHODOLOGY

The main purpose of this work is to investigate the potential of converting lignin into value-added bio-products. In order to accomplish this, the following steps will be taken:

1. Simulate temperature profiles within selected materials exposed to microwave heating (MWH).
2. Design and manufacture an innovative thermometer that does not suffer from the drawbacks of traditional thermometers.
3. Design and build an original thermogravimetric analyzer that works using MWH and is equipped with a product manifold, for kinetic purposes.
4. Study the reaction kinetics of microwave pyrolysis (MWP), in contrast to conventional pyrolysis (CP) and interpret the obtained results.
5. Study the composition and structure of the condensable gases produced by MWP of kraft lignin using different analysis techniques.
6. Design a kinetic model of the MWP products of kraft lignin, both quantitatively and qualitatively.

Chapters 4 to 7 will present the achievement of these objectives and the scientific findings. Chapter 3 will first present a three-dimensional mathematical model to simulate temperature profiles inside a material exposed to electromagnetic irradiation at 2.45 GHz. In order to do this, COMSOL-Multiphysics applications will be used to simulate the transient temperature profiles of pinewood, carbon, Pyrex, and combinations of such under different conditions. Chapter 4 will present a kinetic investigation of the MWP of sawdust using an original MW-TGA. In this chapter, the full descriptions of the MW-TGA will be presented. Chapter 5 will discuss the detailed compositional analysis and structural investigation of a condensable gas phase obtained from the MWP of kraft lignin. In this chapter, different degradation pathways of a lignin network will be presented after analysing the obtained liquids. Chapter 6 will present a kinetic modeling of MWP products from kraft lignin using a lumped approach. Further investigations for the oil

phase will be presented using different techniques, which will enable modeling of the extracted chemicals as well. Finally, Chapter 7 will present the conclusions of this work and the recommendations for the future investigations.

CHAPTER 3 ARTICLE 1: TEMPERATURE PROFILE PREDICTION WITHIN SELECTED MATERIALS HEATED BY MICROWAVES AT 2.45GHz

Sherif Farag[a], Amr Sobhy[a], Cevdet Akyel[b], Jocelyn Doucet[a] and Jamal Chaouki[a]

[a]CRIP-Biorefinery Centre, Department of Chemical Engineering, École Polytechnique de Montréal.

[b]Department of Electrical Engineering, École Polytechnique de Montréal.

P.O. Box 6079, Station Centre-ville, Montréal, QC, Canada H3C 3A7.

(Published in Applied Thermal Engineering Journal - doi:10.1016/j.applthermaleng.2011.10.049)

Presentation of the article: A three-dimensional mathematical model to simulate transient temperature profiles within selected materials exposed to electromagnetic irradiation will be presented. COMSOL-Multiphysics applications will be employed to simulate the temperature profiles of pinewood, carbon, Pyrex, and combinations of such using different scenarios. The predicted results will be compared against experimental data to validate the model.

Abstract

This work presents a three-dimensional mathematical model to simulate temperature profiles inside a material heated by electromagnetic waves (EMW) at 2.45 GHz. COMSOL-Multiphysics was used to simulate transient temperature profiles of pinewood, carbon, Pyrex, and combinations of such under different conditions. The model predicts that, upon exposing an 86mm wooden cube to 2.45 GHz EMW for 300 s, the core temperature reached 595 K at a setting of 60K/min, while the outer surface 365 K at 15 K/min. By mixing 50% carbon with the wooden block, the model anticipated the cube core to reach 990 K at 140 K/min, compared to 1350 K at 212 K/min with 75% carbon at the same power and after the same time. By inserting a 125 cm^3 carbon cube inside the wood cube, the core reaches 3200 K, while the outer surface was 375 K and 636 K for free convection (FC) and perfect insulator (PI), respectively. Placing the same volume of carbon on the surface of the wood cube yielded a maximum temperature of 660 K under FC, compared to 1280 K with PI. Changing the material of the core cube from Carbon to Pyrex yields a temperature of 324 K in the core, with 365 K and 605 K on the outer surface in the case of FC or PI, respectively. The average percentage relative error between the measured and the predicted temperatures was ±4% and ±15% inside the pinewood and carbon respectively.

Keywords: Microwave heating, Temperature profiles, Absorbing power, Temperature prediction, Heat equation, Energy efficiency.

3.1 Introduction

A number of industrial sectors have benefited from the contrast between of microwave heating (MWH) mechanisms and conventional heating (CH). Most importantly, MWH mechanisms reply on energy conversion directly with the target material, leading heat generation volumetrically rather than through the surface of the material, as is the case with CH. Furthermore, it is well established that electromagnetic waves (EMW) have a high interaction with powder samples (Durka, Van Gerven et al. 2009, Li, Zhang et al. 2009). This can be used to distribute hot spots inside the media being heated to increase the microwave-induced energy transfer. Under controlled conditions, it has been demonstrated that MWH can reduce energy consumption and allow for higher product selectivity in certain reactions compared to CH (Camelia Gabriel and Mingosb 1998, Thostenson and Chou 1999, Oloyede and Groombridge 2000, Datta and Ni 2002, Jones, Lelyveld et al. 2002, Will, Scholz et al. 2003, Domínguez, Menéndez et al. 2005, Zhu, Wu et al. 2006, Geedipalli, Rakesh et al. 2007, Orozco, Ahmad et al. 2007, Badamali, Clark et al. 2008, Tang, Xia et al. 2008, Xu, Jiang et al. 2008, Budarin, Clark et al. 2009, Chiavaro, Barnaba et al. 2009, Durka, Gerven et al. 2009, Ma, Liu et al. 2009, Wan, Chen et al. 2009, Mutyala, Fairbridge et al. 2010).

Theoretically, MWH should lead to equivalent heat generation within the material. However, in practice, it is likely to produce a non-uniform temperature distribution (Yang and Gunasekaran 2001, Cuccurullo, Berardi et al. 2002, Pandit and Prasad 2003, Campañone and Zaritzky 2005, Rattanadecho 2006, Gunasekaran and Yang 2007, Ciacci, Galgano et al. 2010). This aspect makes modeling of the heat transfer mechanisms rather complex. As an example, Figure 3-1 shows wooden blocks heated in a microwave oven for 360 s at different power settings. Although Figure 3-1-A and Figure 3-1-B were heated at same power setting (2.3 kW), use of thermal insulation on the outer surface influenced their core temperature. While Figure 3-1-C was heated at 2.7 kW for the same time (360 s), Figure 3-1-B still produced a higher temperature compared to others. These variances result from different parameters, the most important being the heat transfer on the outer surface (Yang and Gunasekaran 2001, Geedipalli, Rakesh et al. 2007).

(A) (B) (C)

Figure 3-1: Wood blocks heated by 2.45 GHz microwaves for 360 s at: (A) 2.3 kW with FC, (B) 2.3 kW with PI, and (C) Power 2.7 kW with FC

Temperature profiles for materials exposed to MWH have been studied in the literature (Klinbun and Rattanadecho , Zhou, Puri et al. 1995, Campañone and Zaritzky 2005); Most of these studies reported that MWH leads to non-uniform distribution of temperature and hot and/or cold spots inside the heated material (Zhou, Puri et al. 1995, Pandit and Prasad 2003, Miura, Kaga et al. 2004, Campañone and Zaritzky 2005, Gunasekaran and Yang 2007, Ciacci, Galgano et al. 2010), but a little effort has been done in order to study how can be controlling in those observations.

The primary objective of this work is to present the development and validation of a mathematical model to predict temperature profiles within a wood cube subjected to MWH. The model was solved using COMSOL-Multiphysics applications, taking into account the effect of (1) heat induction in a wooden cube of known dielectric and physical properties upon irradiation by 2.45 GHz microwaves at 2.3 KW nominal power and (2) heat transfer due to free convection or perfect insulator (FC or PI) at the surface of the cube. The software COMSOL-Multiphysics will then be used to predict temperature profiles within the wood cube (1) subjected to surface heat loss, (2) subjected to perfect insulation at the surface, (3) upon replacing a volume of wood with an excellent converter of microwave to heat (carbon), and (4) upon replacing the same volume of wood with a microwave-transparent material (Pyrex). Cases (3) and (4) are compared to (1) and (2) to highlight the variation of temperature profiles within composite exposed to MWH in the presence of materials of contrasting dielectric, and physical properties. Such discussions aim at (1) improving the understanding of temperature profiles within composite materials heated by microwaves and (2) developing approaches to influence/control temperature profiles through material selection.

3.2 Fundamentals of MWH

3.2.1 Microwave/Material Interaction

Electromagnetic waves consist of an electric and magnetic field orthogonal to each other. The dominant mechanism of microwave-induced heating at 2.45 GHz involves the agitation of molecular dipoles due to presence of an oscillating electric field (for non-magnetic materials). In the presence of an oscillating field, molecular dipoles reorient themselves in order to be in phase with the alternating field. These orientations are restricted by molecular interaction forces, increasing molecular kinetic energy. As kinetic energy increases, system temperature increases within a short time. This period of time depends on the electrical and physical properties of the heated material (Thostenson and Chou 1999, Clark, Folz et al. 2000, Oloyede and Groombridge 2000, Yang and Gunasekaran 2001, Durka, Gerven et al. 2009, Robinson, Kingman et al. 2009, Budarin, Clark et al. 2010).

Materials can be classified into three categories depending on their response to the EMW:

- Materials that reflect waves (highly conductive materials) e.g., metals.
- Materials that are considered EMW-transparent e.g., ceramics, quartz, glass.
- Materials that absorb waves, e.g., carbon, water, methanol. This category has the highest response to microwaves and most of them are relevant to microwave chemistry as they have high thermal response (Miura, Kaga et al. 2004, Budarin, Clark et al. 2010).

In order to apply microwave energy to a chemical process, at least one or more components of the system must be a good microwave absorber. Fortunately, many organic compounds, metal oxides and popular solvents are good or, at least, moderate absorbers for the EMW as they have high thermal response.

3.2.2 The Main Parameters Describing MWH

For non-magnetic material, the main parameter which describes the level of heat generation inside a microwave absorbent material is the complex permittivity (ε^*) as represented in equation (3-1).

$$\varepsilon^* = \varepsilon^{/} - \mathrm{j}\varepsilon^{//} \tag{3-1}$$

The real part of the complex permittivity is called dielectric constant ($\varepsilon^{/}$) which represents the amount of electric energy that can be stored within the heated material. The imaginary part is called "loss factor" ($\varepsilon^{//}$) and represents the ability of the heated material to dissipate microwave energy. The ratio between these parts is called "loss tangent"; it is used to convert microwave energy to thermal energy within a material (Camelia Gabriel and Mingosb 1998, Clark, Folz et al. 2000, Chiavaro, Barnaba et al. 2009, Durka, Gerven et al. 2009, Castro-Giráldez, Fito et al. 2010, Guo, Wang et al. 2010), as represented in equation (3-2).

$$tan\delta = \frac{\varepsilon^{//}}{\varepsilon^{/}} \tag{3-2}$$

3.2.3 Dissipated/Absorbed Power

The dissipated power inside a microwave cavity could be represented as energy generated inside a heated material. For non-magnetic materials, it can be represented in the form of equation (3-3).

$$P = \omega\, \varepsilon_0\, \varepsilon_{eff}^{//}\, E_{rms}^2 \tag{3-3}$$

or

$$P = 2\pi f\, \varepsilon^{/}\, tan\delta\, E_{rms}^2 \tag{3-4}$$

Where P is the absorbed power per unit volume [W/m^3], $\varepsilon_{eff}^{//}$ is the effective dielectric loss factor ($\varepsilon_0\varepsilon_{eff}^{//}=\varepsilon^{/}tan\delta$) [-], ω is the angular frequency ($\omega = 2\pi f$) [s^{-1}], and E_{rms} is the root mean square of the electric field [V/m].

In the case of magnetic materials, equation (3-4) should be replaced by equation (3-5) (Rattanadecho 2006, Manoj Gupta 2007, Robinson, Kingman et al. 2009, Ramasamy and Moghtaderi 2010).

$$P = \omega\, \varepsilon_0\, \varepsilon''_{eff}\, E^2_{rms} + \omega\, \mu_0\, \mu''_{eff}\, H^2_{rms} \tag{3-5}$$

Where μ''_{eff} is the effective magnetic loss factor [-], and H_{rms} is the magnetic field [A/m].

Microwave frequencies ranged between 10^6 (radio frequencies) and 10^{12} Hz (infrared frequencies). Frequencies allocated for commercial applications are 0.915, 2.45, 5.8, and 22 GHz. In laboratory experiments, a frequency of 2.45 GHz is typically used (Tang, Xia et al. 2008, Chiavaro, Barnaba et al. 2009, Mutyala, Fairbridge et al. 2010).

3.2.4 Penetration Depth and Power Penetration Depth

Electric fields and generated power decay exponentially inside the material. The penetration depth (D) is defined as the depth where the magnitude of the electric field drops by a factor $1/e$ with respect to the surface value. In a similar manner, the power penetration depth (D_p) is the distance where the power density is reduced by a factor $1/e$ of the surface. Equation (3-6) describes the relationship between D and D_p, where α is called the attenuation factor and can be represented generally by equation (3-7). For high loss ($\varepsilon''_{eff} \gg \varepsilon'$) and low loss ($\varepsilon''_{eff} \ll \varepsilon'$) mediums, equations (3-8) and (3-9) apply, respectively (Campañone and Zaritzky 2005, Manoj Gupta 2007).

$$D_p = \frac{D}{2} = \frac{1}{2\alpha} \tag{3-6}$$

$$\alpha = \omega \sqrt{\frac{[\mu'/\mu_o\, \varepsilon'\, \varepsilon_o] \left[\left(1 + (\varepsilon''_{eff}\ /\ \varepsilon')^2\right)^{1/2} - 1\right]}{2}} \tag{3-7}$$

$$\alpha = \frac{\omega}{2}\sqrt{\frac{\mu^{/}\mu_o\ \varepsilon_o}{\varepsilon^{/}}}\,\varepsilon_{eff}^{//} \tag{3-8}$$

$$\alpha = \frac{\pi\varepsilon_{eff}^{//}}{\lambda_0\sqrt{\varepsilon^{/}}} \tag{3-9}$$

Lambert's law describes the power penetration in one dimension as shown in equation (3-10) (Zhou, Puri et al. 1995, Bail, Koutchma et al. 2000, Yang and Gunasekaran 2001, Rattanadecho 2006, Manoj Gupta 2007).

$$P = P_o e^{(-2\alpha y)} \tag{3-10}$$

In a nutshell, equation (3-4) represents generated power, while equation (3-10) represents local value of the power at a certain distance from the surface of the heated material.

3.2.5 Estimation of the Dissipated/Absorbed Power Term

Due to the difficulty of measuring and calculating the electric field strength inside a microwave cavity, an energy balance was performed to estimate the power term using an empirical approach (Campañone and Zaritzky 2005) as shown in equation (3-11).

$$\frac{\sum m\ C\ \Delta T}{V\ t} = 2\pi f\ \varepsilon^{/}\ tan\delta\ E_{rms}^2 \tag{3-11}$$

Where m is the water mass, C is the specific heat, ΔT is the temperature difference, V is the water volume, and t is the heating time. It is then assumed that $2\pi f E_{rms}^2$ is independent of the material but is related to the specific microwave oven used at a specific power. For that purpose, an experimental setup was used to heat a constant mass of water ($\varepsilon^{/} = 78$, $\varepsilon^{//} = 12$, and $D_p =$ 1.44cm @2.45 GHz (Manoj Gupta 2007)) in a Pyrex cylinder with a PI on the outer surface. For 9.9 g (10 ml) of water, ΔT=68 K and t=20 s @ 2.3 kW setting power. By substituting in equation

(3-11) a general absorbed energy equation is obtained for any material heated by the microwave oven (Microwave Research Inc; Model: BP-211, 230 V, and Total power 3.2 kW). This calculation was done with a power setting of 2.3 kW. For this specific power, the following equation can be derived (3-12):

$$(P_o)_{material} = 2.25 \times 10^6 (\varepsilon' \ tan\delta)_{material} \ \ \mathrm{W/m^3} \quad (3\text{-}12)$$

3.3 Mathematical Model

Consider an element of volume of dimensions Δx, Δy, and Δz from a larger block element with dimensions *l, h,* and *w* in the *x, y,* and *z* coordinates system. The following assumptions are made:

1) Variation of volume and physical/electrical properties are considered negligible.
2) All materials considered are non-magnetic material, i.e., magnetic field's interaction is negligible.
3) Neglect any effect related to chemical reaction during the heating process.
4) Uniform distribution of the EMW inside the oven cavity.

By applying the energy balance on this element with the set of assumptions and initial conditions, it is possible to obtain the final form of the energy equation as shown in equation (3-13).

$$k\,\nabla^2 T + \frac{P_o}{3}\sum_i \left(e^{\frac{-i}{D_p}} + e^{\frac{i-l}{D_p}}\right) = \rho\, C\, \frac{\partial T}{\partial t} \quad (3\text{-}13)$$

Where *i* refers to the Cartesian coordinates: *x, y,* and *z.* The term *l* must be replaced by *h* and *w* when *i* is *y* and *z* respectively.

Initial and Boundary Conditions:

At t=0: T=T_0 at any point inside or outside the block

In the case of FC heat transfer by conduction is equal to by convection therefore;

@ t>0 i.e. x=0, l; $-k\frac{\partial T}{\partial x} = h(T - T_0)$

y=0, h; $-k\frac{\partial T}{\partial y} = h(T - T_0)$

z=0, w; $-k\frac{\partial T}{\partial z} = h(T - T_0)$

In the case of PI there is no heat transfer by conduction

@ t>0 i.e. x=0, l; $-k\frac{\partial T}{\partial x} = 0$

y=0, h; $-k\frac{\partial T}{\partial y} = 0$

z=0, w $-k\frac{\partial T}{\partial z} = 0$

The electric field components have a maximum value at the air/material interface; these components are decayed through the heated material according to equation (3-10).

By substituting equation (3-12) for equation (3-13), the final form of the energy balance equation (related to this microwave oven) can be obtained as shown in equation (3-14).

$$k\,\nabla^2 T + \frac{2.25\times10^6}{3}(\varepsilon'\,tan\delta)_{material}\ \sum_i(e^{\frac{-i}{D_p}} + e^{\frac{i-l}{D_p}}) = \rho\,C\,\frac{\partial T}{\partial t} \qquad \mathrm{W/m^3} \qquad (3\text{-}14)$$

Figure 3-2 shows the schematic of the problem in one direction: +*x*; includes the three energy terms of the equation (3-14) within the element considered.

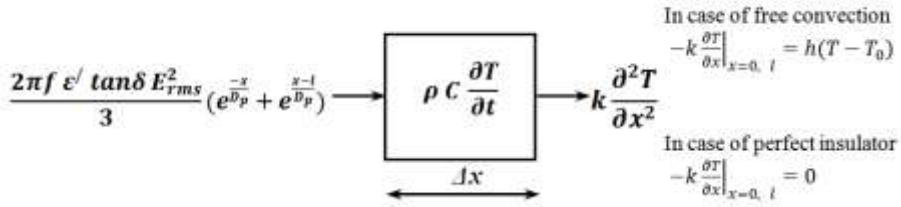

Figure 3-2: Schematic representation of the thermal balance on a dielectric element in the system

3.4 Results

In order to simulate equation (3-14) COMSOL-Multiphysics is applied under selected conditions and materials with a convective heat transfer coefficient of 100 W/m^{2}K (Ciacci, Galgano et al.

2010) and initial temperature 290 K. Table 3.1 shows the physical and electric properties of different materials which are used in this simulation.

Table 3.1: Input parameters for MWH model (Vos, Mosman et al. 2003, D.E. Clark 2005, Kol 2009)

Sample type	C (kJ/kg K)	ρ (kg/m^3)	k (W/m K)	ε'	ε''	D_p (mm)
Pinewood	2.5	470	0.17	2.7	0.53	59
Carbon	0.93	380	0.11	7	2	26
Pyrex	0.75	2230	1.005	4	0.005	7800
25% carbon and 75% wood	2.1	447.5	0.155	3.77	0.9	42
50% carbon and 50% wood	1.7	425	0.14	4.85	1.27	34
75% carbon and 25% wood	1.3	402	0.125	5.92	1.634	29

Upon entering system geometry and defining boundary and initial conditions in COMSOL-Multiphysics, the selected element was given the characteristics shown in Table 3.2. The time-dependent solver algorithm applied the Finite Element Method to solve the partial differential equation. The time range was from 0 to 300 s with a step of 60 s. Relative and absolute tolerances were 0.01 and 0.001 respectively, and the number of the solved degrees of freedom was 136738. The needed time to find the solution is around 160s for each simulation.

Table 3.2: Domain characteristics defined in the model

Maximum element	4.73 mm
Minimum element size	0.344 mm
Maximum element growth rate	1.4
Resolution of curvature	0.4
Resolution of narrow regions	0.7
Time stepping has initial step	0.001 s
Maximum step	0.1 s

3.4.1 The Effect of D_p on the Temperature Profile for a Pinewood Block

The first simulation of this study considers a wood cube with a side length of 86 mm. The second simulation uses side lengths of 200 mm and 400 mm. Temperature profiles are drawn for a one-dimensional line as shown in Figure 3-3. Figure 3-4 shows the temperature profiles along this line based on heating times ranging from 60 to 300 s. Both FC and PI cases are shown. Based on Figure 3-4-A, the heating rate at a point on the outer surface (x=y=43 mm and z=0 mm) is 15 K/min, compared to 60 K/min at the block core (x=y=z=43 mm). After 60, 120, 180, 240 and 300 s of MWH the differences between these two points are 32, 77, 125, 175, and 225 K, respectively. It could be observed that the condition of perfect thermal insulation on the outer surface has a considerable effect and yields a uniform distribution of temperature as shown in Figure 3-4-B.

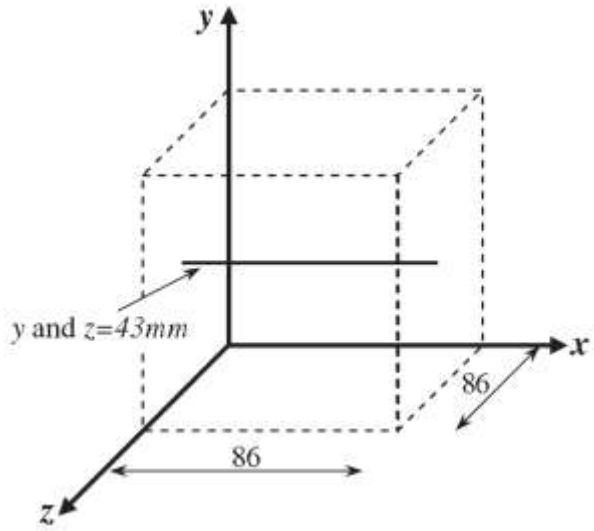

Figure 3-3: Line selected to simulate and measure the temperature profiles

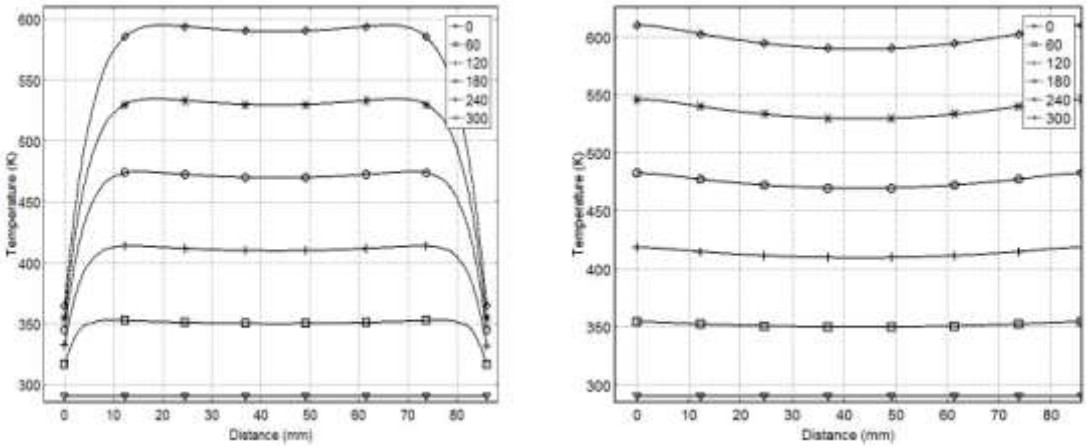

(A) (B)

Figure 3-4: Temperature profiles on the selected line parallel to *x* axis and has 43 mm in *y* & *z* axis (time in seconds): (A) With FC and (B) With PI

In order to study the effect of long heating times, temperature profiles were generated in the case of FC, as shown in Figure 3-5. These suggest that as heating time increases a parabolic profile replaces the flat section, indicating a considerable temperature difference between the surface and the core of the block.

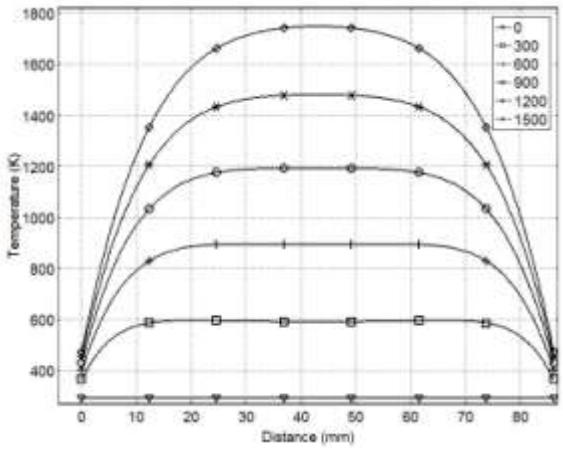

Figure 3-5: The effect of heating time at constant microwave power on temperature profiles

Figure 3-6-A presents the temperature profile for a block with a 200 mm side length. Compared to the smaller block presented earlier (86 mm); the temperature profile has a noticeably different shape. In fact, larger dimensions emphasize the effect of penetration depth where the local power density diminishes exponentially with distance. The fine balance between convection on the surface and heat generation (Beer-Lambert law) yields a maximum value a few centimeters below the surface and not in the core.

Penetration depth for wood is around 60 mm. For the smaller block (86 mm), the side length is less than twice the wood D_p value, and will therefore experience full power density as the waves penetrate 60 mm from each face. Increasing the side length illustrates the impact of the D_p value and explains why it has a non-negligible effect on the temperature profiles with larger wood blocks (200 mm and 400 mm).

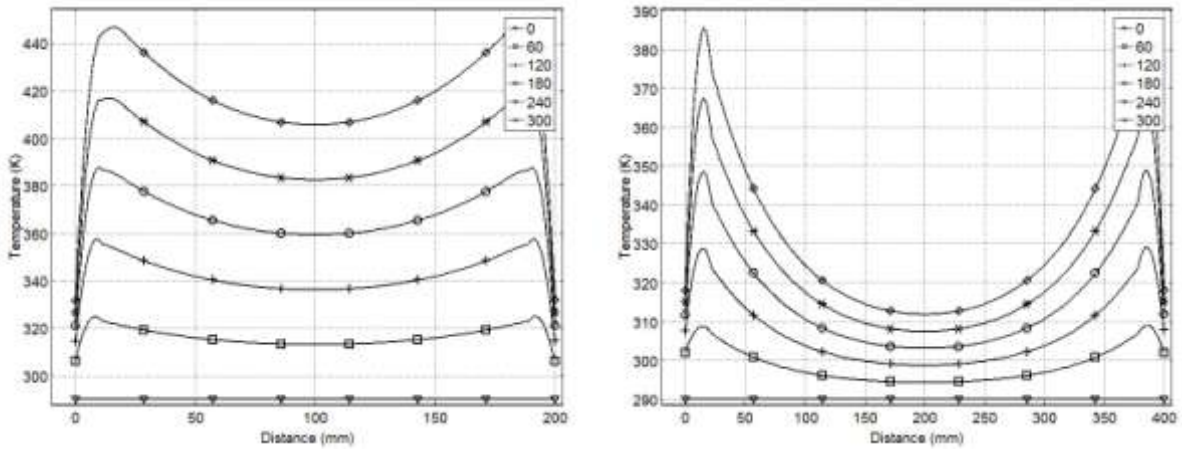

(A) (B)

Figure 3-6: Temperature profiles for FC: (A) For 200 mm cube side length and (B) For 400 mm cube side length

To investigate the effect of thermal conductivity (k) of the target material, the model was resolved for two values of thermal conductivity: 0.25 and 0.5 W/m K. The results are shown in Figure 3-7 and compared to the thermal conductivity of 0.17 W/m K. It is observed that the

maximum temperature decreases with increasing *k* as a result of heat transfer by conduction. It is also clear that the effect of the thermal conductivity on the temperature gradient is negligible compared to the effect of D_p.

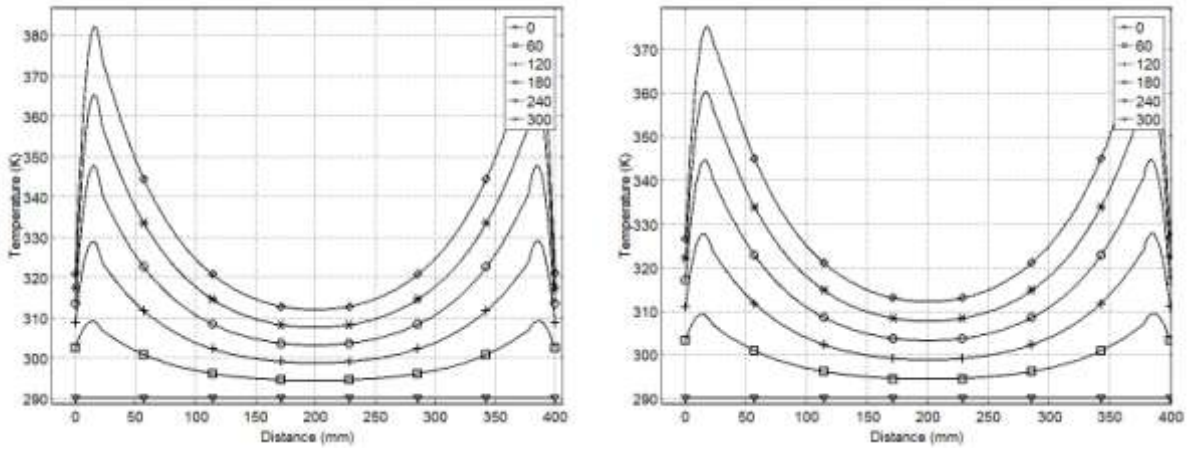

(A) (B)

Figure 3-7: The effect of thermal conductivity values on D_p: (A) k=0.25 and (B) k=0.5

3.4.2 The Effect of Different Material Types

3.4.3 The Effect of Adding Material with Stronger Interaction with the EMW

Carbon is one of the materials that strongly absorb microwaves and convert them to heat. Table 3.1 presents selected physical and electric properties of Carbon. In comparison, pinewood and carbon have a value of $\varepsilon^{/}$ =7 and $\varepsilon^{//}$ =2 (Vos, Mosman et al. 2003), and of $\varepsilon^{/}$= 2.7 and $\varepsilon^{//}$ =0.5 for pinewood, respectively (Kol 2009). Therefore, carbon offers better interaction with microwaves than pinewood as a result of larger values. Furthermore, its density and heat capacity are about 3/4 and 1/3 the values of pinewood, respectively. Therefore carbon can be used as a good microwave thermal catalyst because it will focalize the energy generated by MWH (Menéndez, Domínguez et al. 2004). Three studies have been performed to further investigate the effect of carbon additives as well as the effect of various concentrations on the temperature profiles.

3.4.4 The Effect of Replacing a Fraction of the Wood Block with Carbon

In this study, the block material is assumed to be a homogeneous composite of pinewood and carbon at two different ratios: 50% and 75% by weight. The physical and electric properties of the new mixture are calculated assuming a linear relationship between the percentage of carbon in the mixture as presented in equation (3-15),

$$P_m = x_C\, P_c + (1 - x_C)\, P_w \tag{3-15}$$

where p_m, p_c, and p_w are properties of the new mixture, carbon and pinewood, respectively While x_C is the percentage of carbon in the mixture.

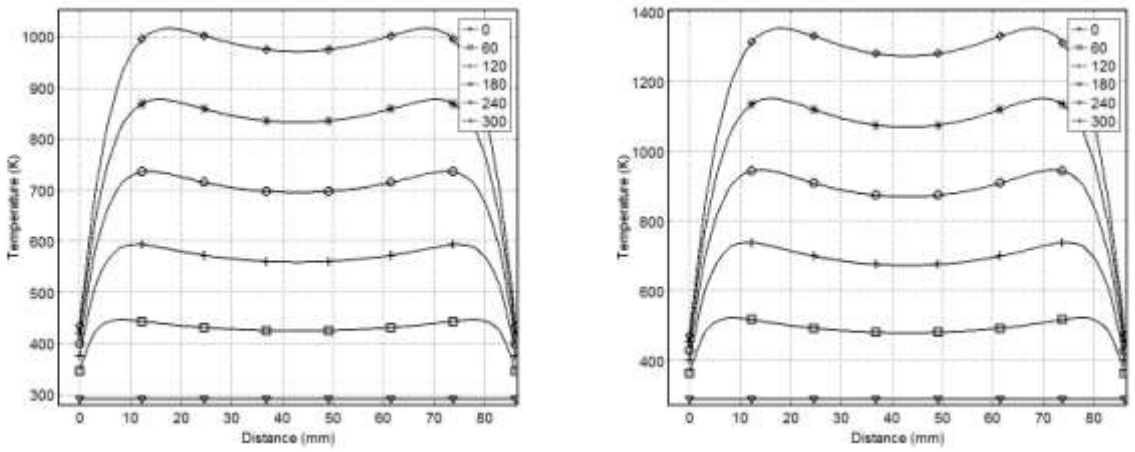

(A) (B)

Figure 3-8: Effect of substituting wood with carbon over 300 s of MWH: (A) 50 wt-% carbon and (B) 75 wt-% carbon

The change on temperature profile as an effect of carbon replacing wood in the block could be seen in Figure 3-8. The baseline case (0% carbon) is presented in Figure 3-4-A. Based on values along the core (centerline), the baseline has a heating rate of 60 K/min and reaches up to 140 K/min and 212 K/min for the 50% and 75% carbon cases, respectively. Therefore, *theoretically*, the replacing 50% of the wood with leads to doubling the heating rate compared to pinewood, while the 75% replacement yields triple the rate. By increasing the carbon percentage from 0 to

75%, the maximum temperature increased from 595 K to 1350 K, meaning that - for the same setting power and heating time- the temperature was 2.3 times that of the original temperature. As a result, using carbon may reduce the overall energy consumption, taking in account that *Dp* is decreased by increasing the carbon percentage as shown in Table 3.1.

3.4.5 The Effect of the Spatial Position of Carbon within the Cube

Two scenarios were considered in order to study the effect of carbon distribution in the mixture. The first one deals with a carbon cube with a volume of 125 cm^3 that is inserted into the core of a larger wooden block. The second scenario deals with covering the outer surface of the same block with an equivalent amount of carbon. In other words, the first case concentrates the carbon in the core and the second case distributes the same mass of carbon on the outer surface. In addition, two different boundary conditions were applied, namely FC as shown in Figure 3-9-A, and PI as in Figure 3-9-B.

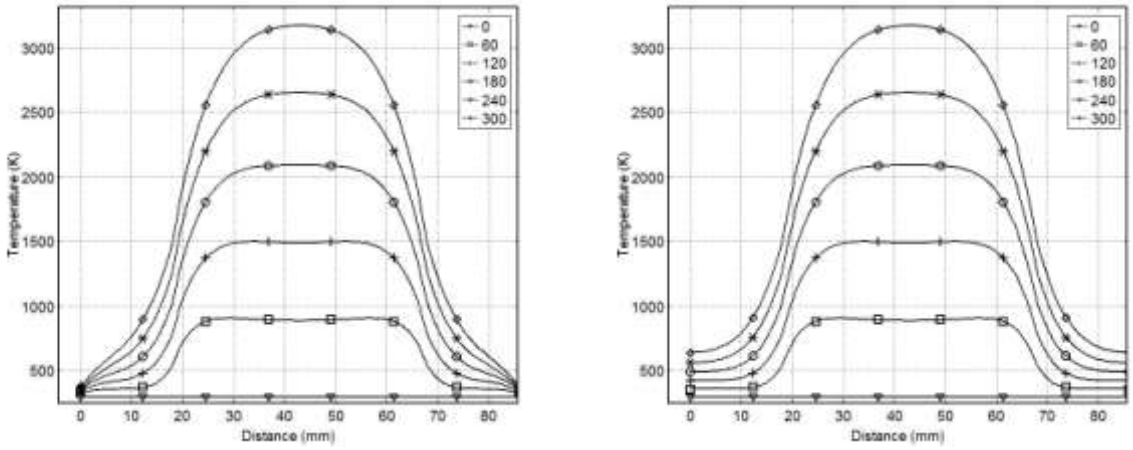

(A) (B)

Figure 3-9: The effect of a carbon cube in the core of the wood block: (A) FC and (B) PI

After 300 s of MWH, the first scenario with FC boundary conditions shows an outer surface temperature of 375 K compared to 636 K in the PI case. Both cases show a similar core temperature of 3200 K. Remarkably, there is a significant difference in the surface heating rate of

17 K/min and 70 K/min in the cases of FC and PI, respectively, and 582 K/min in the core for both instances.

In the case of the second scenario with an evenly-distributed 3 mm layer of carbon on the surface, two boundary conditions were also investigated, as shown in Figure 3-10. Figure 3-10-A shows that the maximum temperature of 660 K is located a few millimetres below the surface in the FC case, while for PI boundary conditions, the maximum temperature of 1280 K is found exactly on the surface. At the interface between the Carbon and the wood, the temperature was 645 K for the FC and 1110 K in the PI. Results clearly demonstrate the strong impact of the presence of carbon in the mixture on heat generation and transfer.

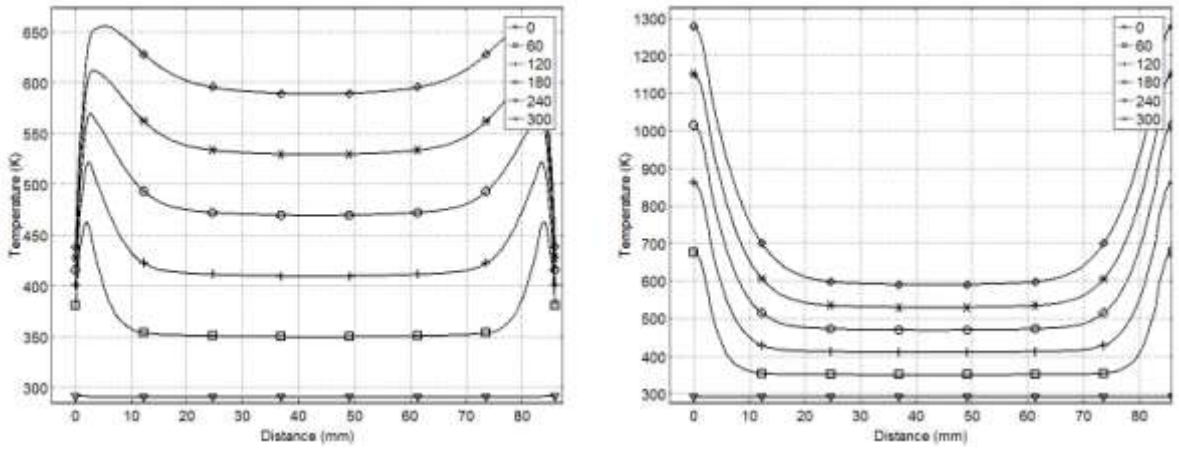

(A) (B)

Figure 3-10: The effect of a 3 mm carbon layer on the surface of the wood block: (A) FC and (B) PI

3.4.6 The Effect of Two Carbon Cylinders in the Wooden Cube

Another scenario was investigated to shed light on the thermal effect of carbon on the temperature profile. For the simulation, two holes with a diameter of 13 mm and a depth of 80mm were created in the block. The two holes were filled with carbon (74 mm) and the remaining 6 mm were filled with wood (same material as the block). Figure 3-11 shows a

representation of this setup. Temperatures were measured in five different locations: two on the outer surfaces (A&E), one in the core (C) and the last two in the interface between the carbon cylinders and the sawdust (B&D). Figure 3-12-A shows the profiles at these five locations, while Figure 3-12-B shows the profiles at the center line. The center of the carbon cylinder reached a higher temperature of 1345 K, as opposed to that in the interface which reached 970 K. Within 6.5 mm there is a temperature ratio of about 1.5 times the interface value.

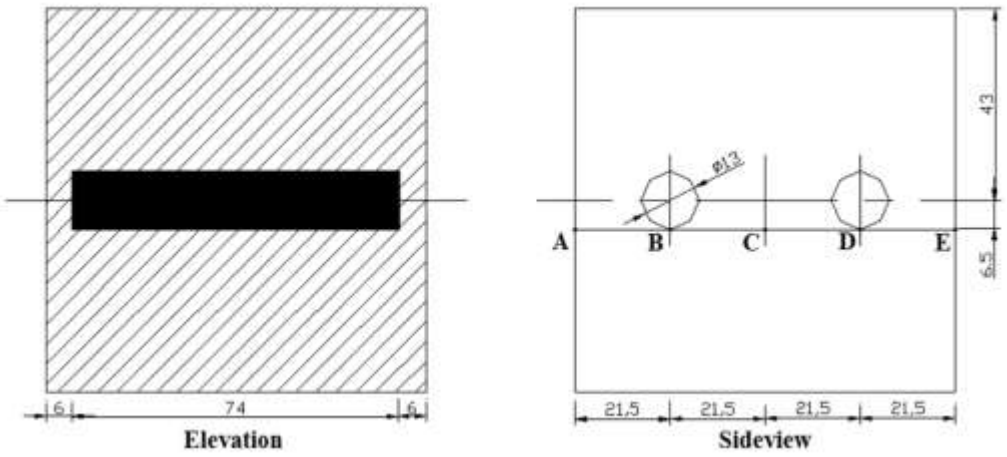

Figure 3-11: Wood block with two holes (D=13 mm)

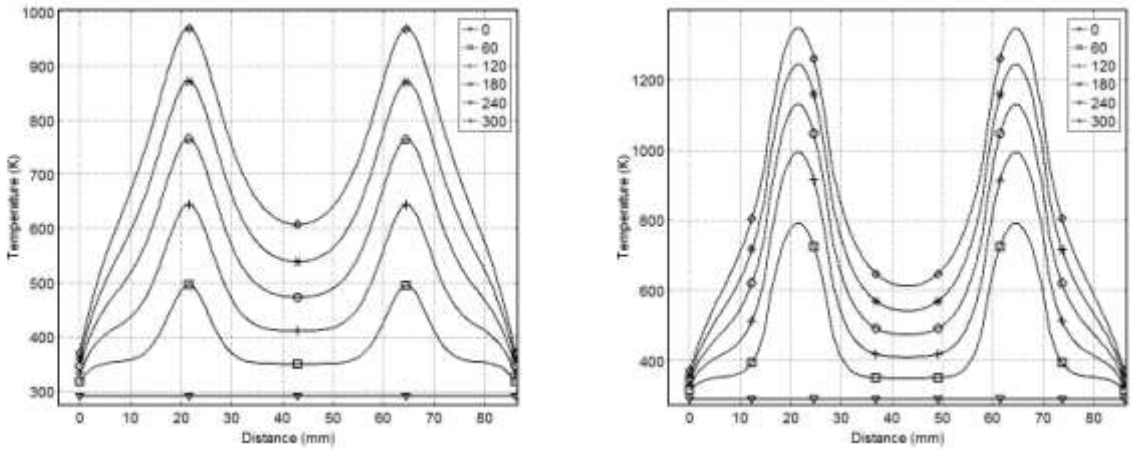

(A) (B)

Figure 3-12: Temperature profiles in the case of two carbon cylinders inside the wood block: (A) At the five points (A, B, C, D, and E) and (B) at the block center line

3.4.7 The Effect of Replacing a Fraction of the Wood with Materials of Weak Interaction with EMW

Pyrex is one of the materials those exhibit weak interactions with EMW at 2.45 GHz. Pyrex has constants of $\varepsilon^{/}$=4 and $\varepsilon^{//}$=0.005 (D.E. Clark 2005). We reproduced the simulations outlined in the previous sections but replaced the carbon core with Pyrex. Figure 3-13 shows the temperature profiles obtained with the same two boundary conditions (FC and PI). In both cases, the core did not exhibit any change in temperature (324 K) while the surface reached 365 K and 605 K for FC and PI, respectively. These results are due to the negligible EMW/Pyrex interaction. Moreover, Pyrex has low thermal conductivity; therefore its core had low temperature.

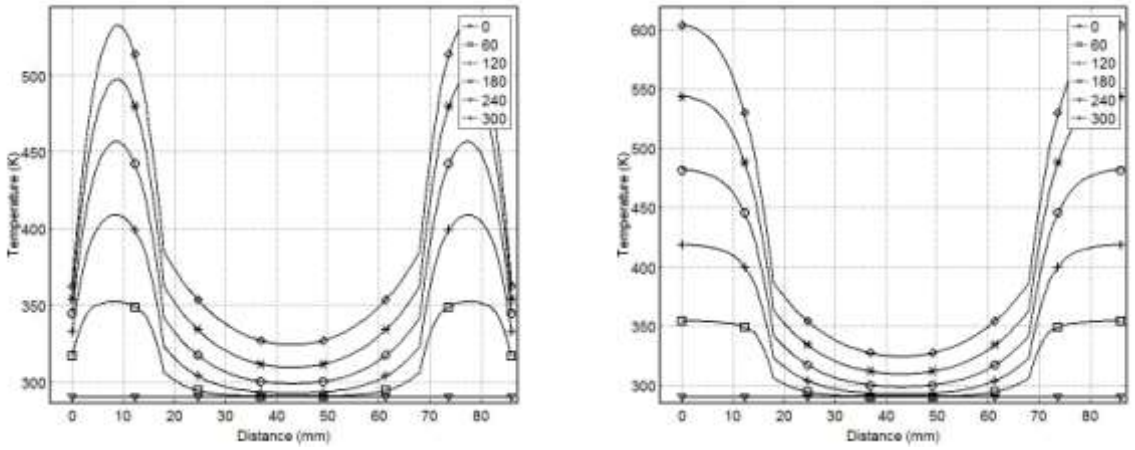

(A) (B)

Figure 3-13: Effect of a Pyrex cube in the wood block core: (A) FC and (B) PI

3.5 Experimental Validation of the Model

Two experimental setups were used for validation. In the first, three experiments were carried out. In each case, a wood cube (86 mm) was heated inside a microwave oven for selected time intervals (60, 120, or 180 s). At the end of the heating period, the cube is removed from the microwave oven and five K-type thermocouples quickly inserted at five points: 0, 21.5, 43, 64.5, and 86 mm. Thermocouples were connected to Data acquisition (OMB-DAQ-3000 Series) to record the temperature values directly at a rate of 6 readings per second. Figure 3-14 shows the

experimental and theoretical results at these three different interval times of MWH. The deviation between predicted and experimental values was calculated as average percentage relative error (Campañone and Zaritzky 2005). The average percentage relative error between the predicted and the experimental values was ±4% of the measured values.

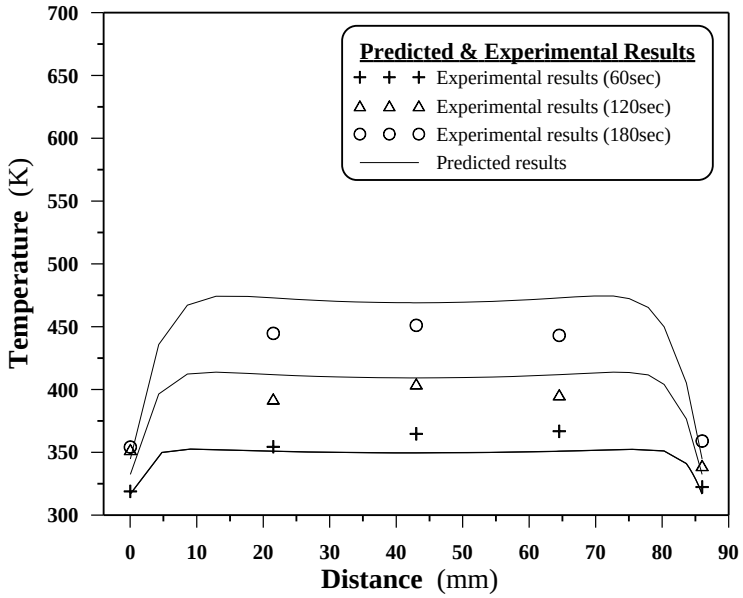

Figure 3-14 Experimental and predicted results for validation of the model for the case of Free Convection (FC)

The second verification setup involved irradiating two wood cubes with carbon insertions to microwaves at 2.3 kW for selected durations. One block was heated for 30 s and the other for 60s. Figure 3-15 presents a comparison of predicted and experimental results. The average percentage relative error between the predicted and the experimental values was ±2.7% for the points A, C, and E, and ±15% at the interface points (B and D). The points B and D have error higher than the others; because the electrical properties of carbon depend on the temperature by a direct proportional relation, while wood does not undergo considerable change up to 550 C (Robinson, Kingman et al. 2009, Ciacci, Galgano et al. 2010). Therefore, in cases involving carbon, the experimental results would be slightly higher than the theoretical results.

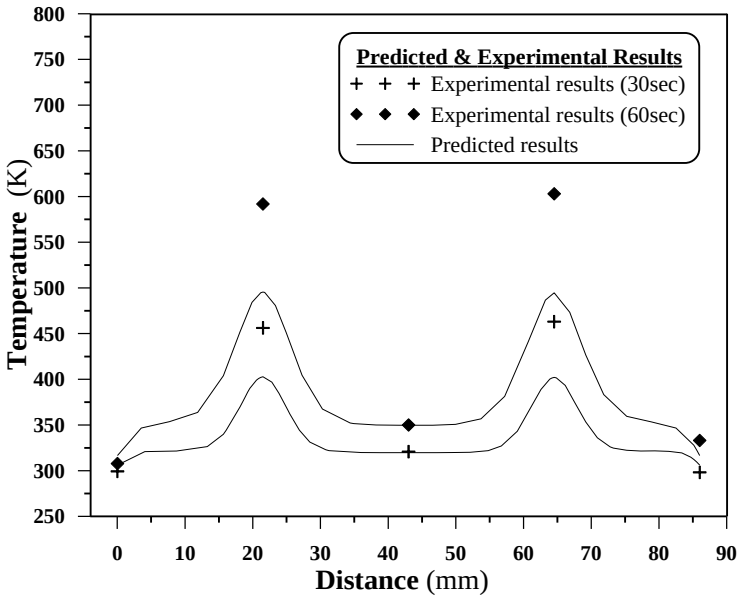

Figure 3-15: Experimental and theoretical results for verification of the model in the case of a wood block with two carbon cylinders

3.6 Conclusion and Future Developments

A three-dimensional mathematical model to predict/control transient temperature profiles within selected materials exposed to MWH at 2.45 GHz has been developed, solved by COMSOL-Multiphysics for different scenarios, and validated.

Key conclusions of this work include:

- MWH leads to non-uniform distribution of temperature which is strongly affected by penetration depth (D_p) and surface heat loss.
- Limiting dimensions of the payload to twice D_p, and placing strong thermal insulation on the surface may minimize temperature gradients significantly.
- Choice of location of materials with contrasting levels of microwave-to-heat conversion may be used to create desired cold/hot zones and achieve a specific temperature profile in the workload.
- Homogenous mixing of materials which are strong microwave-to-heat converters with the payload leads to maintaining the shape of the temperature profile while exhibiting a

significant increase in temperature compared the virgin material exposed to the same power and heating time.

- Simulation scenarios involving the placement of materials which heat strongly by microwaves at specific locations within the payload could provide insights in applications where creating a hot spot to induce thermal cracking or obtain a specific product is desired. For example, generation hot spots in pyrolysis/gasification process to increase gas yield (Domínguez, Fernández et al. 2008, Fernández, Arenillas et al. 2009).
- Simulations involving the placement of materials which act as embedded heaters in the core of the payload may be relevant to applications requiring a significant temperature gradient between the core and the surface. Examples include processes where sufficient pressure difference is generated to enhance extractive applications such as the extraction of moisture content in drying sector and the extraction of valuable bio-chemicals in pyrolysis sector. Other simulations, where materials which heat strongly are concentrated on the surface, may be useful for surface treatment, coating, joining applications
- Finally, simulations involving partial substitution of a weak converter of microwaves with a strong one could be helpful in applications designed for heating two different materials: carbon and metals are pre-mixed with biomass in order to enhance thermal/catalytic processes. A similar appraoch is adopted for sewage sludge, crude oil, and contaminated soil (Monsef-Mirzai, Ravindran et al. 1995, El harfi, Mokhlisse et al. 2000, Menéndez, Inguanzo et al. 2002, Menéndez, Domínguez et al. 2004, Li, Zhang et al. 2009).

Future work will attempt to incorporate mass transfer considerations and chemical reaction kinetics in the existing model in order to predict both temperature profiles and product yield, with focus on microwave pyrolysis of kraft lignin to extract phenols and aromatics.

Acknowledgements

The authors would like to thank Laurent Spreutels (PhD student), Mr. Robert Delisle (Technician at Ecole Polytechnique Montreal) for their assistance in experimental design and COMSOL simulations. In addition, the authors are grateful for the financial and technical support from

Canadian research networks: LIGNOWORKS (lignoworks.ca), and the (Agricultural Biorefinery Innovation Network) ABIN.

CHAPTER 4 ARTICLE 2: A KINETIC INVESTIGATION OF MICROWAVE PYROLYSIS OF SAWDUST USING AN ORIGINAL MICROWAVE –THERMOGRAVIMETRIC ANALYZER

Sherif Farag and Jamal Chaouki

[a]CRIP-Biorefinery Centre, Department of Chemical Engineering, École Polytechnique de Montréal.

P.O. Box 6079, Station Centre-ville, Montréal, QC, Canada H3C 3A7.

(Submitted in Journal of Analytical and Applied Pyrolysis)

Presentation of the article: In this article, a kinetic investigation of microwave pyrolysis of sawdust in contrast to conventional pyrolysis will be presented. To accomplish this investigation, an original microwave thermogravimetric analyzer equipped with an innovated thermometer was built. The kinetics parameters in both cases were estimated and subsequently used to compare the predicted results against the experimental data.

Abstract

The main objective of this work is to investigate reaction kinetics of microwave-pyrolysis (MWP) of sawdust in contrast to conventional pyrolysis (CP). To achieve this objective, an original microwave thermo-gravimetric-analyzer was built and equipped with an innovated thermometer. This thermometer does not suffer from the traditional thermometer drawbacks. The kinetic parameters, activation energy, pre-exponential factor, and reaction order (E_a, k_o, and n), were estimated using a MATLAB® program code. The obtained result demonstrates that the estimated value of k_o in MWP is around three-times that of CP. Accordingly, MWP may have a faster reaction rate than that of CP. This could be due to the molecular chaotic motion resulting from the oscillating-electromagnetic-waves. Nevertheless, this tangible effect on k_o, the estimated value of E_a is almost the same in the two cases. This may be related to the wavelength of the oscillating-electromagnetic-waves, which is much longer than the intermolecular-distance of the heated material.

Keywords: Microwave Heating, Thermo-gravimetric Analyzer, Microwave-Thermo-gravimetric Analyzer, Microwave Pyrolysis, and Reaction Kinetics.

4.1 Introduction

Microwave heating (MWH) is a volumetric energy conversion mechanism which is the result of agitating the dipoles of the heated material due to exposure to an alternating electromagnetic field. Under controlled conditions, MWH demonstrates some advantages in contrast to conventional heating (CH), e.g., temperature gradients inside and outside the heated material, and no direct contact between the heated material and the heating source. Further information regarding MWH was reported in Farag, S., et al. (Farag, Sobhy et al. 2012).

For non-magnetic materials, the main parameter that describes how EMW are converted to thermal energy is called complex permittivity (ε^*). It is defined in equation (4-1) (Camelia Gabriel and Mingosb 1998, Clark, Folz et al. 2000, Durka, Gerven et al. 2009, Castro-Giráldez, Fito et al. 2010, Guo, Wang et al. 2010, Farag, Sobhy et al. 2012). The real part of ε^* is called the dielectric constant, while the imaginary part is called the loss factor.

$$\varepsilon^* = \varepsilon^{/} - \mathrm{j}\varepsilon^{//} \tag{4-1}$$

Loss tangent ($tan\delta$) is defined by the ratio between the imaginary and the real parts as in equation (4-2). To maximize conversion of EMW to thermal energy $tan\delta$ should be chosen with a high value (Monsef-Mirzai, Ravindran et al. 1995, Menéndez, Domínguez et al. 2004, Li, Zhang et al. 2009).

$$tan\delta = \frac{\varepsilon^{//}}{\varepsilon^{/}} \tag{4-2}$$

The power absorbed by the heated material decays exponentially according to Lambert's law as in equation (4-3) (Zhou, Puri et al. 1995, Bail, Koutchma et al. 2000, Yang and Gunasekaran 2001, Rattanadecho 2006). Where D_p is the power penetration depth, and y is the measured distance from the outer surface.

$$P = P_o\, e^{(\frac{-y}{D_p})} \tag{4-3}$$

In the scientific literature, a great effort has been made to investigate effects of MWH on chemical reactions. Most of the reported effects were observed on reaction rate, product quality, and energy consumption. Table 4.1 shows some of the reported effects in different reactions.

Table 4.1: Summary of the effects of MWH on different reactions

The authors and objective	Conclusion
Chandra Shekara, Jai Prakash et al. 2012 (Chandra Shekara, Jai Prakash et al. 2012) Solventless acylation of p-cresol with different carboxylic acids over BEA zeolite	MWH achieves more conversion in contrast to CH: 50-80% compared to less than 20% in CH
Paixão, Monteiro et al. 2011 (Paixão, Monteiro et al. 2011) Modification of MOR zeolites via desilication treatments with NaOH	MWH is promoting Si extraction from the zeolite framework without a significant loss in crystallinity, MWH allows modification of the porosity of samples, MWH is faster with less energy consumption compared to CH
Patil, Gude et al. 2011(Patil, Gude et al. 2011) Transesterification of Camelina sativa oil using metal oxide catalysts	In MWH, the reaction rate constants are two orders of magnitude higher than those obtained with CH
Zhang and Zhao 2010 (Zhang and Zhao 2010) Production of 5-hydroxymethylfurfural and furfural from lignocellulosic biomass (Corn stalk, rice straw, and pine wood) in an ionic liquid	MWH increases product yield and decreases reaction time
Pan, Wu et al. 2009 (Pan, Wu et al. 2009) Preparation of platinum dioxide nanoparticles via MWH and CH.	The obtained nanoparticles via MWH are smaller and more narrowly distributed than those obtained by CH, In the hydrogenation of cyclohexene the obtained particles have a higher catalytic activity

	than those obtained by CH
Budarin, Clark et al. 2009 (Budarin, Clark et al. 2009) Preparation of high-grade bio-oils by MWP of wheat straw as a pellet form	The produced oil via MWP contains few impurities and is rich in aromatics compared to the other oil produced by the conventional methods
Zhou, Zhong et al. 2009 (Zhou, Zhong et al. 2009) Crystallization of zeolite T using MWH as well as CH	MWH has a faster reaction than that in CH
Guiotoku, Rambo et al. 2009 (Guiotoku, Rambo et al. 2009) Investigating of hydrothermal carbonization of Pine sawdust and cellulose	MWH increases the carbonization yield
Krzan and Zagar 2009 (Krzan and Zagar 2009) Liquefaction of wood with glycols using p-toluenesulfonic acid as a catalyst	MWH decreases liquefaction time with minimum catalyst use
Dogan and Hilmioglu 2009 (Dogan and Hilmioglu 2009) Dissolution of cellulose in N-methylmorpholine-N-oxide.	MWH has a shorter time compared to the traditional methods
Sithambaram, Nyutu et al. 2008 (Sithambaram, Nyutu et al. 2008) K-OMS catalyzed oxidation of tetralin	MWH enhances the conversion compared to CH: (52–88%), and (42–80%), respectively
Orozco, Ahmad et al. 2007 (Orozco, Ahmad et al. 2007) Studying dilution of grass and cellulose in phosphoric acid at different concentrations with water	MWH produces high yields of glucose in a short time compared to the traditional methods. MWH has a high reaction rate at moderate temperature, which prevents the formation of hot spots.
Karthikeyan, Balasubramanian et al. 2006 (Karthikeyan, Balasubramanian et al. 2006) Polycyclic aromatic hydrocarbon extraction from airborne particles	The extraction time in MWH can be completed in minutes compared to hours as in the traditional methods, with more different chemical components.

Zhu, Wu et al. 2005 (Zhu, Wu et al. 2005) Pre-treatment of rice straw using microwave/alkali	Rice straw treatment by microwave/alkali has higher cellulose, lower moisture, lignin, and hemicellulose than that produced by alkali treatment only.
Lucchesi, Chemat et al. 2004 (Lucchesi, Chemat et al. 2004) Solvent-free microwave extraction of oil from basil, garden mint, and thyme	First oil droplet was after 5min of MWH compared to 30min in the case of CH. The energy consumption was 0.25kWh compared to 4.5kWh in CH.
Menéndez, Domínguez et al. 2004 (Menéndez, Domínguez et al. 2004) Pyrolysis of four wet sewage sludges from different treatment plants	Pyrolysis process is faster than that in CP, MWH has a lower production of non-condensable gases compared to the CH.

As shown in Table 4.1, many significant effects for MWH on different reactions have been reported in contrast to CH. However, few researchers have attempted to find an explanation for these effects. Despite this modest effort, some points of consideration had to be taken into account, which had not been previously, e.g., temperature gradient within the heated material, and the dielectric properties of the heated material as well as the carried reactor. Therefore, the main objective of this work is to investigate the kinetic parameters of microwave pyrolysis (MWP) in contrast to conventional pyrolysis (CP) of sawdust, considering the previous points. In order to achieve this objective the following steps were carried out: (1) A developed MW-setup works as a thermo-gravimetric analyzer (TGA), (2) An innovated thermometer to measure the transient mean temperature within the heated material, (3) Experimental work on MWP, and CP of sawdust, and (4) Estimate the kinetic parameters in each case then explain the obtained results. Such discussions are so significant that would improve understanding and controlling of a chemical reaction.

4.2 The Experimental Work

4.2.1 The Material

In this investigation, the material used was chosen so it does not have a high resistance to thermal degradation. Therefore, one type of plant biomass was used: sawdust with an elemental analysis

of C=48.3%, H=6.22%, O=45.2%, N=0.22% and S=0, and proximate analysis of Char=16%, Volatile= 81%, and Ash=2.9%.

4.2.2 The Experimental Setup

The experimental work was carried out in a bench scale microwave oven (MW-O) (Microwave Research Inc; Model: BP-211, 230 V, 2.45 GHz, and power setting up to 3.2 kW). Two opposing holes were drilled into the oven side-walls, 24 mm in diameter, to connect the inlet and outlet lines to the reactance carried reactor as well as to enable visual access during the heating process. An alumina box (muffle) was used inside the oven cavity to protect the oven's electronic devices from the emitted heat or unwanted/unexpected explosions, or combustion during the MWP. The dimensions of the oven cavity are 510×250×320 mm, whereas the dimensions of the muffle are 390×180×170 mm. A Pyrex cylinder semi-batch reactor with a volume of 0.37 *l* was used inside the muffle. Limitations of the penetration depth were carefully considered while designing the used reactor and choosing the sample weight.

In order to achieve the main objective of this work two modifications were made to make this traditional MW-O work as a TGA with MWH rather than CH, which explains why it is called MW-TGA. The first modification makes it possible to measure weight-loss of the heated material during exposure to EMW. This was done by connecting the carrier reactor with a scale (Denever Instrument; Model: SI-2002, Weighting capacity: 2000 g, Readability: 0.01 g, Repeatability <±0.01 g, Linearity: <±0.02 g, and Response time (average): 1.1 s) fixed on the top of the MW-O via the two opposite holes as shown in Figure 4-1.

The total weight of the designed system, i.e., the reactor, the long bar, and the suspension wires, is ≈ 800 g. This weight, however, does not affect the measurements because the key parameter is the characteristics of the scale used. The scale capacity is 2000 g and the readability is 0.01 g, i.e., as long as the total weight of the designed system and the sample is less than 2000 g, this system can be used.

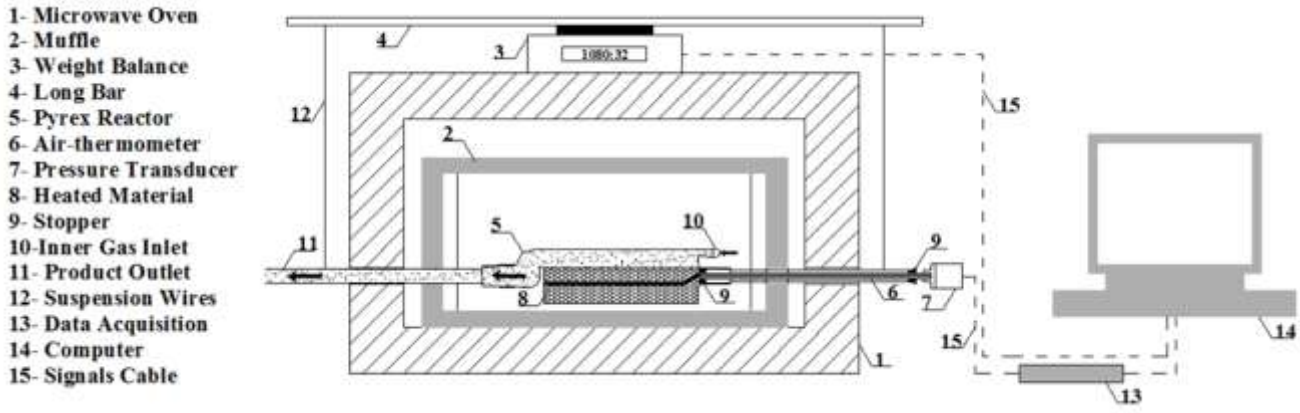

Figure 4-1: The microwave thermo-gravimetric analyzer setup

Specific procedures were followed to load a sample into the MW-TGA. First, the reactor was filled with the virgin material via the left side port, outside the oven cavity. Second, it was inserted inside the muffle-cavity, and the two side tubes were connected, with male/female connections. Third, the air-thermometer (it will be explained in details in the next section) was inserted carefully inside the right-side tube after which the whole system was suspended using the wires that were connected with the metallic bar. Then, the signal cables of the scale and the pressure transducer were connected, as shown in Figure 4-1. Finally, the traditional procedures of pyrolysis as in the conventional TGA were implemented, as will be mentioned later. To insure the re-productivity, the experiments in CP and MWP were repeated and the average values will be processed.

The second modification makes the MW-TGA possible to measure transient mean temperature within the heated material. The following section describes in detail this development.

4.3 The Development for Measuring the Transient Mean Temperature

The three most popular techniques used for measuring the temperature are the thermocouple, the infrared, and the fiber optics thermometer. Using a thermocouple-thermometer inside a MW-O and during the heating process is dangerous with low accuracy due to the metallic probe

interaction with EMW. The thermocouple-thermometer has been used in some publications inside the MW-O but after switching off the oven-power (Zhang, Hayward et al. 2003, Lucchesi, Chemat et al. 2004, Gunasekaran and Yang 2007, Ma 2009, Sun, Wang et al. 2012). It should be noted that there is heat lost after switching off the oven-power. The infrared-thermometer is the best way to measure the temperature without any contact between its probe and the heated material. However, it measures surface temperature only; thus, it is suitable only for thin materials. Moreover, it has high sensitivity to ambient conditions and reactor material; therefore, it needs frequent recalibration (Stuerga and Gaillard 1996, Will, Scholz et al. 2003, Lucchesi, Chemat et al. 2004, Menéndez, Domínguez et al. 2004). The fiber optics-thermometer has many advantages compared to the previous two thermometers, e.g., frequent recalibration is not necessary, it is independent of reactor material, and it can be used to measure the temperature at any point within the heated material. However, it measures a point temperature, and special attention must be paid to avoid damaging the probe (Durka, Van Gerven et al. 2009).

In order to solve this problem, an innovated thermometer to measure transient mean temperature within a material exposed to EMW was made, called an air-thermometer. As shown in Figure 4-2, the air-thermometer consists of two Quartz tubes. The first one is used as a thermometer-probe, while the second is used to transfer the pressure built-up inside the probe to a pressure transducer (Dynisco Model: PT311, Fluch Giaphram pressure transducer, Range: 0-25 psi and Accuracy: ±0.5% full scale). These tubes are made of Quartz to eliminate the interaction with EMW: $\varepsilon^{/} = 3.8, \varepsilon^{//} = 0.0001$, and $\tan\delta$=0.00003 @2.45GHz, while it is 1.006, 0.0, and 0.0, respectively, for air (Durka, Van Gerven et al. 2009), which is used as a working media. To record the built-up pressure signals directly, the pressure transducer is connected to a data acquisition (OMB-DAQ-3000 Series, 1-MHz, 16Bit USB Data Acquisition Modules), and a particular interface is used (OMEGASOFT Data Acquisition Software Rev7.0 501470B-01).

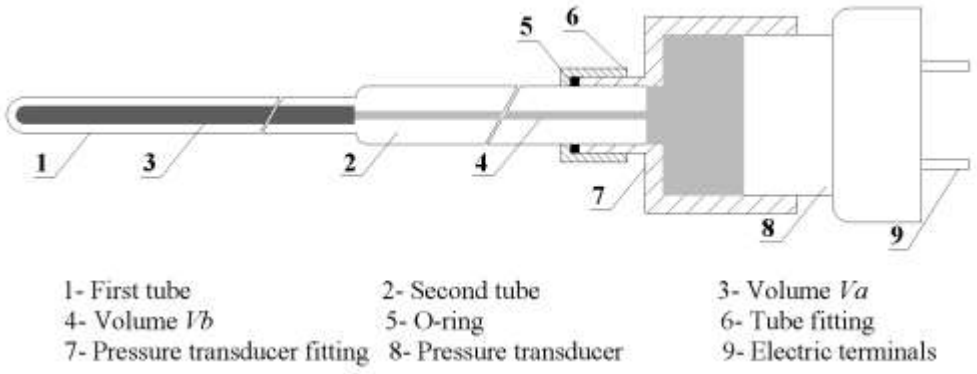

Figure 4-2: Drawing of the air-thermometer

A mathematical derivation was carried out to obtain a mathematical formula that connects the pressure built-up and the probe surrounding-temperature. A type-K thermocouple was used to validate this formula in a range from ambient temperature up to 1100 K, using a CH-oven. The temperature values that were measured by the air-thermometer and the reference values that were measured by the thermocouple were plotted against the heating time, as shown in Figure 4-3.

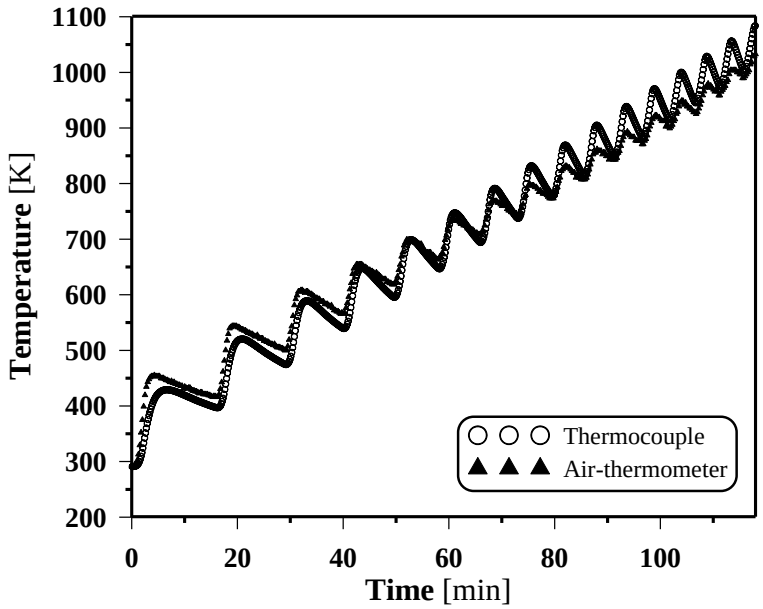

Figure 4-3: The measured and the reference temperature values vs. the heating time

The response time of the air-thermometer was investigated, using a CH-oven controlled by an automatic controller. This controller works by switching on/off during the heating time, and then compares the achieved temperature with the setting value. If the achieved-temperature is less than the setting value, the controller switches On then Off again, etc. As shown in Figure 4-3, the air thermometer follows each interval of heating with an acceptable response time. The deviation between the measured and the reference temperatures was calculated as an average percentage relative error (*APRE*) as in Farag, S., et al (Farag, Sobhy et al. 2012). *APRE* was ±5% of the reference value. Above 850 K, some of the measured values have an error around 50 K, which should be considered. Nonetheless, herein, the presented result is not really affected by this error as the applied temperature range is not greater than 800 K. Besides, further effort is in progress to improve the thermometer accuracy.

Another verification was done by comparing the measured values during the pyrolysis of sawdust and the values predicted by the mathematical model that was published by Farag, S., et al. 2012 (Farag, Sobhy et al. 2012). This model was developed to be suitable for the geometry of the heated material and the carrier reactor as well as the setting power that was used in this work. In addition, the transient values of the physical and electric properties of sawdust were considered.

The predicted temperatures were obtained by applying the energy balance on an element with the dimensions Δx, Δy, and Δz from the heated material, using the set of boundaries and initial conditions that were published in Farag, S., et al (Farag, Sobhy et al. 2012). Upon entering the system geometry in COMSOL-Multiphysics, the time-dependent solver algorithm applied the Finite Element Method to solve the partial differential equation of the energy balance, with a time range from 0 to 320 s. Further details regarding this model were published in Farag, S., et al (Farag, Sobhy et al. 2012).

The dielectric properties of sawdust were measured at a temperature range of 298-900 K, using a "Microwave and millimeter-wave vector network analyzer" (Anritsu 37369D Microwave, 2-Port Vector Network Analyzer, 40 MHz to 40 GHz), and a circular resonance cavity at 2.45 GHz. An inert environment (N_2) was kept during these measurements to keep the transient composition of the material similar to that produced during the pyrolysis. A linear fitting was found for each step

as in equations (4-4) and (4-5) for the dielectric constant and the loss factor, respectively. The obtained equations are only presented here, while the graphs are not presented.

$$\varepsilon^{/}_{(298-740)K} = 3 \times 10^{-4}T + 1.49$$
$$\varepsilon^{/}_{(740-900)K} = 4 \times 10^{-3}T - 1.42 \quad (4\text{-}4)$$

$$\varepsilon^{//}_{(298-806)K} = 2.43 \times 10^{-5}T + 0.07$$
$$\varepsilon^{//}_{(806-900)K} = 5 \times 10^{-3}T - 4.05 \quad (4\text{-}5)$$

The nearly-horizontal line (298-740K for $\varepsilon^{/}$, and 298-806K for $\varepsilon^{//}$) represents the dielectric properties during pyrolysis, while the rapid-increase line (740-900 K for $\varepsilon^{/}$, and 806-900 K for $\varepsilon^{//}$) represents when char is formed (The solid product from the pyrolysis of sawdust). Char has a high interaction with EMW as its elemental composition is ≈90% carbon. Therefore, the dielectric properties of sawdust increased rapidly once char is formed. This result is in agreement with that was reported by Robinson, J.P., et al. 2009 (Robinson, Kingman et al. 2009).

Figure 4-4 illustrates the predicted axial transient temperature profiles within the sawdust, and Figure 4-5 shows the transient mean values of these profiles compared to the measured values using the air-thermometer. The *APRE* was ±6% of the measured value.

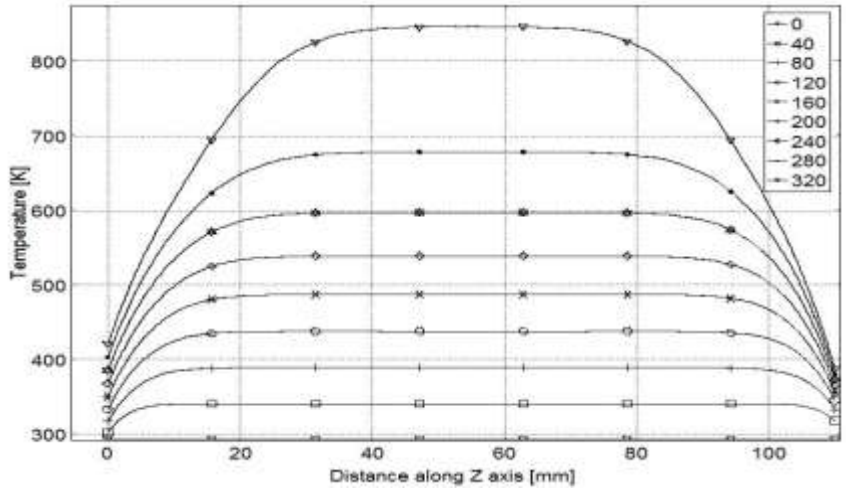

Figure 4-4: The axial transient temperature profiles within the sawdust (time in seconds)

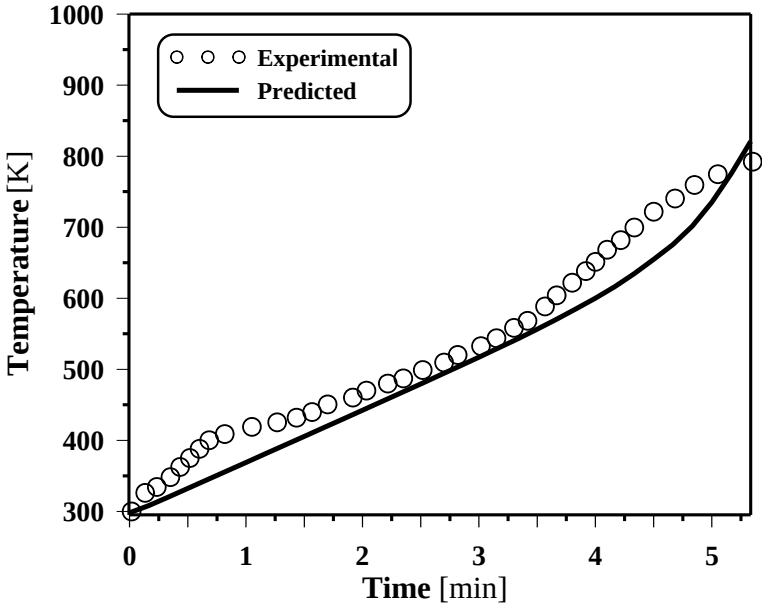

Figure 4-5: The predicted mean temperatures vs. the experimental, within the heated material

As depicted in Figure 4-4, the outer surface of the heated material has a low temperature compared to the core as a result of the temperature gradient within the heated material. Therefore, measuring a mean temperature is needed rather than a local temperature, especially when a large payload is used, and a local investigation is not required. Furthermore, D_p for the reactor and the heated material should be considered.

4.4 The Conventional Pyrolysis Method

Conventional pyrolysis of sawdust was carried out in a TGA (TGA Q5000 Autosampler). The crucible used was made of platinum with a height of ≈ 1mm and a diameter of ≈ 10mm. The weight loss of the sample was measured during pyrolysis at atmospheric pressure and under controlled inert gas flow and temperature. The following procedures were employed during pyrolysis: the sample was placed at room temperature then heated in a nitrogen atmosphere with a flow rate of 50 ml/min and a constant heating rate of 30 ^{o}C/min. Once the temperature reached 600 ^{o}C, an isothermal process was started for 5 min under the same inert gas flow rate, and then the pyrolysis process was stopped.

Different experiments on sawdust at different initial masses (5, 10, 15 mg) and particle sizes (1 mm-355 µm) were carried out in a TGA by Radmanesh et al. 2006 (Radmanesh, Courbariaux et al. 2006). The obtained results show no distinct change in weight loss curves for the different initial weights and particle sizes used. In addition, as a preliminary step in this work different initial masses (5 mg - 35 mg) were used in the CP, to extend the initial mass range used in Radmanesh's study. The same result was obtained; therefore, the used sample with the used particle size is below the limit where inter- and intra-particle transformation may affect the kinetics. As a result, the mass transfer limitations were not considered in this study.

The heat transfer limitations in the case of CP were investigated. The calculated Biot number was less than 0.1, which means that heat transfer by conduction inside the heated material is higher than heat transfer by convection. Therefore, heat transfer limitations were not considered in this work as well.

4.5 The Kinetic Model

A kinetic model with *n* reaction order was employed to estimate kinetic parameters in the MWP and CP of sawdust; as shown in equation (4-6).

$$\frac{dx}{dt} = K\,(1-x)^n \tag{4-6}$$

Where x is the decomposition fraction of the virgin material [-], and K is the reaction rate constant; it is defined by the Arrhenius equation, as in equation (4-7).

$$K = k_o^*\; e^{\frac{-E_a}{R}\left(\frac{1}{T}-\frac{1}{T_r}\right)} \tag{4-7}$$

Where $k_0^* = k_0\, exp(-E_a/R\, T_r)$; k_0 is the pre-exponential factor [time^{-1}]; it represents of molecular mobility and depends on molecule vibration frequency (Lidström, Tierney et al. 2001). E_a is the activation energy [J/mol] that is needed to breakdown the molecule bonds. R is the universal gas constant [J/mol K], T is the reaction temperature [K], and and T_r is a reference temperature [K], 600K. Therefore, equation (4-6) can be rewritten as shown in equation (4-8).

The decomposition fraction can be defined as in equation (4-9), where V is the weight lost up to time t. It equals the difference between the initial weight (W_0) and the weight at this time (W_t). V^* is the maximum available volatility from the virgin material and can be obtained by proximate analysis.

$$\frac{dx}{dt} = k_o^*\; e^{\frac{-E_a}{R}\left(\frac{1}{T}-\frac{1}{T_r}\right)}\,(1-x)^n \tag{4-8}$$

$$x = \frac{W_o - W_t}{W_o - W_\infty} = \frac{V}{V^*} \tag{4-9}$$

In order to generalize this model to be independent of the pyrolysis heating rate (β), equation (4-8) was divided by β, hence equation (4-8) is rewritten as in equation (4-10).

$$\frac{dx}{dT} = \frac{k_o^*}{\beta}\; e^{\frac{-E_a}{R}\left(\frac{1}{T}-\frac{1}{T_r}\right)}\,(1-x)^n \tag{4-10}$$

4.6 Parameter Estimation

Equation (4-10) was implemented in a MATLAB® program code. Multidimensional unconstrained/constrained nonlinear minimization (MATLAB's fminsearch/fminsearchbnd) was used to estimate the model parameters (k_o, E_a, and n) using the initial conditions obtained from the experimental work. The optimum values of these parameters were chosen based on minimizing the square difference between the predicated and the experimental results (x^{Model} and x^{Exp}). In addition, a contour map was performed to obtain an overall view of the complete suitable values, and then the optimal ones were chosen.

To solve the non-linear ordinary differential equation, equation (4-10), MATLAB's ODE45 using the default options was employed. The deviation of x^{Model} from x^{Exp} was calculated according to equation (4-12), where N is the number of fitted points (experimental points) and p is the number of model parameters (Chen, Zhang et al. , Radmanesh, Courbariaux et al. 2006).

$$Obj = \frac{1}{N-p}\sum_{i=1}^{n}(x_i^{Model} - x_i^{Exp})^2 \quad (4\text{-}11)$$

$$Deviation - \% = 100 \times \sqrt{Obj} \quad (4\text{-}12)$$

4.7 The Results

4.7.1 The Decomposition Fraction vs. Temperature

In order to investigate the kinetics of MWP in contrast to CP, the pyrolysis of sawdust was carried out with a mass of 50 g in the MW-TGA @ 2.7 kW and 35 mg in a conventional TGA. Figure 4-6-A and Figure 4-6-C show the decomposition fraction vs. temperature in each case, and Figure 4-6-B and Figure 4-6-D depict the contour maps for the suitable values of k^*_o and E_a, and the corresponding deviations in both cases.

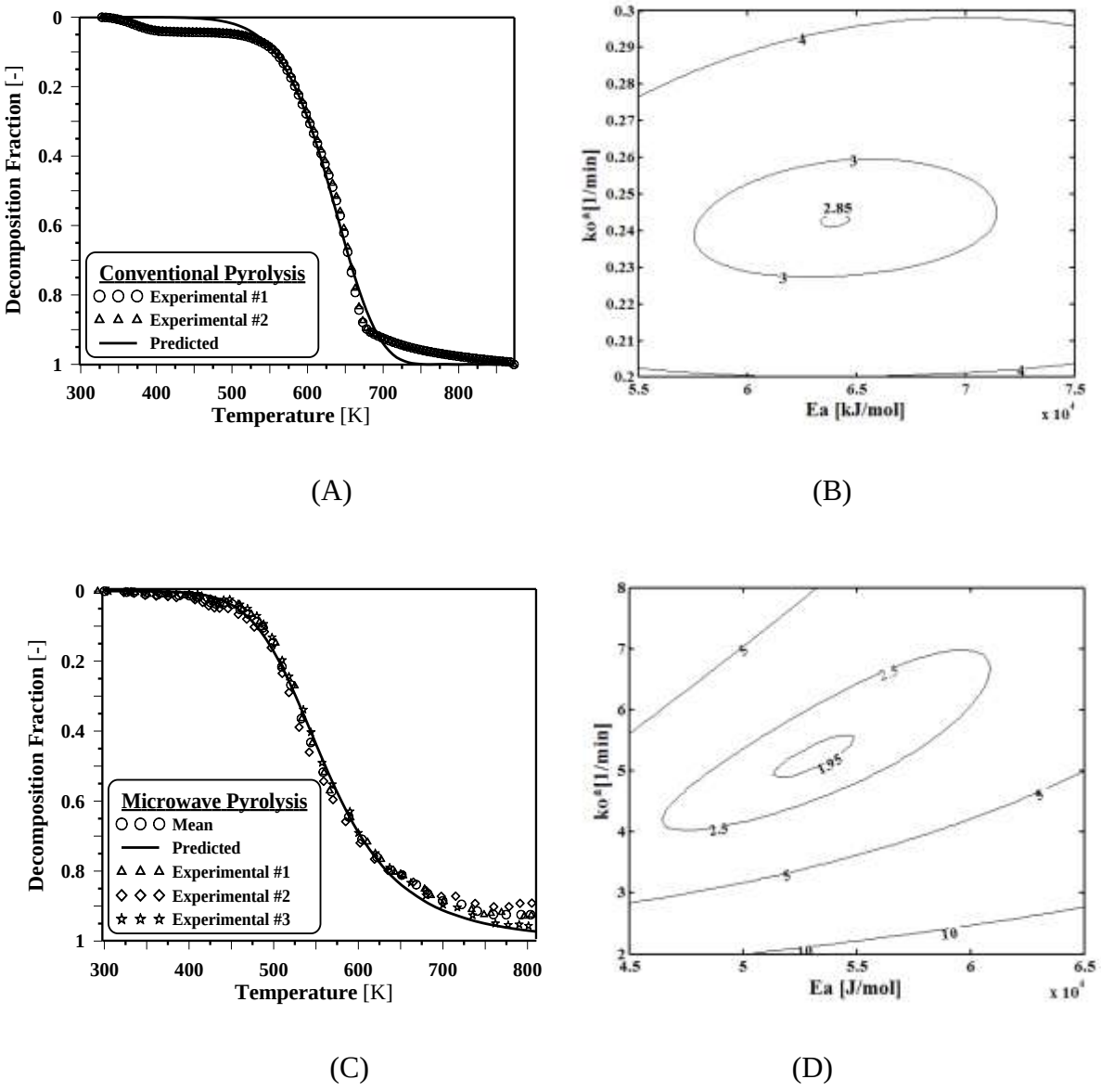

Figure 4-6: (A) & (C) the decomposition fraction vs. temperature, experimental and predicted; and (B) & (D) the contour maps of CP and MWP respectively

4.7.2 The Estimated Kinetic Parameters

To estimate E_a, k_o, and n in each case, equation (4-10) was solved for the measured temperature values using the strategy discussed in the parameter estimation section. Different reaction orders were tested in each case to obtain the optimum fitting and to understand the effect of n on k_o, and

E_a. The estimated kinetic parameters were listed in Table 4.2. These values are in agreement with those reported by Aqsha, Mahinpey et al. 2011 (Aqsha, Mahinpey et al. 2011).

Table 4.2: The estimated kinetic parameters in MWP and CP of sawdust

E_a [kJ/mol]	k_o [min^{-1}]	n [-]	Process
65	1 x 10^5	2	CP
55	3 x 10^5	1	MWP

Figure 4-7 demonstrates a validation of the presented model, which compares the predicted results against the experimental data in each case. As it is obvious, the presented model, at the selected temperature, has a high capability to estimate the decomposition fraction with minor deviations.

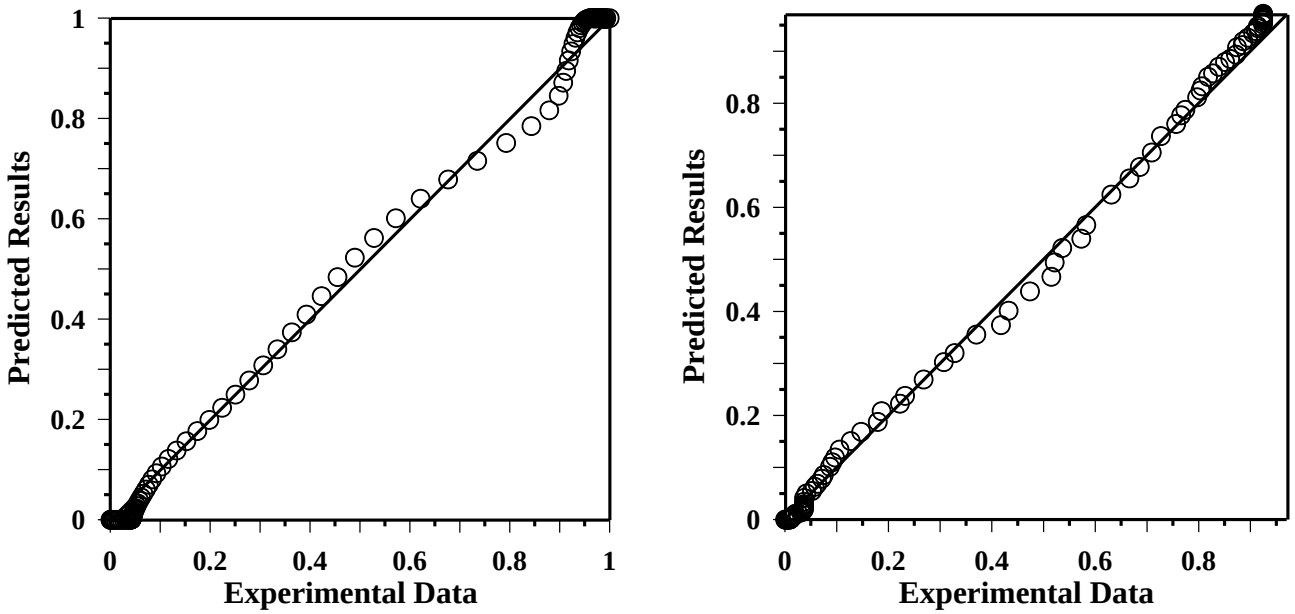

(A) (B)

Figure 4-7: The capability of the presented model: (A) CP and (B) MWP

4.8 The Discussion

According to the estimated kinetic parameters, there may not be evidence on the effect of MWH on E_a as the MWP and CP have almost the same estimated value; however, the effect on k_o is obvious. The estimated value of k_o in the MWP is more than three-times that of the CP. As mentioned in the introduction, the nature of the MWH mechanism mainly depends on agitating the dipoles of the heated material, which results in more chaotic motion. In addition, k_o was interpreted as a collision frequency, determined using the kinetic theory. Indeed, these two facts can elucidate that MWH could enhance the molecule collisions, which leads to an increase in k_o. A similar explanation was documented by Yadav and Borkar 2006. Despite this tangible effect on k_o, E_a is almost the same in both cases. This could be due to the huge difference between the wavelength of the oscillating EMW, which is 12.24 cm at a frequency of 2.45 GHz, and the intermolecular distance of the heated material, which is negligible compared to the wavelength. This renders the effect of the EMW on E_a doubtful as EMW cannot hack the molecular bonds directly.

Table 4.3 demonstrates different kinetic investigations of different reactions, some of which have reported that k_o was increased under MWH, while E_a is either constant or decreased. On the other hand, some investigators have claimed that E_a and/or k_o were decreased under MWH. Indeed, this inconsistent could be a result of using one of the traditional thermometers without considering its drawbacks, as mentioned previously. In addition, it could be related to the employed parameter estimation technique.

Table 4.3: Effect of MWH on reaction kinetics compared to CH

Author	Objective	Thermometer	E_a	k_o
Adnadjevic and Jovanovic 2012 (Adnadjevic and Jovanovic 2012)	A kinetic investigation of sucrose hydrolysis at the acidic ion-exchange resin using CH and MWH	A fibre optics thermometer	less	less
Adnađević, Gigov et al. 2008 (Adnađević, Gigov et al. 2008)	A kinetic study of fullerol formation in MWH and CH	A thermocouple thermometer	less	less
Fukushima, Kashimura et al. 2013(Fukushima, Kashimura et al. 2013)	Study of reduction behavior of copper (II) oxide in MWH	An infrared thermometer	less	
Sun, Wang et al. 2012 (Sun, Wang et al. 2012)	A kinetic study of the decomposition of waste printed circuit boards under MWH and CH	Offline and online thermocouples	less	
Chen, Wang et al. 2013 (Chen, Wang et al. 2013)	A kinetics investigation of Glycolysis of Poly (ethylene terephthalate) using MWH		less	
Yan, Hu et al. 2012 (Yan, Hu et al. 2012)	Investigation of emulsifier-free emulsion polymerization of N-hydroxymethyl acrylamide, methyl methacrylate, and styrene using MWH		less	
Mazo, Estenoz et al. 2012(Mazo, Estenoz et al. 2012)	Investigate the transesterification of castor oil with maleic anhydride using CH and MWH	A thermocouple thermometer	equal	less
Adnadjević and Jovanović 2012 (Adnadjević and Jovanović 2012)	The isothermal kinetics of ethanol adsorption from aqueous solution onto a zeolite type carbon molecular sieve under CH and MWH	A fibre optic thermometer	less	more
Li, Han et al. 2013 (Li, Han et al. 2013)	A kinetic investigation of the microwave liquefaction of corn stove in the presence of ethylene glycol using sulfuric acid as a catalyst	A fibre optic thermometer	less	more

Temur Ergan and Bayramoğlu 2011(Temur Ergan and Bayramoğlu 2011)	Kinetics investigation of the decomposition of potassium persulfate	Infrared thermometer	more	more
Yadav and Borkar 2006(Yadav and Borkar 2006)	Generation of perlauric acid directly from lauric acid and hydrogen peroxide.	Four-blade pitched turbine impeller was used for agitation	equal	more

Herein, the presented exegesis could be helpful to explain some of the observations reported in the literature regarding effects of MWH on reaction rates (Salmoria, Dall'Oglio et al. 1998, Lidström, Tierney et al. 2001, Lucchesi, Chemat et al. 2004, Menéndez, Domínguez et al. 2004, Karthikeyan, Balasubramanian et al. 2006, Orozco, Ahmad et al. 2007, Dogan and Hilmioglu 2009, Guiotoku, Rambo et al. 2009, Krzan and Zagar 2009, Zhang and Zhao 2010, Patil, Gude et al. 2011). This explanation was arrived at based on a reaction kinetics investigation and without investigating the selectivity side, which would be different. Therefore, the future work will attempt to investigate the effect of MWP on product selectivity in contrast with CP. Such discussion is so significant that it would improve the understanding and control of a chemical reaction.

4.9 The Conclusion

This work investigated the kinetics of microwave pyrolysis (MWP) in contrast to conventional pyrolysis (CP) of sawdust. In order to complete this investigation, an original MW-TGA was built and equipped with an innovated thermometer. This thermometer measures transient-mean temperature, which could eliminate the drawbacks suffered by the traditional thermometers.

The temperature profiles within the heated material were estimated using COMSOL-Multiphysics applications. To make this estimation, the dielectric properties of sawdust were measured at the same temperature range that was used in MWP. Based on the estimated profiles,

measuring a point/surface temperature of a material exposed to electromagnetic irradiation will give a temperature completely different from the temperature of all the bulk material, which cannot be employed in kinetic purposes.

The kinetic parameters were estimated in MWP and CP using a MATLAB® program code. The obtained result demonstrates that MWP may have a reaction rate faster than that of CP, for the molecular chaotic motion. This is the result of agitating the heated material dipoles by the oscillating electromagnetic waves. On the other hand, the estimated activation energy is almost the same in the two cases. This may be related to the wave length of the oscillating electromagnetic field, which is much longer than the intermolecular distance of the heated material. This exegesis was achieved by a kinetic investigation, and without investigating the selectivity side, which would be different.

Acknowledgements

The authors would like to thank Mr. Cédric Ginart (Glassblower at Montreal University) and Mr. Robert Delisle (Technician at Ecole Polytechnique Montreal) for their assistance in the experimental setup, and Dr. Levent Erdogan (Electrical Engineering Department, Ecole Polytechnique Montreal) for his assistance in this work. In addition, the authors are grateful for the financial and technical support from Lignoworks NSERC Strategic Network (www.lignoworks.ca).

CHAPTER 5 ARTICLE 3: A DETAILED COMPOSITIONAL ANALYSIS AND STRUCTURAL INVESTIGATION OF A BIO-OIL FROM MICROWAVE PYROLYSIS OF KRAFT LIGNIN

Sherif Farag[a], Dongbao Fu[b], Philip G. Jessop[b], and Jamal Chaouki[a]

[a]CRIP-Biorefinery Centre, Department of Chemical Engineering, École Polytechnique de Montréal.

P.O. Box 6079, Station Centre-ville, Montréal, QC, Canada H3C 3A7.

[b] Department of Chemistry, Queen's University, 90 Bader Lane, Kingston, Ontario K7L 3N6, Canada.

(Journal of Analytical and Applied Pyrolysis)

Presentation of the article: This article presents a detailed structural investigation of condensable gases produced via microwave pyrolysis of kraft lignin at various conditions. Different analysis techniques are performed on the oil phase, such as GC-MS, ^{31}P NMR and ^{13}C. Furthermore, different degradation pathways based on the obtained analyses will be explained.

Abstract

A detailed structural investigation of a bio-oil produced via microwave-pyrolysis of Kraft lignin was accomplished. The investigated variables were thermal-microwave-catalyst (20-40 wt%) and nominal-setting-power (1.5-2.7 kW). The measured temperatures after applying the selected conditions for 800 s were 900, 980, 1065, 1150, and 1240 K. The obtained yields of the aqueous phase, oil phase, gas, and solid were 17-21%, 15-20%, 21-27%, and 32-40%, respectively. The maximum liquid yield was obtained at 1240 K. The oil phase was mostly aromatic compounds; whereas, the aqueous phase was mostly water. The identified concentrations of guaiacols, phenols, and catechols were 97-132 mg/g, 38-60 mg/g, and 18-30 mg/g of the oil phase, using GC-MS. However, the concentrations of 583-707 mg/g of the oil phase could not be identified using this technique. ^{31}P and ^{13}C NMR spectroscopy were implemented to provide detailed structure information for the whole oil phase and the virgin material. Up to 80% of the identified carbon bonds in the oil phase were aromatic carbons. The aliphatic hydroxyl group was significantly eliminated after MWP; it was attributed to water forming in the interim of pyrolysis. The decreased concentrations of *C5* substituted/condensed phenolic hydroxyl groups after MWP were attributed to an increment in the concentrations of guaiacyl, *p*-hydroxyphenyl, and catechol hydroxyl groups. In addition, further degradation of the guaiacyl hydroxyl group was attributed to the formation of catechol hydroxyl group.

Keywords: Microwave Pyrolysis, Kraft Lignin, ^{31}P NMR, ^{13}C NMR, and GC-MS.

5.1 Introduction

Recently, biomass has been employed as a renewable resource of value-added bio-chemicals. Developing bio-chemicals is one opportunity for dealing with the unexpected challenges that have faced the forest industry in North America for the past few years, such as decreasing demand and competition with low cost sources of wood. As well, generating energy from biomass is one way to compensate for the rapid increase in energy demand expected in the next few years .

Lignocellulosic biomass is composed of three intertwined components: cellulose, hemicellulose, and lignin. The dry basis weight of each is 35-45%, 25–30%, and 20–35%, respectively (Zakzeski, Bruijnincx et al. 2010, de Wild, Huijgen et al. 2012, Mu, Ben et al. 2013).This distribution depends on the species, the environment in which it was grown, and other factors.

Lignin is a three dimensional amorphous polymer, one of the most complex organic aromatic polymers in nature (Zakzeski, Bruijnincx et al. 2010, Kibet, Khachatryan et al. 2012, Mu, Ben et al. 2013), but the exact structure of the untreated lignin network is unknown. However, it is believed to be based upon three aromatic alcohols: p-coumaryl, coniferyl, and sinapyl alcohol, as depicted in Figure 5-1 (Zakzeski, Bruijnincx et al. 2010, de Wild, Huijgen et al. 2012, Kibet, Khachatryan et al. 2012).

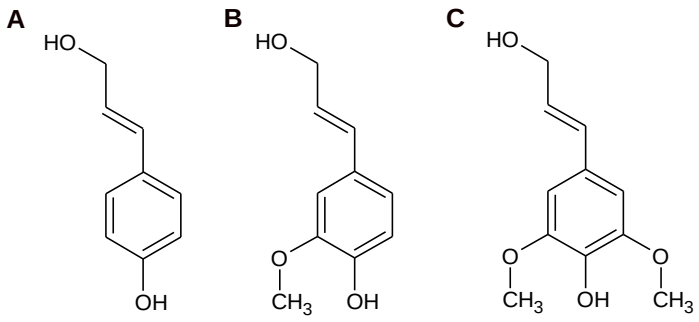

Figure 5-1: The three monolignols of a lignin network: (A) coumaryl alcohol, (B) coniferyl alcohol, and (C) sinapyl alcohol

Even though lignin is the only renewable source of aromatics in nature and the third-most abundant natural polymer after cellulose and hemicellulose, it has received less attention in research than the other biomass components (Ben and Ragauskas 2011, Mu, Ben et al. 2013)**.** In addition, the annual product of lignin in the US paper industry is over 50 million tons, yet only 2% of this material is converted to bio-products (Ben and Ragauskas 2011), whereas the rest is combusted to recover energy.

Lignin can be converted into chemicals and/or energy using thermal, biological, or physical technology. One of the techniques applied in thermal technology is pyrolysis. Pyrolysis is a thermal decomposition of chemical bonds by supplying heat energy in an oxygen-free environment. The main pyrolysis products are: (1) solid, mostly carbon, which can be used as a solid fuel, soil additive, and other applications. (2) Condensable gas, which is a potential source for value added chemicals that could replace petrochemicals; and (3) non-condensable gas, which is combustible (de Wild, Huijgen et al. 2012, Doucet, Laviolette et al. 2013). The needed heat energy for pyrolysis can be provided by heat transfer from a heating source. Otherwise, it can be generated within the heated material by an electromagnetic exposure (microwave heating). This pyrolysis is called “microwave pyrolysis” (MWP).

Microwave heating (MWH) is a volumetric energy conversion mechanism within the target material rather than superficial heat transfer as in conventional heating (CH). MWH has been established in different sectors as it can eliminate several issues/limitations in contrast to CH such as formation of a temperature gradient inside and outside the heated material, and char layer formation of pyrolysis material. Furthermore, it has been demonstrated that a desired temperature gradient and/or hot or cold spots can be generated within the payload in a simple way, compared to CH (Farag, Sobhy et al. 2012). In addition, under controlled conditions, MWH can reduce energy consumption and award higher product selectivity compared to CH (Camelia Gabriel and Mingosb 1998, Thostenson and Chou 1999, Oloyede and Groombridge 2000, Datta and Ni 2002, Jones, Lelyveld et al. 2002, Will, Scholz et al. 2003, Domínguez, Menéndez et al. 2005, Zhu, Wu et al. 2006, Geedipalli, Rakesh et al. 2007, Orozco, Ahmad et al. 2007, Badamali, Clark et al. 2008, Tang, Xia et al. 2008, Xu, Jiang et al. 2008, Budarin, Clark et al. 2009, Chiavaro, Barnaba

et al. 2009, Durka, Gerven et al. 2009, Ma, Liu et al. 2009, Wan, Chen et al. 2009, Mutyala, Fairbridge et al. 2010). Further details regarding MWH can be found in (Farag, Sobhy et al. 2012).

Pyrolysis of lignin and characterization of the liquid product have been investigated over the past two decades. Zheng, Chen et al. 2013 have investigated fast pyrolysis of lignin under the catalytic effect of $Mo_2N/\gamma\text{-}Al_2O_3$ (Zheng, Chen et al.). The experimental work was carried out using a pyrolysis-gas chromatography/mass spectrometry system (Py-GC-MS). The authors reported that using $Mo_2N/\gamma\text{-}Al_2O_3$ in the fast pyrolysis of lignin significantly decreased oxygenated volatile organic products and increased aromatic hydrocarbons, mostly benzene and toluene. The maximum yield is obtained at 700 ˚C. Lou, Wu et al. 2010 have examined the effect of temperature and catalysts (sodium chloride, Permutite) on the pyrolysis of bamboo lignin (Lou, Wu et al. 2010). Py-GC-MS was employed for this study. The obtained results show that the degradation of bamboo lignin took place over the temperature range from 250 ^{o}C to 600 ^{o}C. The catalysts enhanced the formation of volatile products (oil and gas pahse) and decreased the yield of solid product. Increasing the catalyst loading enhanced the yields of small molecular compounds acetic acid, benzene series, furfural, and phenol. Choi and Meier 2013 investigated the pyrolysis of Kraft lignin under the effect of different temperatures and catalysts (Zeolite HZSM-5, FCC and Olivine) (Choi and Meier 2013). GC-MS/GC-FID were used to analyze the liquid product. The obtained results show that increasing the pyrolysis temperature decreased the solid and non-condensable gas yields, whereas the liquid yield was increased. Yields of acids, sugars, benzenes and phenols were almost the same when the catalysts were applied but the guaiacols yields were decreased when HZSM-5 was applied. Increasing the pyrolysis temperature decreased the yield of higher molecular weight compounds and increased the yield of lower molecular weight compounds. Zhang, Resende et al. 2012 studied the pyrolysis of three lignin types: prairie cord grass, aspen, and synthetic Kraft lignin (Zhang, Resende et al. 2012). In this study, Py-GC-MS and TGA/FTIR were employed. The authors reported that prairie cord grass lignin released more alkyls than the other two types of lignin. On the other hand, aspen lignin produced a high yield of liquid product. Jiang, Nowakowski et al. 2010 investigated the temperature dependence of the composition of lignin pyrolysis products using Pr-GC-MS (Jiang, Nowakowski et al. 2010). The authors reported that the maximum yield of phenolics was

obtained at 600^{o}C. Most of the phenolic compounds had a concentration less than 1%. De Wild, Huijgen et al. 2012 investigated the pyrolyis of lignin from two different biomass sources using a fluidized bed reactor (de Wild, Huijgen et al. 2012). GC-MS was employed to analyze the liquid product. A liquid yield was found in the range of 40-60 wt%, and the solid product was found in 30-40 wt% . The yields of the extracted chemicals were affected by changing the biomass source. Luo, Wang et al. 2012 have studied the thermal behaviour of organosolv lignin under the catalytic effect of zeolites (Luo, Wang et al. 2012). TGA-FTIR was used in this study. The results showed that the catalysts inhibited the remaining solid product and decreased the yields of oxygenated compounds. In addition, the formation of CO_2 and CH_4 was increased.

As has been shown, most of the previous work has been done by employing GC-MS, TGA, or FT-IR. Nevertheless, the complexity of the pyrolysis crude liquid limits the use of these instruments due to different issues. Consequently, many chemical components could not be identified. For instance, around 40 wt% of the pyrolysis oil could not be identified using GC-MS. In addition, the ability of FT-IR for the quantitative analyses of a complex mixture is limited (Ben and Ragauskas 2011). Therefore, the main goal of the present study was to investigate the structures of Kraft lignin pyrolysis liquids under different MWP conditions. This was accomplished using quantitative NMR to analyze the liquid products and the virgin material as it can provide detailed structural information. Such investigations improve understanding about MWP mechanisms, which leads to more control in the degradation pathways.

5.2 The Experimental Work

5.2.1 The Virgin Material

The virgin material used in this work was softwood Kraft lignin received from FPInnovations, Montreal, Canada. It was precipitated from a Canadian Kraft mill by using a patent pending process that is called "The LignoForce System$^{(tm)}$". Lignin was characterized via CHNS analysis: C=63.27%, H=5.79%, N=0.07%, and S=1.56%, and approximate analysis: fixed carbon=37%, volatiles=62%, and ash=1%. In addition, it was analysed using quantitative ^{13}C NMR and ^{31}P NMR spectroscopy as will be shown later. Since lignin does not interact well with microwaves, it

was mixed with char, which is the solid product of lignin pyrolysis; in order to improve the conversion of microwaves to heat.

5.2.2 The Experimental Design

To study the effect of MWP conditions on product distribution and crude liquid structure, a central composite experimental design method was applied. This method gave the optimal number of experiments as well as the conditions of each. In this work, two independent parameters were chosen (A_i): (1) the concentration of a MW-thermal-catalyst (A_1 [wt%]) with $A_{1,min}$= 20 and $A_{1,max}$= 40 in the total initial mass (lignin + char) and (2) the MW-nominal setting power (A_2 [kW]) with $A_{2,min}$= 1.5 and $A_{2,max}$= 2.7. The variables A_i were coded as a_i according to equation (5-1).

$$a_i = \frac{A_i - A_o}{\Delta A} \tag{5-1}$$

where a_i is a dimensionless coded value, A_i is the real value of an independent variable, and A_o is the real value of the independent variable at the center point (0,0). ΔA is the step change, which equals 10 for the first parameter and 0.6 for the second one. Table 5.1 shows the coded and actual values for the independent parameters. In order to guarantee the reproducibility, each experiment was repeated three times, and the average value was represented as will be shown later.

Table 5.1: The coded vales and the corresponding actual values applied in MWP of Kraft lignin

Run #	Coded value		Actual value	
	Char wt%	Nominal Power	Char wt%	Nominal power [kW]
1	-1	-1	20	1.5
2	-1	1	20	2.7
3	0	0	30	2.1
4	1	-1	40	1.5
5	1	1	40	2.7

5.2.3 The Experimental Setup

The experimental work was carried out in a bench scale Microwave-oven (MW-O) (Microwave Research Inc; Model: BP-211, 230 V, 2.45 GHz, and setting power up to 3.2 kW). The oven cavity has inner dimensions of 510×250×320 mm. As electronic devices are highly affected by the surrounding temperature, an alumina box (muffle) with the dimensions of 390×180×170 mm was kept inside the oven cavity during the heating. This muffle protects the oven's electronic devices from most of the emitted heat and unwanted/unexpected explosions, or combustion during MWP. A quartz semi-batch cylinder reactor was used after connecting it to a condensation system to collect the condensable gas while the non-condensable gas passes directly through, as shown in Figure 5-2.

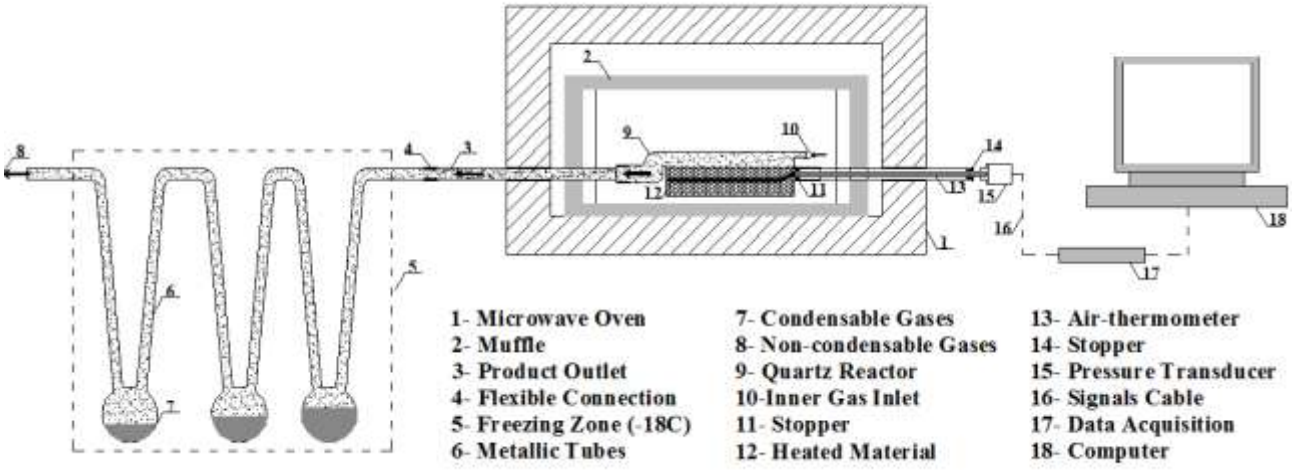

Figure 5-2: The experimental set-up

The employed condensation system consists of a set of vertical metallic tubes. These tubes were connected in series at one end while the other ends were connected via a 500 ml two neck Pyrex flask. The reactor outlet was connected to the condensation system via a metallic connection. This connection was kept at 200 ^{o}C, to avoid any condensation before the freezing zone.

Temperature measurement was done using the innovated thermometer that was used in Farag. and Chaouki. 2013; refer to that paper for a detailed description, calibration, and validation of this thermometer (Farag. and Chaouki. 2013). Figure 5-3 shows the transient mean temperatures within Kraft lignin at two different concentrations of char, 20 and 40 wt%, and one nominal setting power, 2.7 kW. In this work, since MWP was done at non-isothermal conditions, the presented temperatures are the final ones, which were reached at the end of the heating period, 800 s.

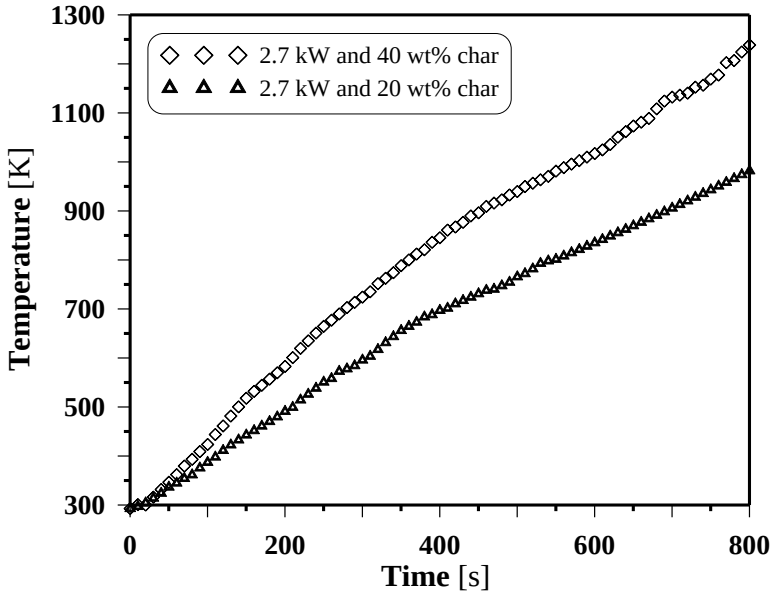

Figure 5-3: The transient mean temperature of MWP of Kraft lignin at two various conditions

5.2.4 The Method

The procedures of each experiment were as follows. First, a constant initial mass of 300 g (char: *x* wt% + lignin: (1- *x*) wt%) was carefully placed in the reactor. Afterward, the reactor was inserted inside the MW-O cavity and then connected for temperature measurement, to the inert gas inlet, and the product outlet, as illustrated in Figure 5-2. Secondly, the whole system was purged in the beginning by an inert gas (N_2); furthermore, N_2 was kept during the pyrolysis. A nominal setting power, according to Table 5.1, was adjusted and held for 800s, which is the microwave exposure time for each experiment.

In the meantime, for each experiment the condensable liquid was condensed within the freezing zone, whereas the non-condensable gas passed directly through. After each experiment, the solid product was collected and weighed as soon as it cooled to ambient temperature. The same approach was used for the liquid product. The mass of non-condensable gas was calculated by subtracting the liquid and solid masses from the initial lignin mass ((1-*x*) times the total initial mass). The collected liquid mixture was separated into two phases: (1) an oil phase, and (2) an aqueous phase which is less dense than the oil phase. Finally, methanol was added (5 wt%) to every liquid product, and the liquids were kept refrigerated until analysis.

The oil and aqueous phases were analysed using GC-MS (PerkinElmer Clarus 680 Gas Chromatograph and a PerkinElmer Clarus 600T Mass Spectrometer), quantitative ^{31}P and ^{13}C NMR spectroscopy (Bruker Avance 500 MHz NMR spectrometer). The detailed methods of these analyses have been published previously (Fu, Farag et al. 2014). Water content of each sample was determined by Karl-Fischer Titration using a Mettler Toledo C20 Coulometric KF Titrator. These analyses and measurements were done on a mix of three samples produced via three repetitions at the same conditions.

5.3 Results and Discussion

5.3.1 The Products Distribution

The power setting and char wt% that were used at each run produced a specific heating rate and therefore a specific final temperature. A comparison made between two runs having the same nominal power setting but different concentrations of char demonstrated that char concentration had a greater effect on the final temperature than the nominal power setting. For instance, when the concentration of char was changed from 20% to 40% at 1.5 kW, the final temperature was increased by 250 ^{o}C. On the other hand, when the power setting was changed from 1.5 kW to 2.7 kW at 20% of char concentration, the final temperature was increased by 80 ^{o}C. This means the same heating rate can be obtained at a lower power setting by raising the char concentration. However, char concentration should be optimized in order to prevent an adverse effect on the product distribution and quality.

Figure 5-4 shows the yields of each product for the conditions under investigation. These yields were calculated based on the initial mass dry basis. The presented values are the average of three repetitions under the same conditions, and the presented error bars are their standard deviations. The maximum deviation was ±2 for the all products except for the aqueous phase, it was ±1. Considering that char does not have any weight loss during pyrolysis, it was examined separately at the measured temperatures.

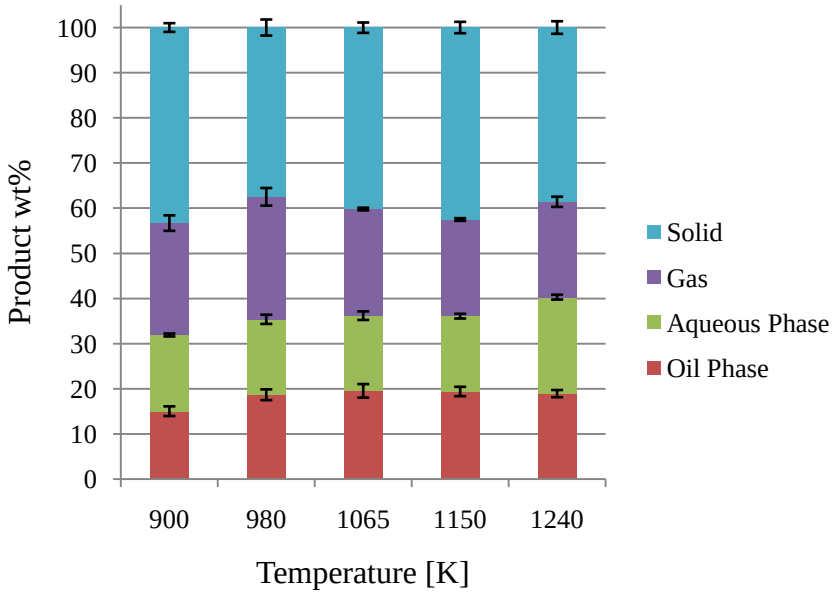

Figure 5-4: The product distribution for the conditions under investigation

As shown in Figure 5-4, increasing the final temperature increased the total liquid product. For example, when the temperature was changed from 900 K to 1240 K, the total liquid yield was increased from 32 wt% to 40 wt%. The same trend has been reported by Choi and Meier. 2013 (Choi and Meier 2013). However, this result could be either beneficial or problematic depending on the structure of the obtained liquid and the yield of the desired chemicals. For this reason, we chose to focus not only on quantitative but also on qualitative characterization of the liquids.

The yield of oil phase (red in Figure 5-4) was calculated from the total liquid yield minus the aqueous phase yield. Although the liquids produced at 1065 K and 1150 K have almost the same yield, the one produced at 1150 K has 12% more oil in the aqueous phase than did the one at 1065 K. In addition, the liquid produced at 980 K, which has the maximum water content in the oil phase, has almost the same total oil wt% as the one at 1065 K.

Table 5.2: The measured water content in the aqueous and oil phase at every run

Run #	Temp [K]	Water content [wt%]			
		Aqueous phase	Oil phase	Total liquid	Relative to initial mass
1	900	91	10	53	17
2	980	76	21	47	17
3	1065	90	14	49	18
4	1150	78	14	44	16
5	1240	73	12	44	18

Alternatively, if another consideration is applied, another condition can be the best. Consequently, different analyses were applied on the liquid products to achieve investigations based on the structure of the obtained liquid, not only based on the obtained quantity of liquids.

5.3.2 The GC-MS Analysis

Simply obtaining a high yield of oil is insufficient; it is important to know and to be able to optimize the composition of the oil. All the liquid products, in total ten samples, were analyzed using GC-MS, for characterizing the extracted chemical compounds via MWP of lignin. Figure 5-5 shows the GC-MS chromatographs for the oil phase, five samples in total, and Table 5.3 lists the 42 organic compounds that were identified quantitatively and qualitatively in the oil and aqueous phases.

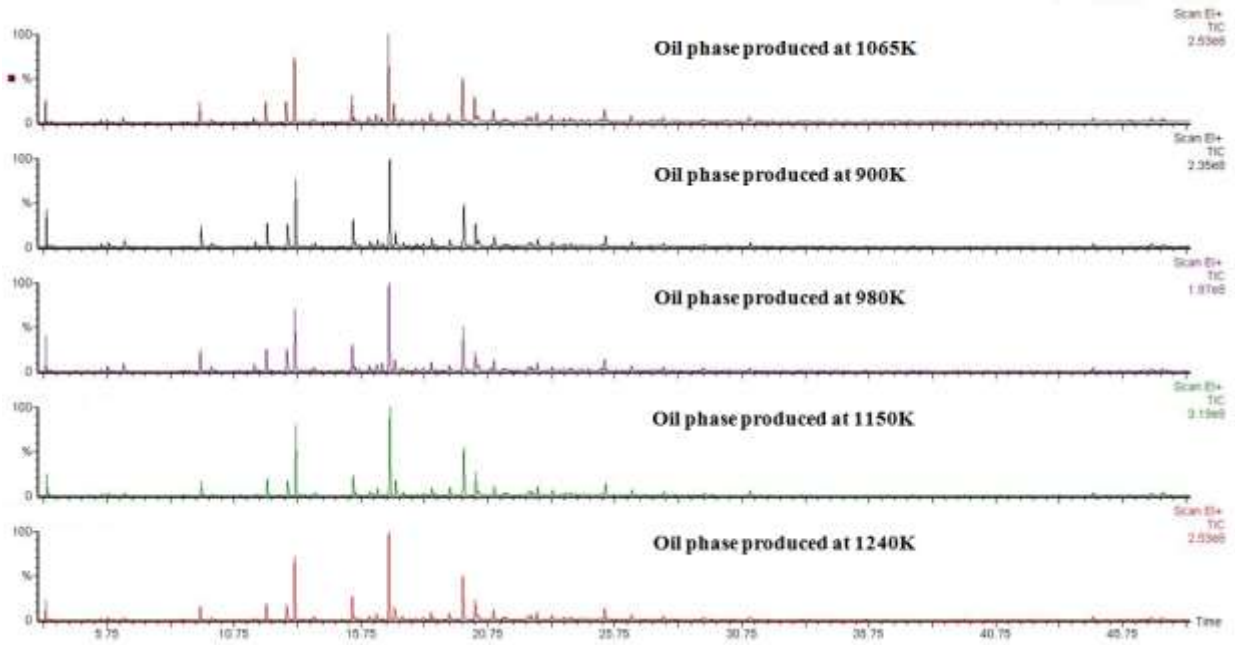

Figure 5-5: GC-MS chromatographs for the oil phase

Table 5.3: The identified chemical components in the oil and aqueous phases using GC-MS

#	RT [min]	Identification by GC-MS	Oil phase [mg/g oil phase]					Aqueous phase [mg/g aqueous phase]				
			900K	980K	1065K	1150K	1240K	900K	980K	1065K	1150K	1240K
		Benzenes	**16.8**	**15.7**	**13.4**	**13.3**	**10**	**0.2**	**0.2**	**0.2**	**0.2**	nd
1	3.38	Toluene	7.7	6.8	5.0	6.1	4.3	0.2	0.2	0.2	0.2	nd
2	6.44	Styrene	3.6	3.1	2.7	1.6	1.4	nd	nd	nd	nd	nd
3	9.90	m-Methylstyrene	2.3	2.5	2.0	1.2	1.2	nd	nd	nd	nd	nd
4	21.46	4-Ethyl-1,2-dimethoxybenzene	1.2	1.2	1.4	1.8	1.1	nd	nd	nd	nd	nd
5	22.50	1,4-Dimethoxy 2,3-dimethylbenzene	2.0	2	2.3	2.6	2	nd	nd	nd	nd	nd
		Phenols	**58.3**	**57.8**	**59.9**	**55.3**	**38.1**	**4.1**	**6**	**4.1**	**3.3**	**1.3**
6	9.46	Phenol	7.0	7.8	7.3	6.5	5.2	1.6	1.8	1.6	1.3	0.5
7	12.06	o-Methylphenol	8.3	7.9	8.2	8	6.4	0.8	1.0	0.8	0.7	0.3
8	12.86	p-Methylphenol	11.4	10.8	11.2	10.2	nd	1.1	1.4	1.0	0.8	0.3
9	13.94	2,6-Dimethylphenol	2.1	2.1	2.3	2.2	1.8	nd	0.1	nd	nd	nd
10	15.45	2,4-Dimethylphenol	11.0	10.2	11	10.6	9	0.4	0.6	0.4	0.3	0.2
11	15.53	2,3-Dimethylphenol	2.4	2.4	2.5	2	1.7	nd	0.1	nd	nd	nd
12	16.10	p-Ethylphenol	2.3	2.3	2.4	2.2	1.8	nd	0.1	nd	nd	nd
13	17.41	2,4,6-Trimethylphenol	2.0	2	2.2	2	1.7	0.1	0.1	0.1	0.1	nd
14	18.22	3-Ethyl-5-methylphenol	1.8	1.8	2.1	1.8	1.6	0.1	0.2	0.1	0.1	nd
15	18.55	3-Methyl-4-ethylphenol	3.9	3.9	4.3	4.3	3.7	nd	0.2	0.1	nd	nd
16	20.37	o-Allylphenol	4.8	5.4	5	3.8	3.6	nd	nd	nd	nd	nd
17	21.40	3-Methoxy-5-methylphenol	1.4	1.3	1.6	1.6	1.5	nd	0.1	nd	nd	nd
		Guaiacols	**101.8**	**96.9**	**112.2**	**132.4**	**100.2**	**4.8**	**7.1**	**5.5**	**5.9**	**2.2**
18	13.18	Guaiacol	22	20.2	22.7	29.3	21.2	2.2	2.6	2.3	2.6	1
19	16.40	6-Methylguaiacol	3.4	3.2	3.8	4.5	3.2	0.1	0.2	0.1	0.1	nd
20	16.89	p-Methylguaiacol	28	28.1	29.9	35.3	28.4	1.3	2.1	1.5	1.5	0.6
21	19.80	4-Ethylguaiacol	17.8	17.6	19.5	24.5	18.2	0.4	0.8	0.5	0.5	0.2
22	21.01	p-Vinylguaiacol	5.0	4.9	5.7	5.7	4.9	nd	0.2	nd	nd	nd
23	22.38	3-Allylguaiacol	3.2	3.0	3.9	4.1	3.1	0.2	nd	0.2	0.2	nd
24	22.72	p-Propylguaiacol	3.8	4.0	4.5	5.6	3.8	nd	nd	nd	nd	nd
25	23.78	5-Formylguaiacol	1.7	1.2	1.9	1.9	1.6	0.2	0.3	0.2	0.2	0.1
26	24.03	4-Propenylguaiacol	1.6	1.6	2.1	2.4	1.7	nd	nd	nd	nd	nd
27	25.38	cis-Isoeugenol	4.8	4.6	5.6	6.3	5.1	nd	0.1	nd	nd	nd
28	26.43	4-Acetylguaiacol	3.1	2.7	3.5	3.7	2.8	0.2	0.3	0.2	0.2	0.1
29	27.68	Guaiacylacetone	2.4	2.1	2.7	3.0	2.2	nd	0.3	0.2	0.2	nd
30	31.08	Homovanillic acid	2.9	2.1	3.3	3.6	2.5	0.3	0.4	0.3	0.3	0.2
31	46.91	Ethyl homovanillate	2.2	1.6	2.9	2.6	1.6	nd	nd	nd	nd	nd
		Catechols	**21.9**	**18.3**	**26.6**	**29.6**	**20**	**9.6**	**10.9**	**9.8**	**9.7**	**5.8**
32	17.12	Catechol	6	4.5	7.1	8.2	5.6	3.4	4	3	2.9	3.2
33	19.25	3-Methylcatechol	3.7	3.2	4.6	5.0	3.5	1.3	1.5	1.6	1.6	0.5
34	20.28	4-Methylcatechol	9.4	8.0	10.7	12.4	8.6	4.1	4.3	4.3	4.3	1.9
35	23.29	4-Ethylcatechol	2.8	2.6	4.2	4	2.3	0.7	1.3	1.0	0.9	0.2
		Others	**12.5**	**14.8**	**15.3**	**6.8**	**5.6**	**0.0**	**0.0**	**0.0**	**0.0**	**0.0**
36	11.58	Indene	2.5	3.3	2.3	nd	1	nd	nd	nd	nd	nd
37	16.61	Naphthalene	1.8	3.6	2.3	nd	nd	nd	nd	nd	nd	nd
38	17.96	2,3-Dihydrobenzofuran	1.6	1.6	1.5	nd	nd	nd	nd	nd	nd	nd
39	25.26	Acenaphthylene	1.7	2.3	2.2	nd	nd	nd	nd	nd	nd	nd
40	29.28	α-Amino-3'-hydroxy-4'-methoxyacetophenone	2.1	1.2	2.6	2.2	1.8	nd	nd	nd	nd	nd
41	44.61	Retene	1.7	1.7	2.3	2.5	1.8	nd	nd	nd	nd	nd
42	47.32	Methyl dehydroabietate	1.3	1.2	2.1	2.2	1.1	nd	nd	nd	nd	nd
Total identified compounds			**211.3**	**203.5**	**227.4**	**237.4**	**173.9**	**18.6**	**24.1**	**19.6**	**19.1**	**9.3**
Total unidentified compounds			**691.7**	**583.5**	**628.6**	**622.6**	**707.1**	**69.4**	**218.9**	**77.4**	**196.9**	**259.7**

RT: Retention Time, nd: not determined, and Total unidentified = 1000-Total identified -Water content

Because the chemical structure of lignin is largely aromatic, all the identified compounds are aromatics as well. The identified chemical compounds in the oil and aqueous phases are presented in five groups: benzenes, phenols, guaiacols, catechols, and others. The aqueous phase contained so little organic content that identified organic compounds totalled only 9.3-24.1 mg/g in the aqueous phase; in contrast, 173.9-237.4 mg/g were found in the oil phase. Consequently, the remainder of this work will focus on the oil phase only.

The most abundant group of compounds in the oil phase was the guaiacols, which were found in a concentration range of 97-130 mg/g. Phenols were found at 38-60 mg/g while catechols were found within 18-30 mg/g. Other identified chemical compounds were collectively found in a concentration of 9-19 mg/g.

In general, the maximum concentration of the total identified compounds (237.4 mg/g of oil phase) was found at 1150 K. The maximum concentration of guaiacols and catechols was produced at 1150K. On the other hand, the maximum concentration of phenols and others was found at 1065 K. The maximum concentration of benzenes was at 900 K. However, there was a concentration from 580 mg/g to 700 mg/g in the oil phase of compounds, probably higher molecular weight compounds that could not be identified using GC-MS. Therefore, GC-MS analysis is inadequate to fully describe the composition.

5.3.3 The Quantitative ^{31}P NMR Analyses for the Oil Phase

Quantitative ^{13}P NMR spectroscopy was used to further characterize the oil phase as well as the virgin material, in a total of six samples. The quantitative ^{31}P NMR spectra were acquired after in situ derivatization with 2-chloro-4,4,5,5-tetramethyl-1,3,2-dioxaphospholane (TMDP) to measure the hydroxyl groups' contents in the samples; this method was developed by Granata and Argyropoulos (Granata and Argyropoulos 1995). Figure 5-6 depicts the ^{31}P NMR spectra for the five oils produced at the selected conditions, and the 6th spectrum for lignin. Table 5.4 summarizes the integration for every sample.

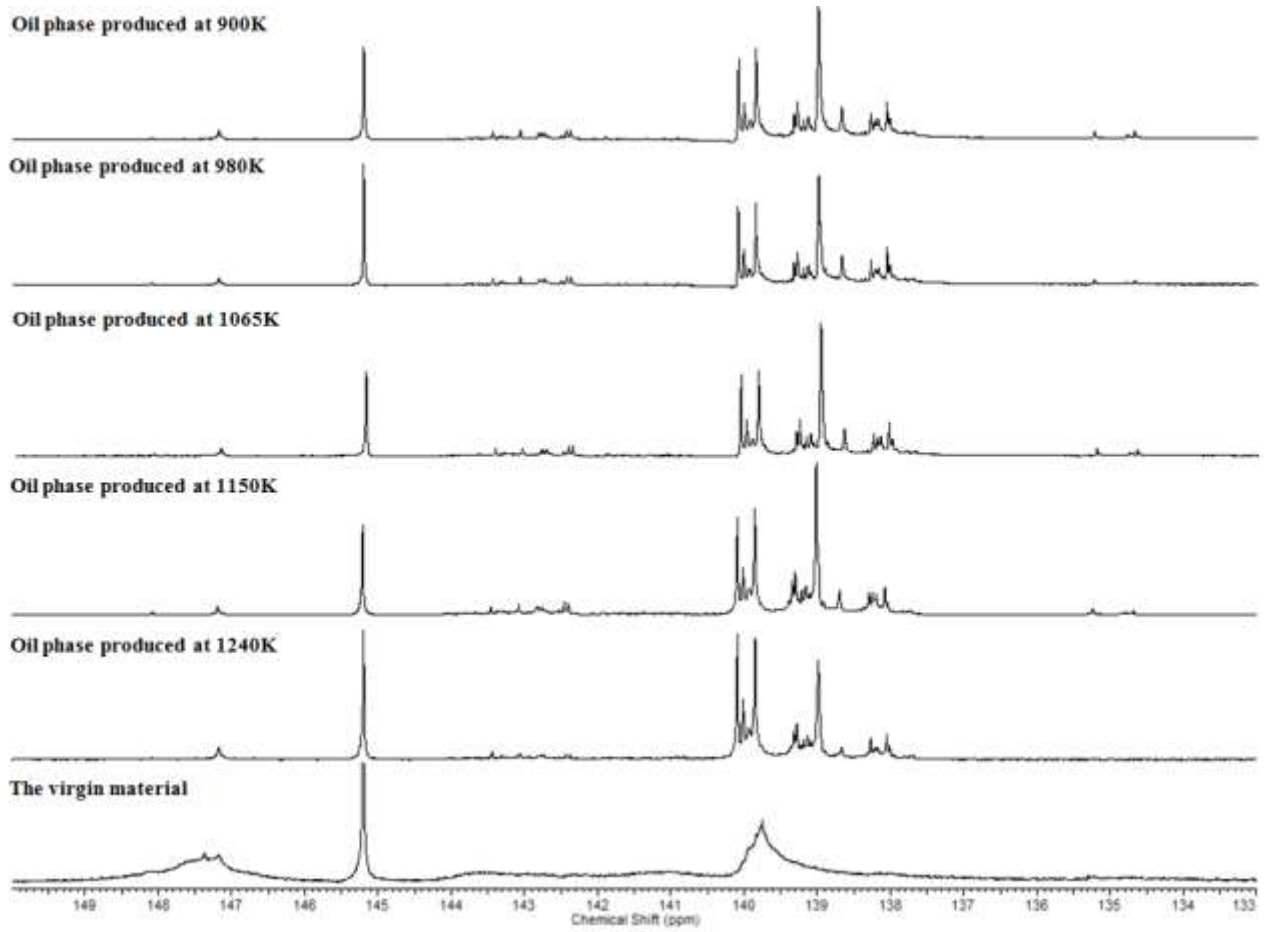

Figure 5-6: Quantitative ^{31}P NMR spectrum for the oil phase and the virgin material

Table 5.4: Concentrations of different hydroxyl groups determined by quantitative 31P NMR spectroscopy of the virgin lignin and the oil phases obtained after microwave pyrolysis at various power levels, char wt%, and temperatures.

Functional group		Integration region (ppm) (Ben and Ragauskas 2011)	Examples	Concentration in oil phase (mmol/g oil)					Conc. in lignin (mmol/g)
				900K	980K	1065K	1150K	1240K	
Aliphatic OH		150.0 – 145.5	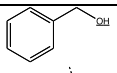	0.18	0.17	0.31	0.06	0.08	1.48
C_5 substituted condensed phenolic OH	β-5	144.7 – 142.8	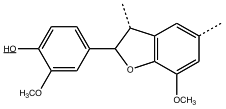	0.25	0.23	0.33	0.33	0.13	0.5
	4-O-5	142.8 – 141.7	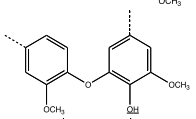	0.22	0.2	0.26	0.29	0.09	0.32
	5-5	141.7 – 140.2	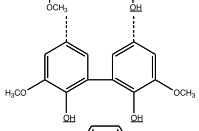	0.03	0.01	0.08	0.15	0.11	0.55
Guaiacyl phenolic OH		140.2 – 139.0	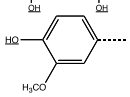	2.12	1.83	2.2	3.08	1.91	1.44
Catechol type OH		139.0 –138.2	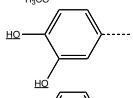	1.64	1.44	1.49	1.2	0.58	0.35
p-Hydroxy-phenyl OH		138.2 – 137.3	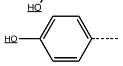	0.89	0.8	0.72	0.44	0.21	0.27
Acid-OH		136.6 – 133.6	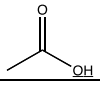	0.57	0.46	0.42	0.08	0	0.43

Each of the oil samples contained a lower concentration of aliphatic and C5 substituted/condensed phenolic hydroxyl groups than in the virgin material. On the other hand, the concentration of guaiacyl, *p*-hydroxy-phenyl, and catechol hydroxyl groups in the oil phase after MWP is higher than that in the virgin material.

The decrease in concentration of the aliphatic hydroxyl group is so considerable that it indicates most of the virgin-material side chain hydroxyl groups were swiftly eliminated during the MWP. The cleavage of these side chains might be attributed to the dehydration of the aliphatic hydroxyl groups to form water and/or unsaturated sites, according to the pathway illustrated in Figure 5-7-

A. On average, the concentration of aliphatic hydroxyl groups decreased by about 90% during the pyrolysis, possibly suggesting the source of the formation of water during MWP of lignin.

The possibility of creating water by means of the decomposition of the carboxyl group is minute as the concentration of carboxyl groups in the virgin material is minimal compared to the concentration of aliphatic hydroxyl groups. Therefore, the decomposition of the carboxyl group is more likely to be the source for the creation of carbon dioxide and/or unsaturated sites during the pyrolysis (Jiang, Nowakowski et al. 2010, Luo, Wang et al. 2012), as shown in Figure 5-7-B. As a result, the level of water measured in the total liquid product corresponds mostly to the decomposition of the side chain aliphatic hydroxyl group.

The decreased concentrations of *C5* substituted/condensed phenolic hydroxyl groups in the oil phase after MWP may be attributed to an increase in the concentrations of guaiacyl, *p*-hydroxyphenyl, and catechol hydroxyl groups. Ben and Ragauskas 2011 have claimed that the thermal cleavage of the *β-O-4* ether bond in the lignin network creates guaiacyl, p-hydroxyphenyl, and catechols, which supports the suggested degradation mechanisms illustrated in Figure 5-8 (Ben and Ragauskas 2011). This Figure demonstrates the possible decomposition pathways for the β-5 bond, the 4-O-5 bond, and the 5-5 bond. As shown in Table 5.4, the concentration of the p-hydroxy-phenyl hydroxyl groups is less than the concentration of the catechol and the guaiacyl hydroxyl groups because the methoxyphenoxy radical, see Figure 5-8-B(3), is more favored than the o-hydroxyphenoxymethyl radical, see Figure 5-8-B(5) (Ben and Ragauskas 2011).

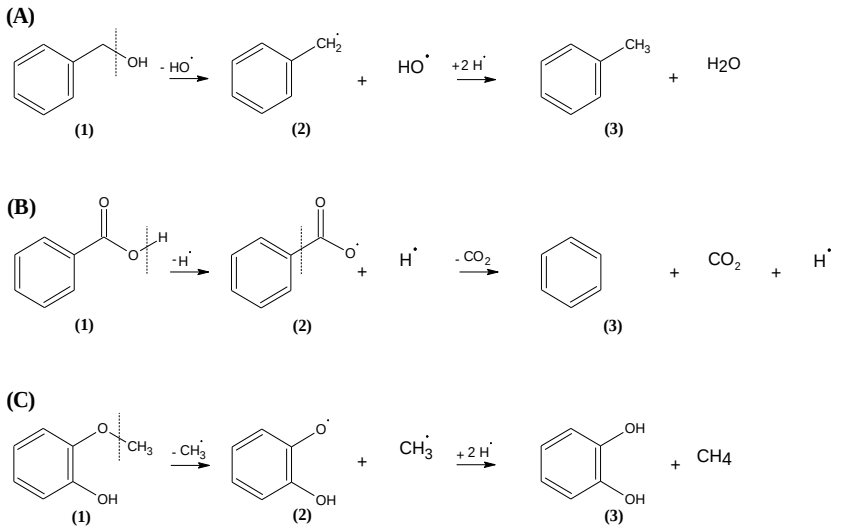

Figure 5-7: Possible degradation pathways for: (A) aliphatic hydroxyl group, (B) carboxyl acid, and (3) guaiacyl hydroxyl groups

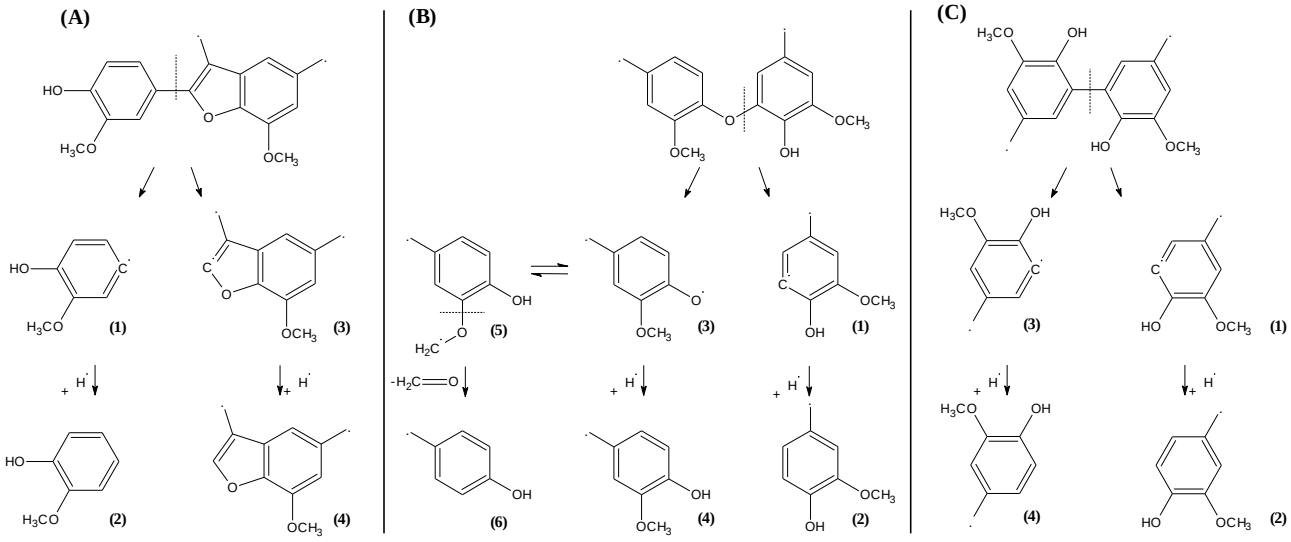

Figure 5-8: Possible degradation pathways of C5 substituted/condensed phenolic hydroxyl group: (A) β-5, (B) 4-O-5, and (C) 5-5

Comparing the increases in the concentrations of guaiacyl (up to 2-fold increase), 4-hydroxyphenyl (up to 3-fold), and catechol hydroxyl groups (up to 5-fold) shows that the

increase in the catechol hydroxyl group is significantly greater than the increase in the guaiacyl, and *p*-hydroxyphenyl groups. This may be due to the further degradation of the guaiacyl hydroxyl group into the catechol hydroxyl group, which is more favored than the degradation of the guaiacyl hydroxyl into the 4-hydroxyphenyl hydroxyl group, as shown in Figure 5-7-C, and Figure 5-8-B(5) respectively. This confirms what was mentioned earlier. However, increasing the pyrolysis temperature decreases the concentration of catechols, as shown in Table 5.4. This might be the result of further degradations of the produced catechols. Ledesma, Marsh et al. 2002 (Ledesma, Marsh et al. 2002) reported catechol pyrolysis at a range of 973-1273 K, using CH, with a residence time of 0.4 s. According to their results, the decomposition of catechol started slowly at 873 K and then increased significantly at 973 K to 1173 K. This is in agreement with the results presented here; catechols concentration decreased from 1.64 to 1.49 mmol/g when the temperature increased from 900 to 1065 K and decreased further when the temperature increased to 1240K. This confirms the occurrence of further degradation of the produced catechols. Many suggested mechanisms for this decomposition reported by Ledesma, Marsh et al. 2002 (Ledesma, Marsh et al. 2002).

The GC-MS analysis presented in Table 5.3 and the ^{31} P NMR analyses are in agreement that the most abundant identified groups are the guaiacols. This suggests that guaiacol groups are abundant in the materials that could not be identified by GC-MS.

Since lignin does not interact well with electromagnetic waves (EMW), the decomposition of aliphatic hydroxyl groups is more sensitive to the char wt% than to the nominal power setting. For instance, at the nominal power setting of 1.5 kW, the concentration of aliphatic hydroxyl groups was decreased from 0.18 to 0.06 mmol/g when the char wt% was increased from 20 to 40%. In addition, at the nominal power setting of 2.7 kW, it was decreased from 0.17 to 0.08 mmol/g, at the same char wt% concentrations, as illustrated in Table 5.4. In other words, the nominal power setting has a negligible effect on the degradation of aliphatic hydroxyl groups compared to the effect of char wt%.

5.3.4 Quantitative 13C NMR Analyses for the Oil Phase

In order to achieve full characterization for the functional groups in the oil phase as well as the virgin material, quantitative ^{13}C NMR spectroscopy was performed on every sample, for a total of six samples. Figure 5-9 depicts a typical ^{31}C NMR spectra and Table 5.5 summarizes the integration for the analysed samples.

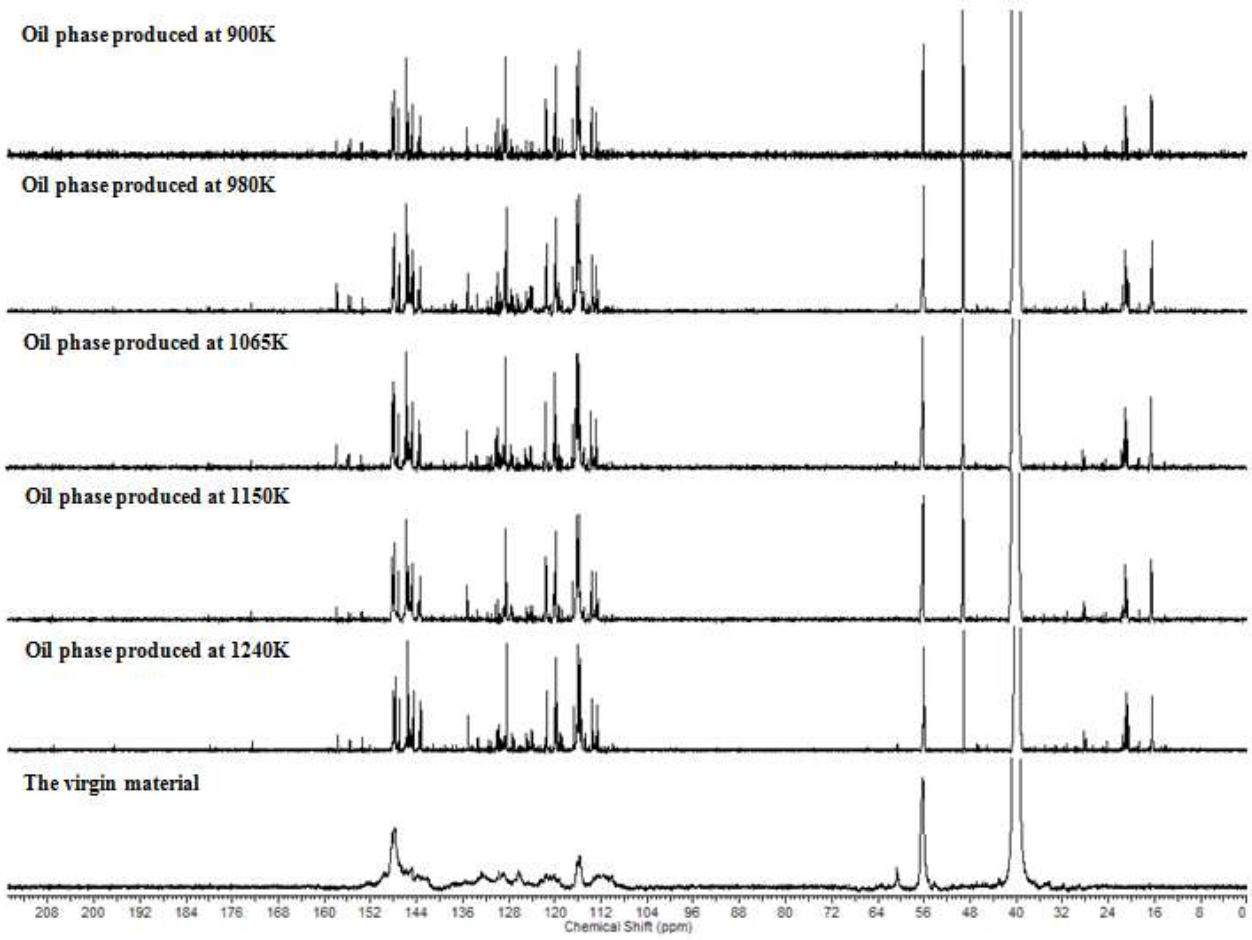

Figure 5-9: Quantitative ^{13}C NMR spectra for the oil phase and the virgin material

Table 5.5: Concentrations of different types of carbon atoms measured by quantitative 13C NMR spectroscopy of the virgin lignin and the oil phase after pyrolysis at different power settings, char wt%, and temperatures

Functional group		Integration region (ppm) (Ben and Ragauskas 2011)	Examples	Concentration in oil phase (C mol%)					Conc. in lignin (C mol%)
				900K	980K	1065K	1150K	1240K	
Carbonyl or Carboxyl		215.0 – 166.5	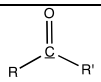	0.11	0.06	0.0	0.0	0.0	0
Aromatic C-O		166.5 – 142.0	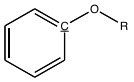	23.5	23.9	26.1	28.4	25.4	32.18
Aromatic C-C		142.0 – 125.0	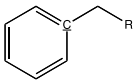	10.8	11.6	11.7	6.2	8.3	21.05
Aromatic C-H		125.0 – 95.8	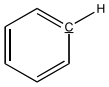	46.1	42.2	39.9	42.2	43.0	21.21
Aliphatic C-O		95.8 – 60.8	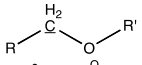	0.0	0.0	0.0	0.1	0.0	0
Methoxyl-Aromatic		60.8 – 55.2	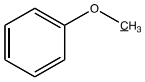	9.5	10.4	11.5	12.3	11.1	22.38
Aliphatic C-C	Total	55.2 – 0.0	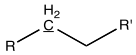	10.0	12.0	10.7	10.8	12.1	3.19
	Methyl - Aromatic	21.6 – 19.1	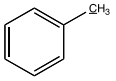	4.3	6.0	5.6	5.4	5.7	0
	Methyl - Aromatic ortho to a hydroxyl or methoxyl group	16.8 – 15.4	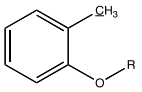	5.4	4.3	4.2	4.3	4.6	0

Up to 80% of the identified carbons in the oil phase are aromatic carbons, which is similar to what was reported by Ben and Ragauskas. 2011, 70-80% (Ben and Ragauskas 2011). This result is very significant because it demonstrates that the oil phase is mostly aromatics, which is logical according to the chemical structure of lignin. The number of aromatic C-O and C-C bonds in the oil phase was less than that in the virgin-material. On the other hand, the number of aromatic C-H bonds in the oil phase was more than that in the virgin material for all the investigated conditions.

Together, the ^{13}C NMR and ^{31}P NMR results support the degradation pathways proposed above. The decreased number of C-O aromatic bonds after the MWP may be due to the decomposition of the ether bond during MWP, as illustrated in Figure 5-8. In addition, the further decomposition

of the *o*-hydroxyphenoxymethyl radical could have contributed to the decrease, as in Figure 5-8-B ((5), (6)), although this is not favored. The decreased number of C_{arom}-C bonds may be due to the degradation of the carboxyl hydroxyl group and the C5 substituted/condensed phenolic hydroxyl groups, as in β-5 and 5-5 bonds, as presented in Figures 5-7-B and 5-8, respectively. On the other hand, the increased number of C_{arom}-H bonds may be due to the decomposition of the ether bond during pyrolysis and the degradation of C_{arom}-C bonds, as illustrated in Figure 5-8. In addition, the changes in the number of C-H bond are interrelated with the modifications in the C-C and C-O bonds. As a result, when the percentage of C-O and/or C-C bonds was reduced, the percentage of C-H bonds increased, as shown in Table 5.5. The increased number of C_{methyl}-C_{arom} bonds may be due to the cleavage of the aliphatic hydroxyl groups, as shown in Figure 5-7-A.

Table 5.6 shows the measured hydroxyl groups in this work in contrast to those published by Ben and Ragauskas, 2011 using CP (Ben and Ragauskas 2011). In general, both methods (CP and MWP) caused the same change, either an increase or a decrease, in the concentrations of the different types of OH groups in the oil relative to the virgin lignin. However, the concentration of most hydroxyl types after MWP at each temperature is lower than that in CP. For example, the concentration of aliphatic hydroxyl groups was lower after MWP than after CP. This resulted in a greater yield of the aqueous phase, in this work, than that reported in Ben and Ragauskas, 2011. Table 5.7 shows the same comparison for the carbon atoms detected by quantitative ^{13}C NMR. Again, in general, both methods (CP and MWP) caused the same change, either an increase or a decrease, in the concentrations of the different types of C atoms in the oil relative to the virgin lignin. Nonetheless, higher concentrations of C_{arom}-O and C_{arom}-H were found after MWP than after CP. The reason for that might be due to differences in the average and maximum temperatures, the difference in the virgin material characteristics, and/or the applied heating mechanism. Accordingly, further effort is needed to explore this point, which will be considered in the future work.

Table 5.6: Concentrations of different hydroxyl groups determined by quantitative 31P NMR spectroscopy of the virgin lignin and the oil phases obtained after microwave pyrolysis and conventional pyrolysis at various conditions

Functional group		**MWP (mmol/g oil)**						**CP (mmol/g oil)** (Ben and Ragauskas 2011)				
		900K	**980K**	**1065K**	**1150K**	**1240K**	**lignin**	**673K**	**773K**	**873K**	**973K**	**Lignin**
Aliphatic OH		0.18	0.17	0.31	0.06	0.08	1.48	0.28	0.36	0.36	0.35	1.73
C_5 substituted condensed phenolic OH	β-5	0.25	0.23	0.33	0.33	0.13	0.5	0.47	0.47	0.4	0.41	0.59
	4-O-5	0.22	0.2	0.26	0.29	0.09	0.32	0.26	0.31	0.31	0.34	0.42
	5-5	0.03	0.01	0.08	0.15	0.11	0.55	0.35	0.35	0.31	0.3	0.76
Guaiacyl phenolic OH		2.12	1.83	2.2	3.08	1.91	1.44	3.05	2.93	2.33	2.28	1.53
Catechol type OH		1.64	1.44	1.49	1.2	0.58	0.35	1.34	1.49	2.02	2.22	0.17
p-Hydroxy-phenyl OH		0.89	0.8	0.72	0.44	0.21	0.27	0.33	0.46	0.49	0.55	0.14
Acid-OH		0.57	0.46	0.42	0.08	0	0.43	0.26	0.33	0.37	0.37	1.05

Table 5.7: Concentrations of different types of carbon atoms measured by quantitative 13C NMR spectroscopy of an oil phase produced after microwave pyrolysis and conventional pyrolysis at various conditions

Functional group		**MWP** (C mol%)						**CP** (C mol%) (Ben and Ragauskas 2011)				
		900K	**980K**	**1065K**	**1150K**	**1240K**	**lignin**	**673K**	**773K**	**873 K**	**973 K**	**Lignin**
Carbonyl or Carboxyl		0.11	0.06	0.0	0.0	0.0	0	0.5	0.6	0.9	0.3	1.6
Aromatic C-O		23.5	23.9	26.1	28.4	25.4	32.18	15.7	16.3	16.7	20.6	27.3
Aromatic C-C		10.8	11.6	11.7	6.2	8.3	21.05	14	15.9	22.7	26.9	25.8
Aromatic C-H		46.1	42.2	39.9	42.2	43.0	21.21	36.5	33.2	29.7	29.4	26.4
Aliphatic C-O		0.0	0.0	0.0	0.1	0.0	0	0.6	0.5	0.1	0.5	5.8
Methoxyl-Aromatic		9.5	10.4	11.5	12.3	11.1	22.38	9.6	8.5	5.4	4.5	12.9
Aliphatic C-C	Total	10.0	12.0	10.7	10.8	12.1	3.19	23.1	25	24.4	17.8	0.3
	Methyl - Aromatic	4.3	6.0	5.6	5.4	5.7	0	3.9	4.3	4.5	3.2	0.0
	Methyl - Aromatic ortho to a hydroxyl or methoxyl group	5.4	4.3	4.2	4.3	4.6	0	2.4	2.7	3.3	2.2	0.0

5.4 Conclusions and Future Work

A detailed compositional analysis and structural investigation of bio-oil produced via microwave pyrolysis (MWP) of Kraft lignin was accomplished. MWP was performed at different conditions of weight-% of a thermal-microwave-catalyst (char, 20-40%) and nominal power setting (1.5-2.7 kW). GC-MS analysis was implemented on the oil and aqueous phases, and ^{31}P and ^{13}C NMR analyses were performed on the oil phase and the virgin material. One of the main conclusions of this work includes the greater effect of char wt% than power setting on the heating rate. Increasing the pyrolysis final temperature augmented the total obtained liquid yield. However, beneficial depending on the structure of the liquid phases as well as the water content. The identified concentrations of chemical compounds obtained in the oil phase were 173.9-237.4 mg/g in contrast to 9.3-24.1mg/g identified in the aqueous phase. Nonetheless, a concentration of 583-707 mg/g of the oil phase could not be identified, due to the limitations of the GC-MS. Therefore, a GC-MS analysis is inadequate to provide a detailed structure of the pyrolysis liquids. On the basis of ^{31}P and ^{13}C NMR analyses, up to 80% of the carbon atoms in the oil phase were aromatic carbons. The concentration of aliphatic hydroxyl groups in the virgin material was significantly decreased by the MWP. This was attributed to water forming during the thermal degradation of the lignin network. The decreased concentrations of *C5* substituted/condensed phenolic hydroxyl groups after MWP could be attributed to the increase in the concentrations of guaiacyl, *p*-hydroxyphenyl, and catechol hydroxyl groups.

One of the demonstrated conditions will be performed in a kinetic modeling study to simulate the MWP products, solid, liquid, and gas, as well as the extracted chemicals phenolics, aliphatics, and tar using a lumping approach.

5.5 Acknowledgements

The authors thank Mr. Yazid Belkhir and Mr. Robert Delisle (Technicians at Ecole Polytechnique Montreal) for their assistance in the experimental setup, and Dr. Levent Erdogan (Electrical Engineering Department, Ecole Polytechnique Montreal) and Ms. Mai Attia (Student at UQAM University Montreal) for their assistance in this work. In addition, the authors are grateful for the

financial and technical support from Lignoworks NSERC Strategic Network (lignoworks.ca), and providing the virgin material from FPInnovations, Montreal, Quebec, Canada.

CHAPTER 6 ARTICLE 4: A LUMPED APPROACH IN KINETIC MODELING OF MICROWAVE-PYROLYSIS OF KRAFT LIGNIN

Sherif Farag[a], Lamfeddal Kouisni[b], and Jamal Chaouki[a]

[a]CRIP-Biorefinery Centre, Department of Chemical Engineering, École Polytechnique de Montréal.

P.O. Box 6079, Station Centre-ville, Montréal, QC, Canada H3C 3A7.

[b]FPInnovations-Pulp&Paper Division, 570 Saint-Jeab Blvd. Pointe-Claire, QC, Canada

(Published in energy & fuels Journal, DOI: 10.1021/ef4023493)

Presentation of the article: The MW-TGA that was built in the second article and the obtained results in the third article will be employed to describe the kinetics of microwave pyrolysis of kraft lignin. Three different models will be presented: the first model, considers the virgin material converted into solid, condensable gas, and non condensable gas. The second model distinguishes between the water and the chemicals extracted in the condensable gas. The third model presents further investigations for the extracted chemicals in the oil phase.

Abstract

This work presents three kinetic models based on a lumping approach to describe the microwave pyrolysis of kraft lignin. The first model considered the formation of the main pyrolysis products, condensable gas, non-condensable gas, and the remaining solid, taking into consideration each as an individual lump. The second model investigated the liquid product while dividing the condensable gas into oil and water products. The oil product contains only chemicals whereas the water product does not contain any chemicals. In the third model, the oil product was separated into four main groups: (1) phenolics, which contain all the identified phenolic components using a GC-MS analyzer; (2) heavy molecular weight components, which contain all the identified heavy molecular weight and undefined components, using GC-MS; (3) non-phenolic aromatics with a single ring; and (4) aliphatics. The comparison of the predicted results using the estimated kinetic parameters against the experimental data showed the high capability of the presented models to estimate the products yield under the selected conditions.

Keywords: Microwave Pyrolysis, Microwave-thermo-gravimetric Analyzer, Kraft lignin, and Reaction Kinetics

6.1 Introduction

Lignocellulosic biomass is composed of three intertwined components: cellulose, hemicellulose, and lignin. The percentage of each varies from one species to another, one environment to another, and depending on many other conditions. Generally, the dry weight basis of each component is 35-45%, 25–30%, and 20–35%, respectively (Zakzeski, Bruijnincx et al. 2010, de Wild, Huijgen et al. 2012, Mu, Ben et al. 2013). Lignin is considered the only renewable source of aromatic hydrocarbons on earth and is the third most abundant natural polymer after cellulose and hemicellulose (Zakzeski, Bruijnincx et al. 2010, Kibet, Khachatryan et al. 2012, Mu, Ben et al. 2013). In the US paper industry, the annual production of lignin as a byproduct is over 50 million tons; however, only 2% of this amount is converted into bio-products, while the rest is combusted to recover energy and recycle the pulping chemicals.

Lignin can be considered as a renewable resource with a great potential as an alternative to fossil fuel based chemicals. This approach would be one of the best routes to valorize lignin and deal with the challenges that have been facing the Canadian forest industry for the last few years. Furthermore, it would help to compensate for the increase in demand and prices for energy and chemicals.

In general, thermal, biological, and physical technologies are the three most popular technologies used to convert lignin into energy and/or chemicals. Pyrolysis is one of the techniques belonging to thermal technology. It is the thermal decomposition of the chemical bonds of a target material by means of supplying heat in an inert environment. The case of providing essential heat energy via electromagnetic irradiation is called microwave pyrolysis (MWP), which is applied in this work. Further information regarding the fundamentals of microwave heating can be found in references (Farag, Sobhy et al. 2012, Doucet, Laviolette et al. 2013).

Pyrolysis of lignin produces three main products: (1) solid, which is mostly carbon ≈ 90 wt%; (2) non-condensable gas, which is combustible; and (3) condensable gas. The condensable gas can be

separated into oil and aqueous phases. The oil phase is denser than the aqueous phase and mostly aromatics, whereas the aqueous phase is mostly water, ≈75 wt% (Farag., Fu. et al. 2013). The yield of these products depends on several parameters, such as pyrolysis temperature, heating rate, residence time, presence of a catalyst, pyrolyser design, and the characteristics of the virgin material, etc.

In the scientific literature, the pyrolysis of lignin has been investigated from several different aspects, such as product distributions (Jiang, Nowakowski et al. 2010, Lou and Wu 2011), presence of a catalyst (Mullen and Boateng 2010, Rutkowski 2011), and reaction kinetics (Ferdous, Dalai et al. 2002, Montané, Torné-Fernández et al. 2005, Mani, Murugan et al. 2008, Faravelli, Frassoldati et al. 2010, Jiang, Nowakowski et al. 2010, Janković 2011). However, only a modest effort was made in these investigations. Nevertheless, in spite of this modest effort, publications that investigate the kinetics of pyrolysis products compositionally are quite scarce in the literature. This is a consequence of the particular requirements in the experimental setup, which forced most of the researchers investigate the kinetic of devolatilization rather than the kinetics of individual products. Accordingly, a kinetic study that takes into consideration the composition of the pyrolysis products is essential. Such a study would lead to an improved understanding of the underlying processes and provide the necessary information for the rational design and scaling-up of pyrolysis reactors. Therefore, this work does not only intend to investigate the kinetics of lignin MWP products, i.e., solid, liquid, and gas, but will also consider further details about the composition of the liquid phase.

In order to achieve this objective, the microwave thermo-gravimetric analyzer (MW-TGA) that was used in Farag and Chaouki 2013 (Farag. and Chaouki. 2013) was modified and employed in this work. The modifications made in this setup make it possible to distribute the vapor product up to 7 parts during MWP, which makes the kinetic investigation of the pyrolysis products compositionally attainable.

This work was carried out by applying the best experimental condition reported in reference (Farag., Fu. et al. 2013), which gave the maximum concentration of phenolics in the liquid product. CHNS, ^{13}C NMR, ^{31}P NMR, and approximate analyses were implemented on the virgin material. Gas Chromatograph-Mass Spectrometer (GC-MS) analysis and water content measurement were performed on the obtained liquids. Subsequently, the results were processed mathematically to calculate the yield of each product at the selected temperatures. Finally, three kinetic models based on the lumping approach were applied, and their kinetic parameters were estimated. The yield of each product was predicted using the estimated parameters and then compared against the experimental data to validate the presented models.

6.2 The Experimental Work

6.2.1 The Virgin Material

In this work, the virgin material was softwood kraft lignin supplied by FPInnovations, Pointe-Claire, Quebec, Canada. It was precipitated from a Canadian kraft mill using The LignoForce System™ a patent pending process that was developed by FPInnovations and licenced to NORAM Engineers and Constructors, Vancouver, BC, Canada for commercialization. Lignin was characterized by CHNS elemental analysis (C=63.27%, H=5.79%, N=0.07%, and S=1.56%), and approximate analysis (fixed carbon=37%, volatiles=62%, and ash=1%). The ^{13}C and ^{31}P NMR analyses were performed on the virgin material and reported in reference (Farag., Fu. et al. 2013) and will, therefore, not be presented here.

According to the dielectric and physical properties of the virgin material, lignin is not a good microwave-to-heat convertor. However, it needs a high temperature to fully decompose as its structure is rather complex. Therefore, enough heat energy must be provided for the occurrence of pyrolysis. Otherwise, the extracted product takes the form of a tar-like product, which is ex-pulsed out of the lignin particles forming an extremely sticky material. Finally, after cooling, the formed material converts into a very strong block, which is exceedingly difficult to break down. Accordingly, lignin was mixed with char, which is the solid product of the MWP of lignin, by a constant ratio of 30% weight basis. Char was only considered as a microwave-to-heat convertor,

which does not have any effect on either the reaction mechanism or the weight loss measurements.

6.2.2 The Experimental Setup

The experimental work was carried out on a bench scale MW-TGA connected with a product manifold, as shown in Figure 6-1: The experimental setup, MW-TGA connected with a product manifold

. MW-TGA consists of a microwave-oven (MW-O) (Microwave Research Inc; Model: BP-211, 230 V, 2.45 GHz, and setting power up to 3.2 kW) with two modifications. The first one makes it possible to measure the weight loss of the heated material during the pyrolysis, and the second enables measuring the transit mean temperature within the heated material. A detailed description of these two modifications was reported in reference (Farag. and Chaouki. 2013) and will, therefore, not be repeated here.

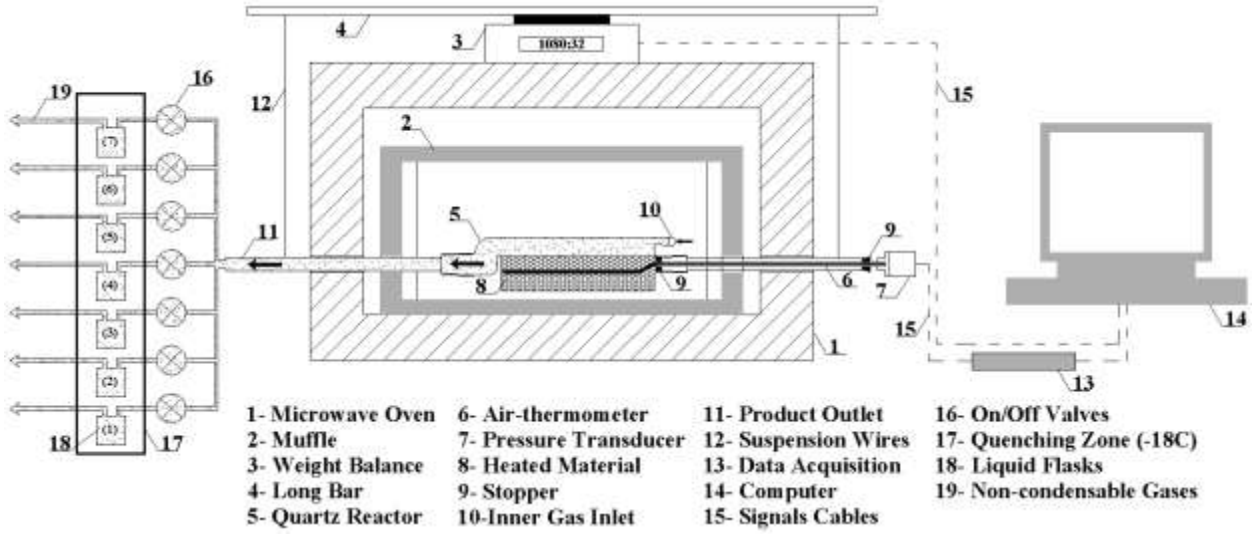

Figure 6-1: The experimental setup, MW-TGA connected with a product manifold

The product manifold consists of seven on/off manual ball valves connected together at one end with the outlet of a semi-batch quartz reactor. Each of the other ends was connected with a

condenser, kept at -18 ^{o}C using a traditional freezer. The condensation system consists of sets of vertical metallic tubes. Each set was connected in series at one end, whereas the other end was connected to a 500 ml two neck Pyrex flask. These flasks were used to collect the condensable gases while the non-condensable gas passes directly through. In order to prevent a vapor condensation barrier to the condensers forming, all the connections and the product manifold were kept at 200 ^{o}C using external-temperature heat cables (Flexible electric heating tape, AWH-051-020D; 760 ^{o}C; 1.3 A; 156 W; and 120 V, HTS/Amptek, USA)

6.2.3 The Method

The procedures of the experimental work are described below. First, the freezing zone was switched on to reduce the condensers temperature to -18 ^{o}C. In the meantime, the electric heaters were switched on to keep the temperature barrier to the condensation system at 200 ^{o}C. Second, the reactor was filled with an initial mass of 70 wt% of lignin + 30 wt% of char and then connected as shown in Figure 6-1: The experimental setup, MW-TGA connected with a product manifold

. Subsequently, the signal cables of the scale and the thermometer were connected with a data acquisition system, and the whole system was purged by an inert gas (N_2). Third, the valves of the product manifold were closed, except for valve number 1, which was kept open. After that, the oven power was adjusted to 2.1 kW and switched on for 800 s, which is the required time for full conversion. Once the payload temperature reached T_1, which is a selected temperature, valve number 2 was turned on, and at the same time valve number 1 was turned off. The same procedures were repeated at the other selected temperatures, T_2, T_3, T_4, T_5, and T_6, which led to the collection of the liquid product within different temperature ranges. Within the limitations of the design setup, 6 liquids in total could be collected. Finally, after 800 s of MWP and once the obtained liquids and the solid product had reached the ambient temperature, they were collected and weighted. The mass of the non-condensable gas was calculated by subtracting the liquid and solid masses from the initial mass of lignin. The obtained liquids were separated into the oil phase, which is the dense one and contains mostly chemicals and the aqueous phase, which is lower in density than the oil phase, and contains mostly water.

The analyses of every liquid sample (12 samples in total) were carried out at FPInnovations, QC, Canada, using a Varian 3900 GC equipped with a Saturn 2100T MS (ion trap) and selective ion chromatogram for peak integration. The column used was DB-1701, 30 m × 0.25 mm ID× 0.25 µm film thickness with an injector temperature of 280 °C. Helium was used as the carrier gas with a constant flow rate of 1 ml/min and a split ratio of 75:1. The MS scan range was 41-650 amu, 70 eV, with an ion trap detector and the transfer line temperature was 300 °C. The oven was held at 70 °C for 2 min and then ramped up at 5 °C/min to 300 °C; the total run time was 48 min.

Prior to the GC-MS injection, 25 µl of each oil phase was diluted to 1 ml of MeOH, while 250 µl of each aqueous phase was diluted to 1 ml of MeOH. Then, every sample was filtered with a 5 µm Teflon membrane to remove the presence of particles. The identification of the individual compound was performed by comparing the mass spectrum to those reported in the "NIST MS Search V2.0" Library. Identification of a probability match using the GC-MS software library is less than 90 for a good portion of the compounds. Quantitation is based on an internal standard with a relative response factor of 1 used for all compounds.

Water content in the oil and aqueous phases was measured using a Metrohm Titrando 836/803 with a KF titration unit.

Transient mean temperatures were measured using the innovated thermometer that was used in Farag. and Chaouki. 2013 (Farag. and Chaouki. 2013); kindly refer to that paper for a detailed description, calibration, and validation of this thermometer. Figure 2 shows the measured values, using this thermometer, and the predicted ones, using the mathematical model published in Farag, Sobhy et al. 2012 (Farag, Sobhy et al. 2012), taking into consideration the characteristics of lignin as well as the pyrolysis conditions.

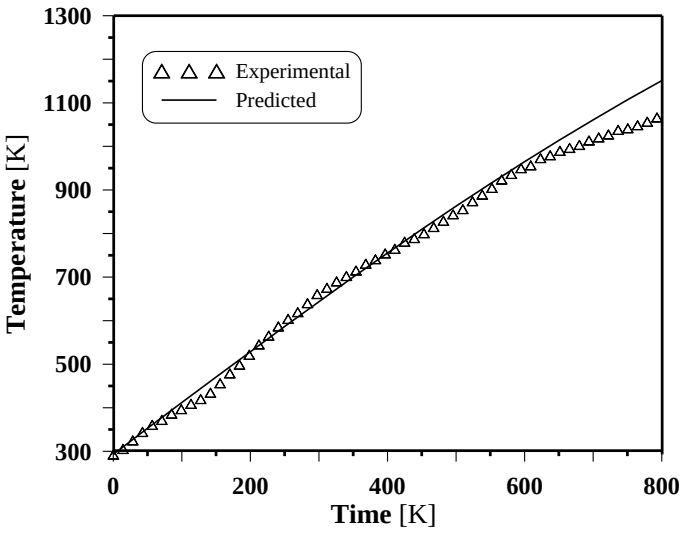

Figure 6-2: The measured and the predicted transient mean temperature of the MWP of Kraft lignin at 2.1 kW and 30 wt% char

6.3 The Implemented Kinetic Models

Three different kinetic models based on the lumping approach were implemented in this work. The first model considered that the virgin material was converted into three main products: solid, condensable gas, and non-condensable gas. The condensable gas was separated into oil and aqueous phases, and the water content was measured in both phases. Subsequently, further mathematical processes were carried out on the measurements to present two products: oil, which has only chemicals with no water content; and water, which does not contain any chemicals. Herein, since the virgin material was first dried, the obtained water was considered as a product, which could be the result of a cleavage of the lignin site chain hydroxyl groups, as was presented in references (Farag., Fu. et al. 2013). Therefore, the second model assumed that the lignin was converted into four main products: solid, oil, water, and non-condensable gas.

GC-MS was performed on the oil phase as well as the aqueous phase. Then, the results were processed mathematically to present the yield of four chemical groups at the selected temperatures: (1) phenolics group, which contains all the identified phenolic components; (2) heavy molecular weight components group (HMWC), which contains all the heavy molecular

weight and unidentified components using the GC-MS analyzer; (3) aromatics with a single ring non-phenolics group (ASR-Non-Ph); and (4) aliphatics group, which contains all the identified aliphatic components. Accordingly, the third model considered that lignin was converted into seven products: the previous four chemical groups, plus solid, water, and non-condensable gas products.

6.3.1 The First Model

The first model assumes the reactant, which is the virgin material, is converted into three products: solid, condensable gas, and non-condensable gas. Each product is formed via a parallel elementary reaction, as follows.

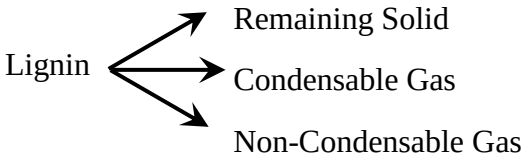

$$\frac{dS}{dt} = -k_{o_s}\left(e^{\frac{-E_{a_s}}{RT}}\right)(S - S_\infty)^{n_s} = -k_{o_l}\left(e^{\frac{-E_{a_l}}{RT}}\right)(S - S_\infty)^{n_l} - k_{o_g}\left(e^{\frac{-E_{a_g}}{RT}}\right)(S - S_\infty)^{n_g} \quad (6\text{-}1)$$

$$\frac{dL}{dt} = k_{o_l}\left(e^{\frac{-E_{a_l}}{RT}}\right)(S - S_\infty)^{n_l} \quad (6\text{-}2)$$

$$\frac{dG}{dt} = k_{o_g}\left(e^{\frac{-E_{a_g}}{RT}}\right)(S - S_\infty)^{n_g} \quad (6\text{-}3)$$

where; k_o is the pre-exponential factor [time^{-1}], E_a is the apparent activation energy [J/mol K], T is the reaction temperature [K], and R is the universal gas constant [J/mol K]. The subscripts *s, l,* and g are referring to the solid product, which is the remaining solid as it is very difficult to distinguish between the un-reacted lignin and the produced char; the liquid, which is the condensable gas; and gas, which is the non-condensable gas, respectively. *S*, *L and G* are the remaining solid, the condensable gas, and the non-condensable gas yields at any time/temperature

[-], respectively. S_∞ is the final solid yield, which is the measured weight of solid at the final temperature to the feed weight of lignin [-].

6.3.2 The Second Model

As mentioned earlier, the second model considers that the virgin material is converted into four products: solid, oil, water, and non-condensable gas. Each was formed via a parallel elementary reaction with its own kinetic parameters, as follows.

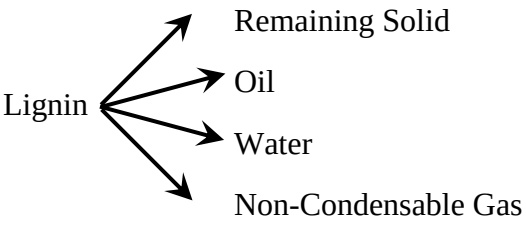

$$\frac{dS}{dt} = -k_{o_s}\left(e^{\frac{-E_{a_s}}{RT}}\right)(S - S_\infty)^{n_s} = -k_{o_o}\left(e^{\frac{-E_{a_o}}{RT}}\right)(S - S_\infty)^{n_o} - k_{o_w}\left(e^{\frac{-E_{a_w}}{RT}}\right)(S - S_\infty)^{n_w} - k_{o_g}\left(e^{\frac{-E_{a_g}}{RT}}\right)(S - S_\infty)^{n_g} \quad (6\text{-}4)$$

$$\frac{dO}{dt} = k_{o_o}\left(e^{\frac{-E_{a_o}}{RT}}\right)(S - S_\infty)^{n_o} \quad (6\text{-}5)$$

$$\frac{dW}{dt} = k_{o_w}\left(e^{\frac{-E_{a_w}}{RT}}\right)(S - S_\infty)^{n_w} \quad (6\text{-}6)$$

where, *o* and *w* refer to the oil and water products. *O* and *W* are the yields of the oil and water products, respectively. The remaining solid and the non-condensable gas yields can be obtained from Equations (6-2) and (6-3), respectively.

6.3.3 The Third Model

The third model takes into consideration the chemical composition of the liquid product. Therefore, it considers the reactant is converted into seven products: remaining solid, phenolics, ASR-Non-Ph, aliphatics, HMWC, water, and non-condensable gas.

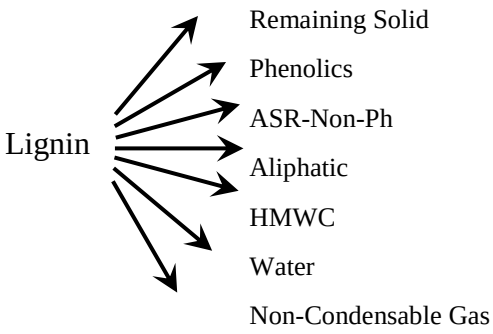

$$\frac{dS}{dt} = -k_{o_s}\left(e^{\frac{-E_{a_s}}{RT}}\right)(S-S_\infty)^{n_s} = -k_{o_{Ph}}\left(e^{\frac{-E_{a_{Ph}}}{RT}}\right)(S-S_\infty)^{n_{Ph}} - k_{o_{ASR-Non-Ph}}\left(e^{\frac{-E_{a_{ASR-Non-Ph}}}{RT}}\right)(S-S_\infty)^{n_{ASR-Non-Ph}} - k_{o_a}\left(e^{\frac{-E_{a_a}}{RT}}\right)(S-S_\infty)^{n_a} - k_{o_t}\left(e^{\frac{-E_{a_t}}{RT}}\right)(S-S_\infty)^{n_t} - k_{o_w}\left(e^{\frac{-E_{a_w}}{RT}}\right)(S-S_\infty)^{n_w} - k_{o_g}\left(e^{\frac{-E_{a_g}}{RT}}\right)(S-S_\infty)^{n_g} \quad (6\text{-}7)$$

$$\frac{dPh}{dt} = k_{o_{Ph}}\left(e^{\frac{-E_{a_{Ph}}}{RT}}\right)(S-S_\infty)^{n_{Ph}} \quad (6\text{-}8)$$

$$\frac{d(ASR-Non-Ph)}{dt} = k_{o_{ASRNP\ h}}\left(e^{\frac{-E_{a_{ASRNP}}}{RT}}\right)(S-S_\infty)^{n_{ASR-Non-Ph}} \quad (6\text{-}9)$$

$$\frac{dA}{dt} = k_{o_a}\left(e^{\frac{-E_{a_a}}{RT}}\right)(S-S_\infty)^{n_a} \quad (6\text{-}10)$$

$$\frac{d(HMWC)}{dt} = k_{o_{HMWC}}\left(e^{\frac{-E_{a_{HMWC\ t}}}{RT}}\right)(S-S_\infty)^{n_{HMWC}} \quad (6\text{-}11)$$

where *Ph*, *ASR-Non-Ph*, *A*, and HMWC are the instantaneous yield of phenolics, aromatics with a single ring non-phenolics, aliphatics, and heavy molecular weight components group,

respectively. The water yield can be obtained from Equation (6-6), whereas the remaining solid and the non-condensable gas yields can be had from Equations (6-2) and (6-3), respectively.

In order to eliminate the effect of the heating rate (β), the reaction rate equations from (6-1) to (6-11) were divided by β. Therefore, they become temperature based rather than time based, which means the left hand side becomes $\frac{d}{dT}$ rather than $\frac{d}{dt}$.

6.4 The Parameters Estimation

In order to estimate the kinetic parameters, k_o, E_a, and n, the reaction rate equations of each model were implemented in MATLAB® program codes after the transfer to a linear domain, as in the form of equation (6-12).

$$y = a_o + a_1 x_1 + a_2 x_2 \tag{6-12}$$

where, the dependent parameter, y, is the natural logarithm (ln) of dS/dT, and a_o, a_1 and a_2 are constants equal to ln k_o/β, E_a/R, and n, respectively. The independent parameters, x_1 and x_2, represent $1/T$ and ln (S- S_∞), respectively.

MATLAB's fminsearch/fminsearchbnd was applied using the initial conditions that were obtained from the experimental work. The optimum values of the estimated parameters were acquired based on minimizing the square difference between the predicated result and the experimental data (y^{Model} and y^{Exp}), according to equations (6-13) and (6-14), where N is the number of fitted points and p is the number of model parameters (Chen, Zhang et al. , Radmanesh, Courbariaux et al. 2006). Furthermore, a contour map was created to obtain an overall view for all the suitable values, and then the optimal ones were chosen.

$$Obj = \frac{1}{N-p}\sum_{i=1}^{n}(x_i^{Model} - x_i^{Exp})^2 \tag{6-13}$$

$$Deviation - \% = 100 \times \sqrt{Obj} \tag{6-14}$$

The estimated parameters were applied to predict the yields of each product using Ode(s) MATLAB's solvers to solve the ordinary differential equation of each implemented model.

6.5 The Results and Discussions

Microwave pyrolysis of kraft lignin was carried out using a constant weight percentage of a microwave-to-heat converter, 30%, and a constant nominal power setting, 2.1 kW. Figure 6-3-A demonstrates the transient remaining solid fraction at the selected temperatures, experimental and predicted. The experimental data was fitted using the scenario explained previously. In order to check the sensitivity of the implemented model, different reaction orders including a first and second order were applied during the fitting procedures. The first and second reaction orders are presented here, while the remaining orders were found in-between and are, therefore, not presented. Figure 6-3-B shows a contour map for the deviations between the experimental data and the predicted results at different estimated values of k_o and corresponding values of E_a. This was performed by applying a first order reaction rate as it is representative of the experimental results much better than the other investigated orders. Consequently, the first order reaction rate was chosen for the remaining solid fraction for the remainder.

Figure 6-3-C shows the condensable gas yield, while Figure 6-3-D illustrates the non-condensable gas yield at the selected temperatures. Table 6.1 presents the estimated kinetic parameters of the remaining solid fraction, condensable gas, and non-condensable gas at a first order reaction rate.

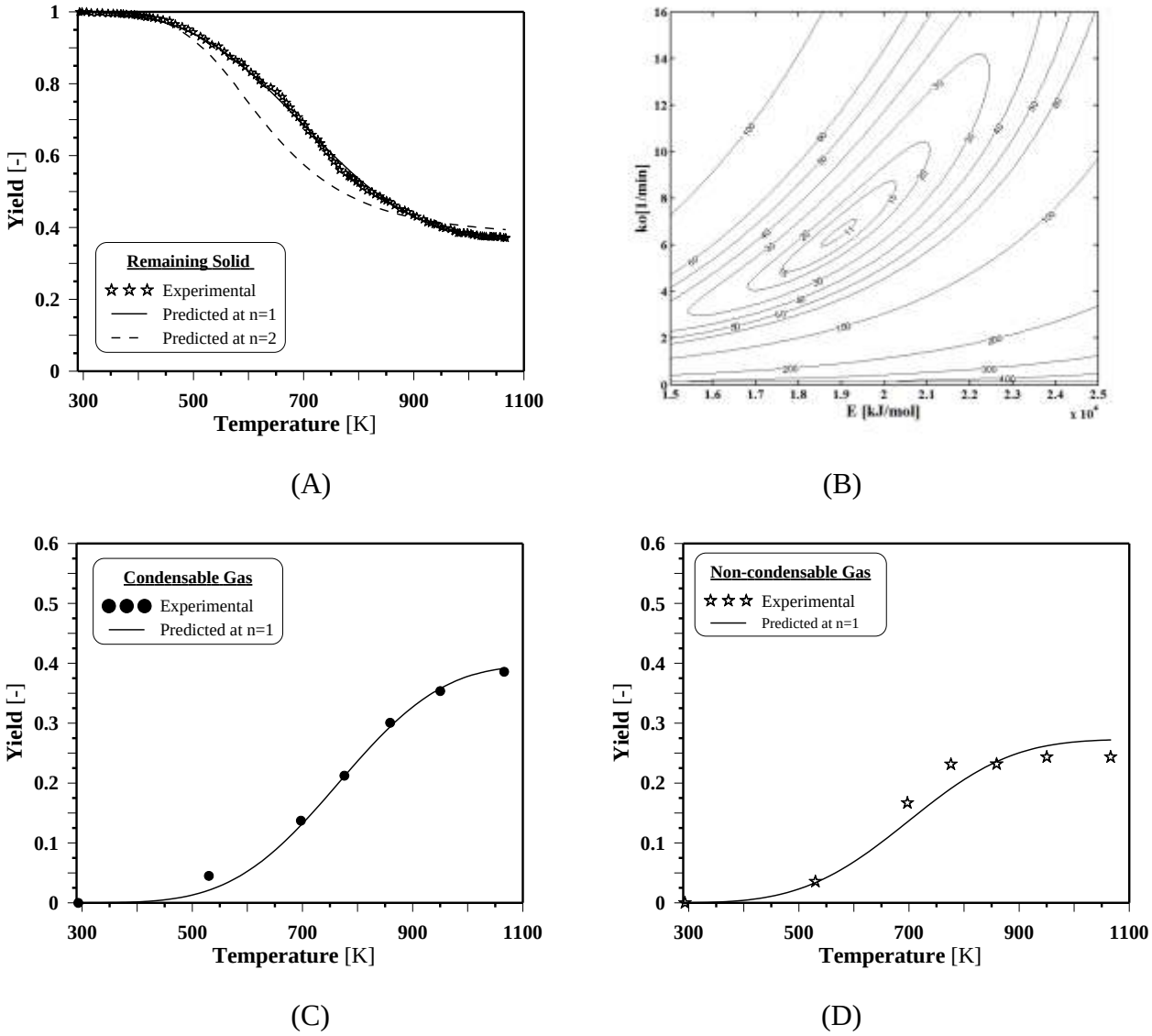

Figure 6-3: (A) The experimental and predicted remaining solid fraction, (B) the contour map of the calculated deviations using a first order reaction rate, (C) the transient condensable gas yield, and (D) the transient non-condensable gas yield

Table 6.1: The estimated kinetic parameters of the 1st pyrolysis model

Product	k_o **[min^{-1}]**	E_a **[kJ/mol]**	n
Remaining Solid	7	19	1
Condensable Gas	22	29	1
Non-Condensable Gas	6	22	1

Comparing between Figure 6-3-C and Figure 6-3-D can show that upon 725 K, the non-condensable gas yield is slightly higher than that of the condensable gas. On the other hand, beyond 725 K, the condensable gas yield continues increasing more than the non-condensable. This could be the consequence of the swift split in lignin site chains, which are mostly aliphatic hydroxyl groups, to form water, non-condensable gas, and/or unsaturated sites. Accordingly, the total water yield should be little higher than the total oil yield during the temperature range from ambient temperature (T_{amb}) to 725 K. Further information regarding this degradation was reported in reference (Farag., Fu. et al. 2013). The increases in the condensable-gas yield beyond 725 K could be the result of decomposing strong chemical bonds of the lignin network. Therefore, the oil yield should be higher than the water yield beyond 725 K.

According to Table 6.1, the rate of thermal cracking of lignin is higher than that of condensable gas, which could point out that the likelihood of secondary reactions is low under these conditions. The estimated activation energy of the non-condensable gas is lower than that of the condensable gas. This is a consequence of the non-condensable gas mostly produced from the decomposition of lignin site chains, while the condensable gas is produced from the breakdown of bonds between lignin aromatic rings. At low temperature/heating rate, the solid yield will be higher than the gas yield, which is known in the case of slow pyrolysis (Motasemi and Afzal 2013).

The condensable gas was divided into oil and aqueous phases and then the water content was measured in both. Table 6.2 shows the measured value in every sample at the corresponding temperatures. The obtained measurements were processed using equation (6-15) to calculate the accumulated yield of water.

Table 6.2: The The measured water content in the aqueous and oil phases

Temperature range [K]	**Aqueous Phase [wt%]**	**Oil Phase [wt%]**
295 - 530	90	8
530 - 697	90	8
679 - 776	80	8
776 - 859	89	8
859 - 950	84	8
950 - 1066	80	7

$$Water\ Yield_T = \frac{\sum_{i=T_{amb}}^{i=T} \left[(w_{aq}\% \times m_{aq})_i + (w_o\% \times m_o)_i\right]}{m_i} \quad (6\text{-}15)$$

$$Oil\ Yield_T = \frac{\sum_{i=T_{amb}}^{i=T} \left[((100 - w_{aq}\%) \times m_{aq})_i + ((100 - w_o\%) \times m_o)_i\right]}{m_i} \quad (6\text{-}16)$$

where, *water yield*$_T$ is the ratio between the weight of the formed water at temperature *T* to the initial feed weight of lignin [wt%]. The w_{aq}% and w_o% are the measured water content in the aqueous and oil phases [wt%], respectively. The m_{aq}, m_o, and m_i are the obtained weights of the aqueous phase, oil phase, and initial feed of lignin [g], respectively. The same scenario was performed to calculate the accumulated yield of oil, using equation (6-16).

Figure 6-4-A demonstrates the accumulated yield of the obtained oil at the selected temperatures, which contains 0% water content. Figure 6-4-B illustrates the yield of the water, which contains 0% chemicals. Table 6.3 shows the kinetic parameters of the two products, while for the solid and non-condensable gas products, the parameters can be obtained from Table 6.1.

As expected, the swift split of the lignin site chains formed mainly water in addition to the non-condensable gas, and/or the unsaturated sites. As a result, the water yield was found to be slightly higher than the oil yield in the temperature range from T_{amb} to 725 K. In contrast, as soon as the temperature reached 725 K, the water yield became lower than the oil yield. As a result, the temperature of 725 K could be a critical temperature as most of the lignin network site chains had been decomposed.

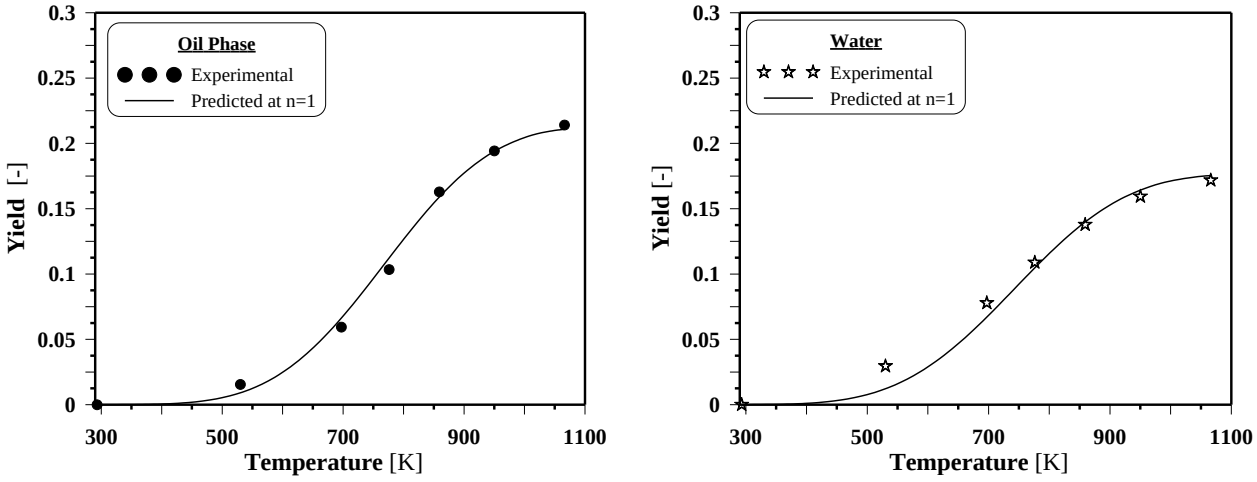

(A) (B)

Figure 6-4: The experimental and predicted yield of: (A) the oil phase and (B) formed water. The points are the experimental, and the line is the fitting

Table 6.3: The estimated kinetic parameters of the water and oil products.

Product	k_o **[min^{-1}]**	E_a **[kJ/mol]**	n
Water	9	27	1
Oil	27	33	1

According to Table 6.3, the estimated activation energy of the water is lower than that of the oil, as the water is mostly formed due to the cleavage of the lignin site chains, whereas the oil is formed due to the decomposing stronger bonds in the lignin network. Therefore, at high temperature, the formation rate of oil is higher than that of formatting the water.

As mentioned above, the third model predicts the yield of the selected chemical groups. To achieve this objective GC-MS was performed on the oil phase as well as the aqueous phase, in a total of 12 samples, using the method that was mentioned above.

Figure 6-5 depicts the typical GC-MS chromatographs of the analyzed samples, and Table 6.4 summarizes the integration for every sample. In the GC-MS spectrum, the numbers from 1 to 6 refer to the collected sample temperature range, e.g., number 1 means the sample was collected within the first temperature range, from 295K to 530K, etc. The letters *h* and *L* refer to the oil phase and the aqueous phase, respectively.

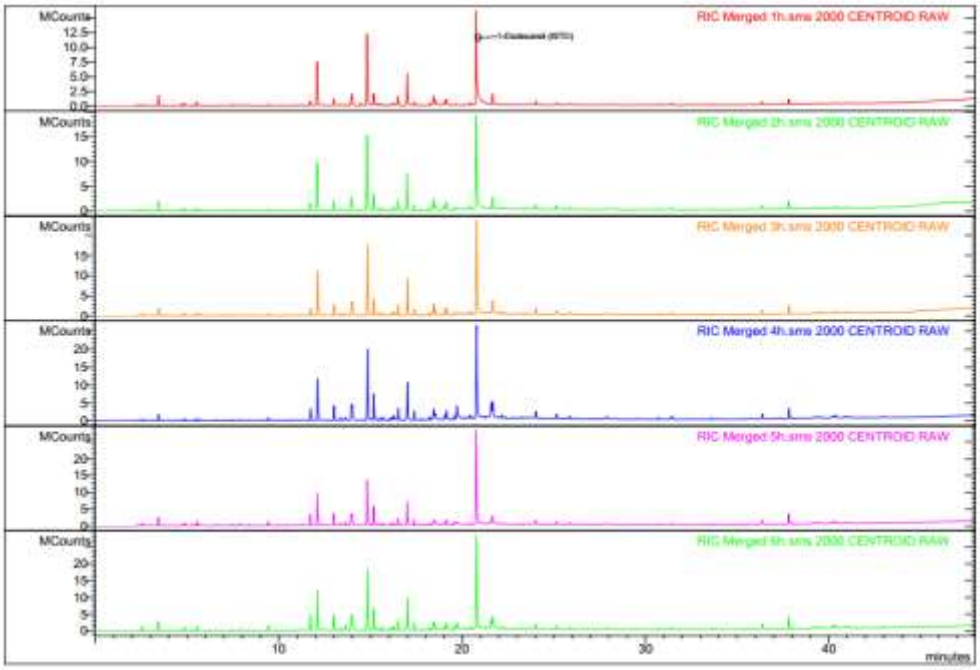

(A)

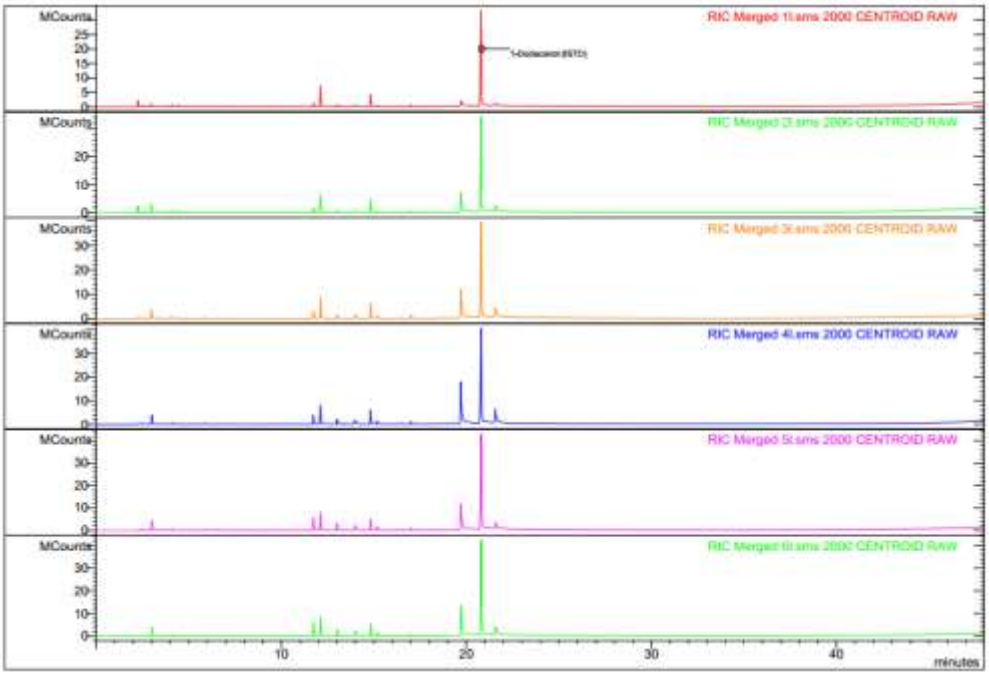

(B)

Figure 6-5: The typical GC-MS chromatographs: (A) the oil phase, and (B) the aqueous phase

Table 6.4: The identified chemical components in the oil and aqueous phases using GC-MS [mg/g]

Identification by GC-MS	The Oil-phase						The Aqueous-phase					
	295-530K	530-697K	697-776K	776-859K	859-950K	950-1066K	295-530K	530-697K	697-776K	776-859K	859-950K	950-1066K
Pentane	2.491	2.337	2.142	1.248	1.291	1.129	0.393	0.000	0.309	0.267	0.346	0.282
Propane, 1,1-dimethoxy-	0.435	0.218	0.000	0.000	0.000	0.000	0.098	0.096	0.018	0.000	0.000	0.000
Acetic acid	0.000	0.000	0.000	0.442	0.000	0.000	0.455	0.958	1.177	0.418	0.336	0.300
Ethanol, 1-methoxy-, acetate	0.000	0.000	0.000	0.000	0.000	0.000	0.000	0.000	0.098	0.037	0.060	0.000
Toluene	19.238	15.800	16.958	11.295	16.223	18.197	0.010	0.019	0.028	0.015	0.043	0.033
Propanoic acid	0.000	0.000	0.000	0.000	0.000	0.000	0.012	0.037	0.063	0.083	0.078	0.002
Methanethiol	0.000	0.000	0.000	0.000	0.000	0.000	0.244	0.213	0.089	0.139	0.000	0.000
Methane, (methylsulfinyl)(methylthio)-	0.366	0.000	0.000	0.000	0.000	0.000	0.228	0.209	0.088	0.000	0.000	0.000
Ethylbenzene	3.926	2.872	2.806	1.422	2.166	2.410	0.000	0.000	0.000	0.000	0.000	0.000
2-Propanol, 1-(1-methylethoxy)-	0.000	0.000	0.000	0.000	0.000	0.000	0.048	0.034	0.024	0.000	0.000	0.000
p-Xylene	1.763	1.445	1.138	1.000	1.758	1.737	0.000	0.000	0.000	0.000	0.000	0.000
1,3,5,7-Cyclooctatetraene	4.048	3.017	2.653	1.983	3.711	4.042	0.000	0.000	0.000	0.000	0.000	0.000
3-Cyclopentene-1-acetaldehyde, 2-oxo-	0.889	1.000	1.160	0.617	0.319	0.000	0.066	0.064	0.066	0.058	0.061	0.022
Propanal, 3-(methylthio)-	0.615	0.388	0.250	0.000	0.000	0.000	0.084	0.040	0.024	0.007	0.010	0.000
Benzene, 1,2,3-trimethyl-	1.206	0.935	0.869	0.620	0.733	0.678	0.000	0.000	0.000	0.000	0.000	0.000
Benzene, 1-propynyl-	2.736	2.536	2.617	3.184	5.833	7.221	0.000	0.000	0.000	0.000	0.003	0.003
Benzenesulfonic acid, 4-hydroxy-	8.384	11.016	13.069	19.486	16.749	23.426	0.560	0.750	1.168	1.508	2.086	2.541
Mequinol (4-Methoxy-phenol)	56.142	49.955	54.998	48.054	30.897	38.329	2.203	2.128	2.401	2.159	1.831	1.985
Phenol, 2-methyl- (O-cresol)	6.744	7.812	10.210	12.578	10.402	12.687	0.185	0.216	0.351	0.401	0.517	0.546
Phenol, 2,3-dimethyl-	2.017	2.086	2.156	2.606	2.221	2.407	0.019	0.022	0.032	0.041	0.041	0.049
Naphthalene	2.140	1.677	2.073	3.568	4.740	7.249	0.000	0.000	0.000	0.000	0.001	0.000
Phenol, 3-methyl- (m-cresol)	8.857	11.485	11.217	15.432	13.192	16.087	0.067	0.110	0.292	0.340	0.310	0.264
Phenol, 2-methoxy-3-methyl-	11.098	9.299	10.363	8.819	5.712	7.412	0.081	0.071	0.103	0.099	0.080	0.066
Phenol, 3-methoxy-2-methyl-	8.640	7.986	17.369	26.144	14.004	20.604	0.280	0.377	0.606	0.528	0.775	0.927
Tetrasulfide, dimethyl	2.568	1.128	0.585	0.000	0.000	0.000	0.000	0.000	0.000	0.000	0.000	0.000
Phenol, 2-methoxy-4-methyl-	68.531	60.401	64.580	57.425	37.907	46.487	1.073	1.098	1.277	1.236	0.856	1.082
Phenol, 2,4-dimethyl-	14.308	17.174	21.975	28.433	19.420	23.398	0.144	0.180	0.299	0.362	0.352	0.401
3,4-Dimethoxytoluene	1.884	1.645	1.892	1.814	1.105	1.394	0.005	0.004	0.005	0.005	0.004	0.003
Phenol, 2,4,6-trimethyl-	2.878	3.024	3.718	4.480	2.989	3.637	0.014	0.016	0.026	0.028	0.030	0.035
Phenol, 4-ethyl-2-methoxy-	2.012	1.721	2.018	1.827	1.154	1.496	0.007	0.000	0.010	0.009	0.006	0.009
Phenol, 2,3-dimethyl-	0.848	1.168	1.648	2.759	1.740	2.394	0.000	0.000	0.019	0.022	0.026	0.034
Phenol, 4-ethyl-	4.258	5.443	6.031	7.787	4.438	6.195	0.021	0.028	0.053	0.069	0.047	0.056
Benzene, 1,4-dimethoxy-2-methyl-	10.325	8.972	10.009	9.178	5.507	7.143	0.037	0.032	0.044	0.049	0.034	0.044
Phenol, 4-ethyl-2-methoxy-	55.602	52.937	63.179	63.448	35.008	46.325	0.330	0.349	0.465	0.455	0.295	0.389
Phenol, 3,4,5-trimethyl-	6.031	8.377	9.300	13.053	7.937	9.129	0.019	0.019	0.046	0.049	0.044	0.035
1,4-Dimethoxy-2,3-dimethylbenzene	2.051	2.228	2.728	3.110	1.746	2.233	0.000	0.000	0.000	0.000	0.000	0.000
Phenol, 3-methoxy-2,4,5-trimethyl-	1.359	1.314	1.603	1.625	0.933	1.276	0.000	0.000	0.000	0.000	0.000	0.000
2-Methoxy-4-vinylphenol	10.983	10.363	10.396	9.948	5.227	7.272	0.036	0.029	0.041	0.017	0.020	0.017
Phenol, 3-methoxy-2,4,5-trimethyl-	6.450	5.737	6.499	0.000	3.897	5.013	0.000	0.000	0.000	0.000	0.000	0.000
Phenol, 2-methoxy-3-(2-propenyl)-(3-Allyl-2-methoxyphenol)	2.950	2.664	3.014	2.993	1.481	2.051	0.006	0.005	0.010	0.008	0.006	0.005
Phenol, 2-methoxy-4-propyl-	12.521	12.926	15.831	17.241	9.161	12.075	0.019	0.019	0.030	0.036	0.020	0.028
1,2-Benzenediol (pyrocatechol)	0.000	0.000	1.664	20.249	2.911	9.163	0.828	3.607	5.539	9.636	4.581	5.785
1-Dodecanol (Internal Standard)	54.331	53.540	53.959	52.075	53.644	51.880	5.576	5.576	5.576	5.576	5.576	5.576
1,2-Benzenediol, 4-methyl-	0.000	0.000	0.000	12.854	3.412	8.372	0.188	0.630	0.925	1.500	0.499	0.735
Phenol, 2-methoxy-4-(1-propenyl)-	9.765	10.204	10.863	11.911	5.475	7.653	0.016	0.000	0.000	0.000	0.000	0.000
Phenol, 2-methoxy-4-propyl-	1.396	2.139	1.716	0.000	0.000	0.000	0.169	0.128	0.049	0.000	0.000	0.000
Ethanone, 1-(4-hydroxy-3-methoxyphenyl)-	7.280	7.218	10.863	11.135	5.112	7.238	0.116	0.106	0.122	0.108	0.054	0.052
2-Propanone, 1-(4-hydroxy-3-methoxyphenyl)-	5.572	7.904	8.898	10.314	5.662	6.677	0.190	0.173	0.171	0.160	0.087	0.072
3,4-Dimethoxy-dl-phenylananine	3.360	4.305	5.060	5.377	3.052	3.626	0.000	0.000	0.000	0.000	0.000	0.000
Benzeneacetic acid, 4-hydroxy-3-methoxy-	0.000	0.000	2.170	3.418	1.744	2.587	0.072	0.058	0.032	0.045	0.000	0.000
1-Phenanthrenecarboxaldehyde, 1,2,3,4,4a,9,10,10a-octahydro-1,4a-dimethyl-7-(1-methylethyl)-, [1S-(1.alpha.,4a.alpha.,10a.beta.)]- (>1 singl ering)	1.832	1.949	2.302	2.589	1.653	1.893	0.000	0.000	0.000	0.000	0.000	0.000
.alpha.-Tetraloxime, 8-fluoro-5,6-dimethoxy- (2rings)	1.300	0.000	1.247	0.000	0.730	0.000	0.000	0.000	0.000	0.000	0.000	0.000
Podocarpa-8,11,13-trien-16-al, 13-isopropyl- (3rings)	1.978	2.162	2.576	2.861	1.767	2.039	0.000	0.000	0.000	0.000	0.000	0.000
10,18-Bisnorabieta-5,7,9(10),11,13-pentaene (3rings)	1.782	1.849	1.938	2.081	1.430	1.564	0.000	0.000	0.000	0.000	0.000	0.000
Phenanthrene, 1-methyl-7-(1-	5.419	6.116	6.465	7.941	5.741	6.301	0.000	0.000	0.000	0.000	0.000	0.000

methylethyl)- (3rings)												
1-Phenanthrenecarboxylic acid, 1,2,3,4,4a,9,10,10a-octahydro-1,4a-dimethyl-7-(1-methylethyl)-, methyl ester, [1R-(1.alpha.,4a.beta.,10a.alpha.)]-(3rings)	14.152	16.964	20.896	23.533	19.214	21.754	0.000	0.000	0.000	0.000	0.000	0.000
Total	**455.461**	**443.440**	**507.670**	**549.954**	**381.149**	**471.878**	**13.896**	**17.399**	**21.671**	**25.471**	**19.112**	**21.378**

The analyzed samples were collected during the selected temperature ranges, which explains why they are not presented at specific temperatures; rather, they are presented at temperature ranges, as shown in Table 6.4. Further mathematical procedures were implemented on this data to obtain the accumulated yields of each group, using the scenario that was discussed earlier. The identified chemical components in the oil and the aqueous phases were classified into four groups: (1) phenolics, (2) HMWC, (3) ASR-Non-Ph, and (4) aliphatics. Figure 6-6 shows the instantaneous experimental and predicted yields of each group, and Table 6.5 shows their estimated kinetic parameters. The rest of the MWP products, which are the remaining solid, water, and non-condensable gas, can be obtained from the first and second models.

The total identified components in the oil phase ranged from 381to 549 mg/g for oil, and 13.9 to 25.7 mg/g for the aqueous phase since the aqueous phase is mostly water. The presented HMWC yield was calculated by subtracting the “water content + the other three identified groups” from 100.

According to Figure 6-6, the formation rate of phenolics and HMWC groups is much higher than that of ASR-Non-Ph and aliphatics groups. This is related to the structure of the lignin network, which is totally poly-aromatics and mostly phenolics compounds. In addition, the nature of the applied heating mechanism could decrease the probability of a secondary reaction to produce aliphatics, as an example.

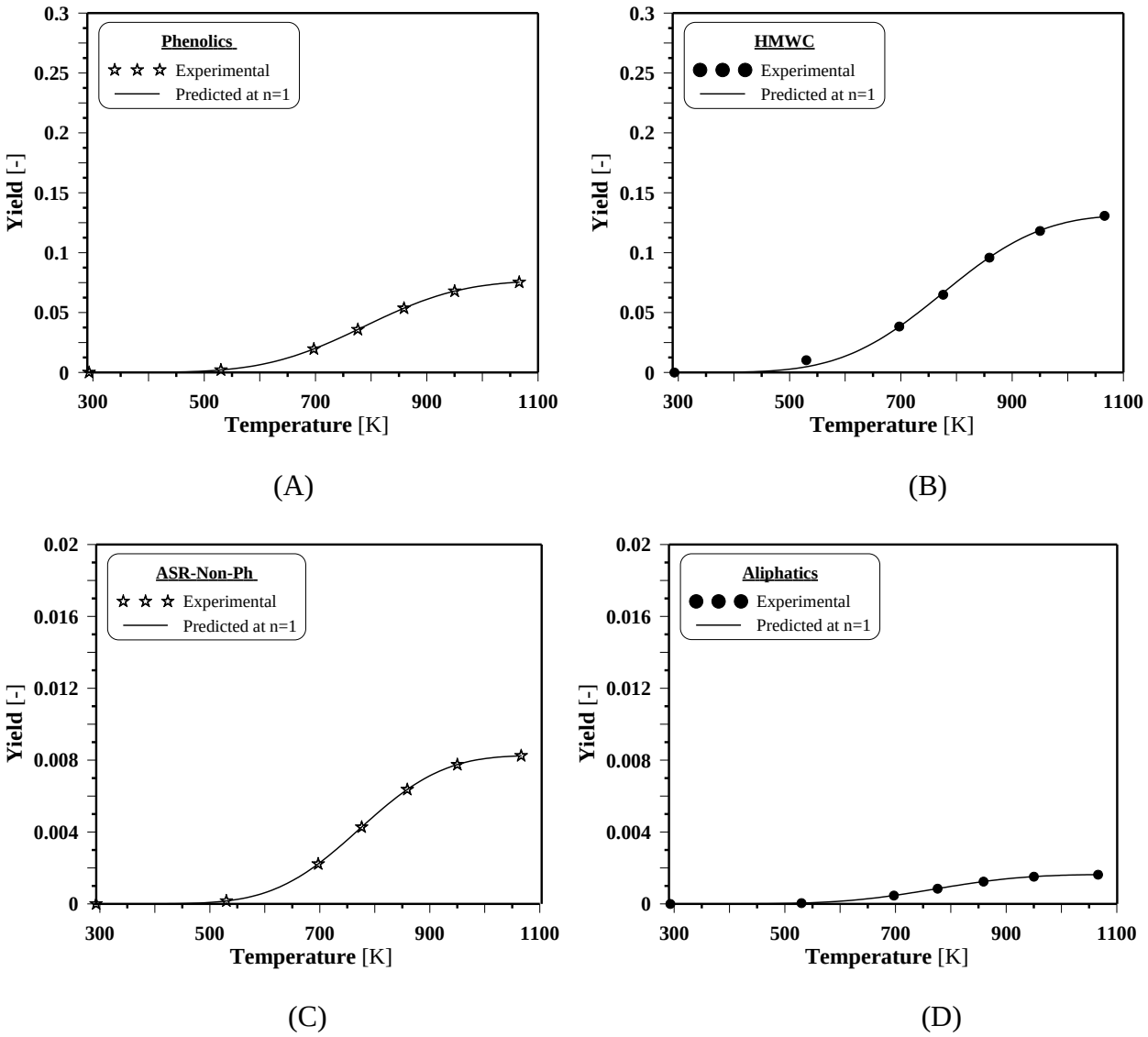

Figure 6-6: The experimental and predicted yields: (A) phenolics, (B) HMWC (C) ASR-Non-Ph, and (D) aliphatics. The points are the experimental, and the line is the fitting

Table 6.5: The estimated kinetic parameters of the extracted chemical groups.

Product	k_o **[min^{-1}]**	E_a **[kJ/mol]**	**n**
Phenolics	21	38	1
HMWC	22	35	1
ASR-Non-Ph	1	40	1
Aliphatics	20	47	1

The activation energy estimated for aliphatics is higher than that estimated for the other groups. This is a consequence of the energy needs to form aliphatics from an aromatic ring, which are higher than those needed to create phenolics or HMWC from lignin directly. On the other hand, the activation energy of HMWC is lower than that of the other groups. This is because the energy needs to produce some aromatic rings connected with each other is lower than the energy needs to produce the same rings but each as an individual ring, such as phenols, for example. Since the structure of phenolics and ASR-Non-Ph is almost similar, as they have a single aromatic ring, their estimated activation energies are similar as well. However, the pre-exponential factor is different as most of the aromatics in the virgin material can produce phenolics much easier than aromatics that are not phenolics.

6.6 Maximize the Phenolics Yield

The estimated kinetic parameters were employed to simulate yields of the phenolics group at different heating rates and the same investigated temperature range, as depicted in Figure 6-7.

Increasing the heating rate from 10-100 K/min enhanced the phenolics yield from 0.024 to 0.1 g/g of lignin; however, the heating rates above 150 K/min resulted in the opposite. As known, at low heating rates, vapor products do not escape rapidly like at high heating rates, which would increase the chance of further decomposition when the products are being formed. On the other

hand, a high heating rate could not enable the molecular bonds to be fully decomposed. Thus, it would increase the heavy products yield; accordingly, the phenolics yield decreased at heating rates above 150 K/min. Among these heating rates, an optimum value that maximizes phenolics yield should be found and applied; theoretically, it is 110 K/min in this work.

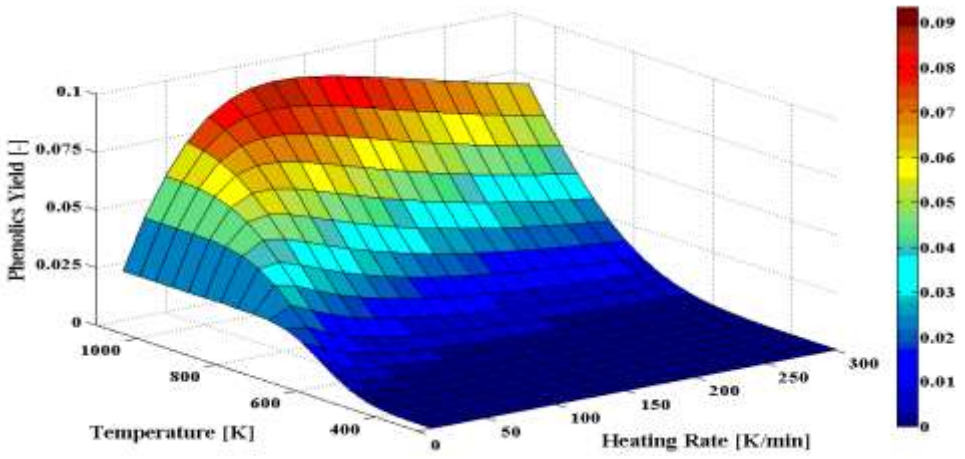

Figure 6-7. The estimated Phenolics yield at different heating rates and temperatures [g/g lignin].

Indeed, besides applying the optimum heating rate, many factors should be considered in this aspect, such as high heat transfer and short vapor residence time. Furthermore, rapidly cooling the vapor product is essential to eliminate further reactions to breakdown the condensable gas into gaseous products. Also, and most importantly, a carefully controlled pyrolysis reaction is essential, particularly at high heating rates.

Further attention will be paid to maximize the phenolics yield using different scenarios and at optimum heating rates obtained from this work; subsequently, the yield of the other groups will be estimated according to the best scenario and considered in future work.

6.7 The Validation of the Presented Models

The presented models were validated against the experimental data, as depicted in Figure 6-8. Figure 6-8 -A -A shows the first model products, condensable gas, non-condensable gas, and

remaining solid. Figure 6-8-B presents the second model liquid products, water and oil; the solid and gas products were demonstrated in Figure 6-8-A. Figure 6-8-C and Figure 6-8-D illustrate the third model oily products, phenolics, HMWC, ASR-Non-Ph, and liphatics; while the remaining products can be obtained from Figure 6-8-A&B. As it is obvious, the presented models have a high capability to estimate the investigated products with minor deviations. This means that these three models can be applied in designing and scaling-up the pyrolysis process, which is essential; thus, they will be considered in the future work.

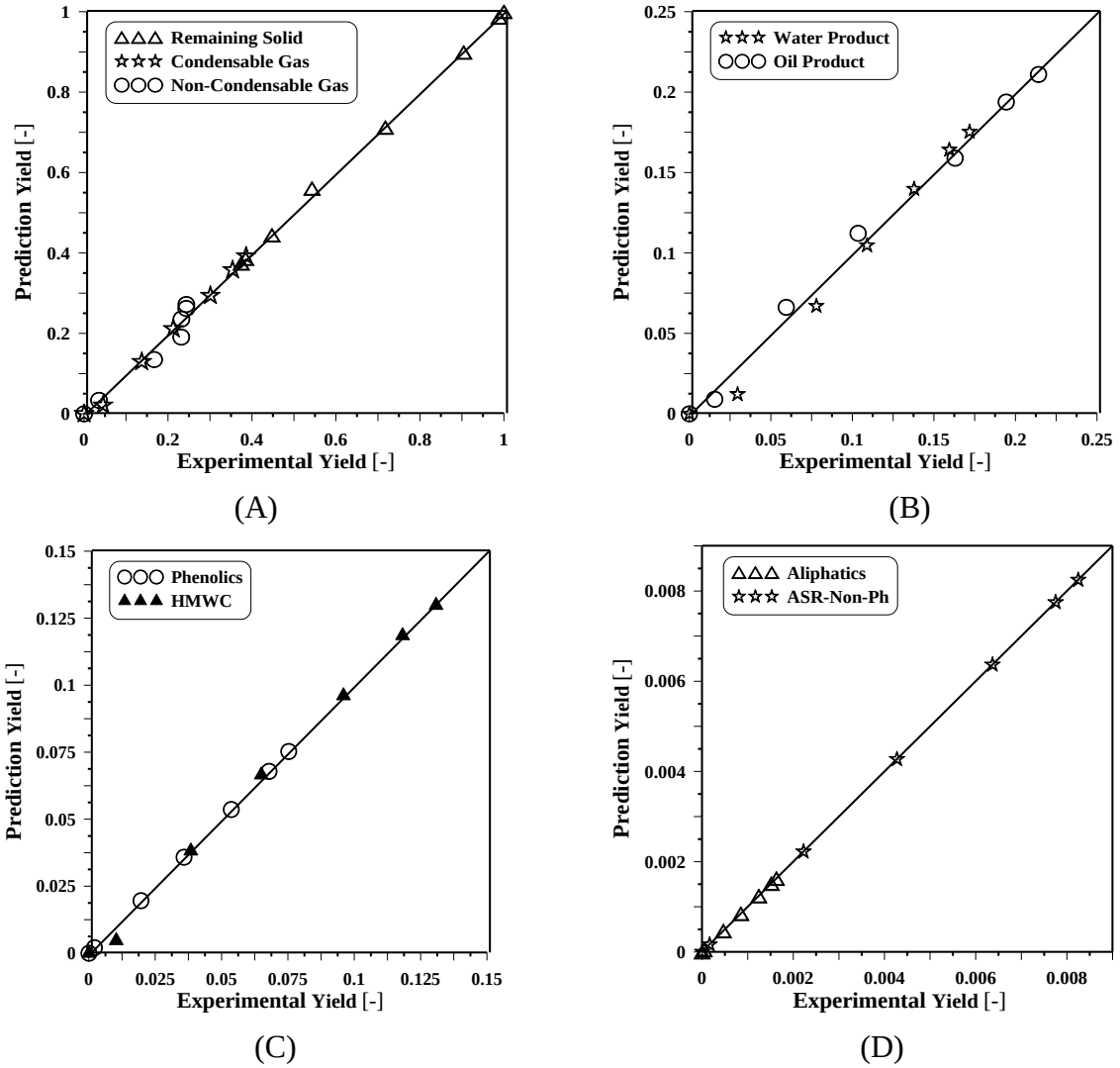

Figure 6-8: The capability of the presented models: (A) the first model, (B) the second model, and (C) & (D) the third model.

6.8 The Conclusion and Future Work

The kinetics of the microwave pyrolysis of kraft lignin was investigated using three different models based on a lumping approach. The first model considered that lignin converted to solid, liquid, and gas product, while the second model divided the liquid product into water and oil products. In the third model, the oil product was divided into four chemical groups, phenolics, aliphatics, HMWC, and ASR-Non-Ph. A microwave thermo-gravimetric analyzer equipped with a product manifold was designed and built to be used in this investigation. The kinetic parameters of every model were estimated, and then applied to predict the yield of each product. In addition, a simulation for the phenolics yield at different heating rates was achieved. The predicted yields illustrate a very small deviation from the experimental data, which validates the presented models. Up to 725 K the yield of non-condensable gas product was slightly higher than that of the condensable gas product, which might be due to the swift split of the lignin network site chains. This increased the water yield more than the oil yield up to this temperature. Beyond 725 K the situation was the opposite, which could be the result of decomposing strong chemical bonds of the lignin network. A comparison between the estimated kinetic parameters showed that the rate of thermal cracking of lignin is higher than that of the liquid phase. This could indicate that the possibility of secondary reactions is low. The rate of formation of the phenolics and HMWC groups is much higher than that of ASR-Non-Ph and aliphatics groups, which is related to the structure of the lignin network and/or the nature of the applied heating mechanism. A heating rate of 110 K/min was found to be the optimum value to maximize the phenolics yield.

The investigations in this work are essential to improve the understanding of the underlying processes and provide the necessary information for the rational design and scaling-up of the pyrolysis reactor.

Acknowledgements

The authors would like to thank Mr. Yazid Belkhir and Mr. Robert Delisle (Technicians at Ecole Polytechnique Montreal) for their assistance in the experimental setup and Mr. Alain Gagné (Principal Technologist at FPInnovations) for his assistance in products characterization with

GC-MS and KF. In addition, the authors are grateful for the financial and technical support from Lignoworks NSERC Strategic Network (www.lignoworks.ca).

CHAPTER 7 GENERAL DISCUSSION

The potential of Canadian forests has established the forest industry one of the cornerstones of the Canadian economy. However, this industry has reached a crossroads because it has been facing unexpected challenges for the past few years. One of the solutions that can be applied to ensure a sustainable future for the industry is the production of value-added forest-based products. Thus, this project investigated the potential for converting one of the lignocellulosic biomass components, lignin, into a value-added bio-product.

One of the routes applied to convert lignin to bio-products is pyrolysis. Pyrolysis is a process of thermal decomposition of the chemical bonds of a target material, which is performed by heating the material in an inert environment. In general, pyrolysis produces three main products, solid, condensable gas, and non-condensable gas. Herein, the required heat energy in pyrolysis is generated within the material itself using microwave heating (MWH); thus, this pyrolysis is called microwave pyrolysis (MWP).

As known, temperature measurement/simulation within a material exposed to electromagnetic waves (EMW) is rather complex. Therefore, as a first step in this project, temperature profiles inside a material heated by EMW at 2.45 GHz were simulated using a three-dimensional mathematical model. COMSOL-Multiphysics was used to simulate transient temperature profiles of pinewood, carbon, Pyrex, and combinations of such under different conditions. Subsequently, the predicted results were compared against the experimental data in order to validate the presented model. The average percentage relative error between the measured and the predicted temperatures was ±4% and ±15% inside the pinewood and carbon respectively.

The presented model predicts that, upon exposing an 86mm wooden cube to 2.45 GHz of EMW for 300 s, the core temperature reached 595 K, while the outer surface 365 K. This means, MWH leads to non-uniform distribution of temperature which is strongly affected by penetration depth (D_p) and surface heat loss. This could be avoided by limiting dimensions of the payload to twice

D_p, and placing a strong thermal insulation on the surface. By mixing 50% carbon with the wooden block, the model anticipated the cube core to reach 990 K, compared to 1350 K with 75% carbon at the same power and after the same time. As a result, homogenous mixing of materials which are strong microwave receptor with the payload leads to exhibiting a significant increase in temperature compared to the virgin material exposed to the same power and heating time. By inserting a 125 cm^3 carbon cube inside the wood cube, the core reaches 3200 K, while the outer surface was 375 K. Placing the same volume of carbon on the surface of the wood cube yielded a maximum temperature of 660 K. Changing the material of the core cube from Carbon to Pyrex yields a temperature of 324 K in the core, with 365 K on the outer surface. Therefore, choice of location of materials with contrasting levels of microwave-to-heat conversion may be used to create desired cold/hot zones and achieve a specific temperature profile in the workload.

Indeed, such discussions could provide insights in: (1) applications where creating a hot spot to induce thermal cracking or obtain a specific product is desired, e.g., generation hot spots in gasification process to increase gas yield. (2) Applications requiring a significant temperature gradient between the core and the surface to generate sufficient pressure difference to enhance extractive applications such as the extraction of moisture content in drying sector and the extraction of valuable bio-chemicals in pyrolysis sector. (3) Applications where surface treatment, coating, joining, etc., are used.

Indeed, this study was extremely useful as a first step in this project to improve the understanding of temperature profiles within composite materials subjected to MWH.

In literature, different kinetic investigations of different reactions have been demonstrated; however, most of them are inconsistent with each other. Actually, this inconsistent might be a result of using one of the traditional thermometers without considering its drawbacks in case of MWH. Therefore, in the second step, the reaction kinetics of MWP of sawdust in contrast to conventional pyrolysis (CP) was investigated. In order to complete this investigation, an original microwave thermo-gravimetric-analyzer (MW-TGA) was built and equipped with an innovated thermometer. This thermometer does not suffer from the traditional thermometer drawbacks

when MWH is applied. Subsequently, the kinetic parameters, activation energy, pre-exponential factor, and reaction order (E_a, k_o, and n), were estimated using a MATLAB® program code. According to the estimated values of the kinetic parameters, there may not be evidence on the effect of MWH on E_a because the MWP and CP have almost the same estimated value; however, the effect on k_o is obvious. The estimated value of k_o in the MWP is more than three-times that of the CP. This could be a consequence of the nature of the MWH mechanism, which mainly depends on agitating the dipoles of the heated material, and results in more chaotic motion. In addition, k_o was interpreted as a collision frequency, determined using the kinetic theory. Indeed, these two facts can elucidate that MWH could enhance the molecule collisions, which leads to an increase in k_o. Despite this tangible effect on k_o, E_a is almost the same in both cases, which might be due to the huge difference between the wavelength of the oscillating EMW and the intermolecular distance of the exposed material. This renders the effect of the EMW on E_a doubtful as EMW cannot hack the molecular bonds directly.

At this point, temperature of a material exposed to MWH can be measured, using the innovated thermometer, and/or estimated, using the mathematical model. Therefore, in the third step, a detailed structural investigation and compositional analysis of a liquid produced via MWP of kraft lignin was accomplished under various conditions. The key variables in this investigation were concentration of a microwave receptor, char, (20-40 wt%) and nominal-setting-power (1.5-2.7 kW). This resulted temperatures after applying the selected conditions of 800 s of 900, 980, 1065, 1150, and 1240 K. The maximum yield of the obtained liquid (oil and aqueous phases) was found at 1240 K; however, beneficial depending on the structure of the liquid phases as well as the water content. GC-MS analysis was implemented on the oil and aqueous phases, and ^{31}P and ^{13}C NMR analyses were performed on the oil phase and the virgin material.

Due to the limitations of the GC-MS analysis, the concentrations of 583-707 mg/g of the oil phase could not be identified using this technique. As a result, GC-MS analysis is inadequate to provide a detailed structure of the pyrolysis liquids. Accordingly, ^{31}P and ^{13}C NMR spectroscopy were implemented to provide detailed structure information for the whole oil phase and the virgin material. Up to 80% of the carbon atoms in the oil phase were aromatic carbons. The

concentration of aliphatic hydroxyl groups in the virgin material was significantly eliminated by the MWP, which might be attributed to form water during the thermal degradation of the lignin network. The decreased concentrations of *C5* substituted/condensed phenolic hydroxyl groups after MWP were attributed to an increment in the concentrations of guaiacyl, *p*-hydroxyphenyl, and catechol hydroxyl groups. Indeed, such investigations improve understanding about MWP mechanisms, which leads to more control in the degradation pathways.

One of the performed conditions in the previous investigation was used to achieve a kinetic modeling of the MWP products quantitatively as well as qualitatively. To perform this modelling, the MW-TGA, which was built in the second step, was equipped with a product manifold to separate the vapor product at various temperatures. This kinetic modelling presents three kinetic models based on a lumping approach. The first model considered that lignin converted to condensable gas, non-condensable gas, and the remaining solid, while the second model divided the liquid product into water and oil products, taking into consideration each as an individual lump. In the third model, the oil product was separated into four main groups: (1) phenolics, contain all the identified phenolic components using a GC-MS analyzer; (2) heavy molecular weight components, contain all the identified heavy molecular weight and undefined components, using GC-MS; (3) non-phenolic aromatics with a single ring; and (4) aliphatics. The kinetic parameters of every model were estimated, and then applied to predict the yield of each product. The predicted yields illustrate a very small deviation from the experimental data, which validates the presented models. Finally, a simulation for the phenolics yield at different heating rates was achieved. The optimum heating rate that maximizes phenolics yield was 110 K/min in this simulation. At heating rates less than 110 K/min, vapor products do not escape rapidly like at high heating rates, which would increase the chance of further decomposition. Heating rates higher than 110 K/min could not enable the molecular bonds to be fully decomposed. Thus, it would increase the heavy products yield; accordingly, the phenolics yield decreased at heating rates above 110 K/min.

CHAPTER 8 CONCLUSION AND RECOMMENDATIONS

8.1 Conclusions

In this study, the potential for converting kraft lignin into value-added bio-products was investigated. Electromagnetic irradiation using a pyrolytic technique was employed to achieve this objective. The obtained results and conclusions of this work are compliant with the objectives described in Chapter 2 and are as follows.

Objective 1: Simulate temperature profiles within selected materials exposed to microwave heating (MWH).

Conclusion 1: Chapter 3 presents a three-dimensional mathematical model developed to predict transient temperature profiles within selected materials exposed to MWH at 2.45 GHz. The key conclusion of this work is that MWH is strongly affected by the surface heat loss and penetration depth (D_p) of the exposed material. Therefore, it leads to non-uniform temperature distribution inside the heated material. However, placing a strong thermal insulation on the surface and limiting dimensions of the target material to twice D_p minimizes temperature gradients significantly. The homogenous mixing of strong microwave-receptive materials with the payload exhibits a dramatic increase in temperature compared the virgin material exposed to the same power and heating time. Furthermore, desired cold/hot zones inside the heated material can be achieved by choosing of location of materials with contrasting levels of microwave-to-heat conversion. Such findings provide insight into applications where creating a hot/cold spot to obtain and/or enhance specific products is essential, such as gasification, pyrolysis, and drying.

Objective 2: Design and manufacture an innovative thermometer that does not suffer from the drawbacks of traditional thermometers.

Conclusion 2: In Chapter 4, an innovative thermometer to measure transient mean temperature inside a microwave oven was designed and manufactured, called an air-thermometer. In order to verify the air-thermometer measurements, the measured temperatures were compared against the

reference values measured by a traditional thermocouple. In addition, further verification was conducted against predicted temperatures using the model presented in Chapter 3. This showed a good agreement between the measured temperatures and the reference temperatures.

Objective 3: Design and build an original thermogravimetric analyzer that works using MWH and is equipped with a product manifold, for kinetic purposes.

Conclusion 3: In Chapter 4, an experimental setup similar to a TGA was built for kinetic purposes, called the MW-TGA, which operates by MWH. In Chapter 6, this MW-TGA was equipped with a product manifold to distribute the vapor product up to 7 parts at selected temperatures/times. According to the sensitivity of the installed balance, MW-TGA has good results, even when using very large samples, compared to those obtaining using a traditional TGA.

Objective 4: Study the reaction kinetics of microwave pyrolysis (MWP), in contrast to conventional pyrolysis (CP) and interpret the obtained results.

Conclusion 4: Chapter 5 presents a kinetic investigation of MWP in contrast to conventional pyrolysis (CP) of sawdust, using the air-thermometer and MW-TGA. According to the estimated kinetic parameters in both cases, MWP may have a reaction rate faster than that of CP. This is a consequence of enhancing the molecular chaotic motion produced by the oscillating electromagnetic field. On the other hand, the estimated activation energy is almost the same in CP and MWP. This may be related to the wavelength of the oscillating electromagnetic field, which is much longer than the intermolecular distance of the heated material. This explanation was achieved based on the kinetic aspect and without investigating from the selectivity side, which would be different.

Objective 5: Study the composition and structure of the condensable gases produced by MWP of kraft lignin using different analysis techniques.

Conclusion 5: Chapter 5 discusses the compositional analysis and structural investigation of liquids obtained from the MWP of kraft lignin under various conditions. The key conclusion of

this discussion includes the greater effect of char wt% than the microwave power setting on the heating rate, as the native lignin is not strong receptive to microwaves. Increasing the heating rate increased the total obtained liquid yield; however, beneficial depending on the liquid structure and the water content. A concentration of 583-707 mg/g of the oil phase could not be identified, due to the limitations of the GC-MS. As a result, GC-MS analysis is inadequate for providing a detailed structure of the pyrolysis liquids. According to ^{31}P and ^{13}C NMR analyses, up to 80% of the measured carbon atoms in the oil phase were aromatic. The concentration of aliphatic hydroxyl groups in the virgin material was significantly decreased by MWP. This was a consequence of the swift cleavage of the lignin side chain hydroxyl groups, which was attributed to water forming during pyrolysis.

Objective 6: Design a kinetic model of the MWP products of kraft lignin, both quantitatively and qualitatively.

Conclusion 6: Chapter 6 examines the kinetics of MWP of kraft lignin using three different models, based on a lumping approach. The first model converts lignin to solid, liquid, and gas products, while the second model divides the liquid into water and oil products. In the third model, the oil product is divided into four chemical groups: phenolics, aliphatics, HMWC and ASR-Non-Ph. The kinetic parameters of these models were estimated and applied to predict the yield of each product. Furthermore, a simulation was designed for the phenolics yield at different heating rates. The predicted yields illustrate a very small deviation from the experimental data, which validates the presented models. A comparison between the estimated kinetics parameters shows that the rate of thermal cracking of lignin is higher than that of the liquid phase, which may indicate that the possibility of secondary reactions is low. The rate of formation of the phenolics and HMWC groups is much higher than that of the ASR-Non-Ph and aliphatics groups, which is related to the structure of the lignin network and/or the nature of the applied heating mechanism. A heating rate of 110 K/min was found to be the optimum value for maximizing the phenolics yield.

8.2 Future Work and Recommendations

1- The further investigation of ways to minimize water content in the liquid product is essential;

2- The further investigation of ways to maximize specific chemical compounds is needed;

3- Different separation techniques for the obtained oil are required; and

4- The process needs to be scaled up and studied economically.

REFERENCES

Adnađević, B., M. Gigov, M. Sindjic and J. Jovanović (2008). "Comparative study on isothermal kinetics of fullerol formation under conventional and microwave heating." Chemical Engineering Journal **140**(1–3): 570-577.

Adnadjevic, B. K. and J. D. Jovanovic (2012). "A comparative kinetics study on the isothermal heterogeneous acid-catalyzed hydrolysis of sucrose under conventional and microwave heating." Journal of Molecular Catalysis A: Chemical **356**(0): 70-77.

Adnadjević, B. K. and J. D. Jovanović (2012). "Kinetics of Isothermal Ethanol Adsorption onto a Carbon Molecular Sieve under Conventional and Microwave Heating." Chemical Engineering & Technology **35**(4): 761-768.

Aqsha, A., N. Mahinpey, T. Mani, F. Salak and P. Murugan (2011). "Study of sawdust pyrolysis and its devolatilisation kinetics." The Canadian Journal of Chemical Engineering **89**(6): 1451-1457.

Badamali, S. K., J. H. Clark and S. W. Breeden (2008). "Microwave assisted selective oxidation of lignin model phenolic monomer over SBA-15." Catalysis Communications **9**(13): 2168-2170.

Bail, A. L., T. Koutchma and H. S. Ramaswamy (2000). "MODELING OF TEMPERATURE PROFILES UNDER CONTINUOUS TUBE-FLOW MICROWAVE AND STEAM HEATING CONDITIONS." Journal of Food Process Engineering **23**(1): 1-24.

Ben, H. and A. J. Ragauskas (2011). "NMR Characterization of Pyrolysis Oils from Kraft Lignin." Energy & Fuels **25**(5): 2322-2332.

Benoit, L. (2008). CANADA'S FOREST INDUSTRY: RECOGNIZING THE CHALLENGES AND OPPORTUNITIES. Report of the Standing Committee on Natural Resources, HOUSE OF COMMONS CANADA. **39th PARLIAMENT:** 1-2.

Budarin, V. L., J. H. Clark, B. A. Lanigan, P. Shuttleworth, S. W. Breeden, A. J. Wilson, D. J. Macquarrie, K. Milkowski, J. Jones, T. Bridgeman and A. Ross (2009). "The preparation of high-grade bio-oils through the controlled, low temperature microwave activation of wheat straw." Bioresource Technology **100**(23): 6064-6068.

Budarin, V. L., J. H. Clark, B. A. Lanigan, P. Shuttleworth and D. J. Macquarrie (2010). "Microwave assisted decomposition of cellulose: A new thermochemical route for biomass exploitation." Bioresource Technology **101**(10): 3776-3779.

Camelia Gabriel, a. S. G., a Edward H. Grant,a,b Ben S. J. Halsteadb and D. Michael P. and Mingosb (1998). "Dielectric parameters relevant to microwave dielectric heating." Chemical Society Reviews **27**: 213-222.

Campañone, L. A. and N. E. Zaritzky (2005). "Mathematical analysis of microwave heating process." Journal of Food Engineering **69**(3): 359-368.

Castro-Giráldez, M., P. J. Fito and P. Fito (2010). "Application of microwaves dielectric spectroscopy for controlling pork meat (Longissimus dorsi) salting process." Journal of Food Engineering **97**(4): 484-490.

Chandra Shekara, B. M., B. S. Jai Prakash and Y. S. Bhat (2012). "Microwave-induced deactivation-free catalytic activity of BEA zeolite in acylation reactions." Journal of Catalysis **290**(0): 101-107.

Chen, D.-Y., D. Zhang and X.-F. Zhu "Heat/mass transfer characteristics and nonisothermal drying kinetics at the first stage of biomass pyrolysis." Journal of Thermal Analysis and Calorimetry: 1-8.

Chen, F., G. Wang, C. Shi, Y. Zhang, L. Zhang, W. Li and F. Yang (2013). "Kinetics of glycolysis of poly(ethylene terephthalate) under microwave irradiation." Journal of Applied Polymer Science **127**(4): 2809-2815.

Chiavaro, E., C. Barnaba, E. Vittadini, M. T. Rodriguez-Estrada, L. Cerretani and A. Bendini (2009). "Microwave heating of different commercial categories of olive oil: Part II. Effect on thermal properties." Food Chemistry **115**(4): 1393-1400.

Choi, H. S. and D. Meier (2013). "Fast pyrolysis of Kraft lignin—Vapor cracking over various fixed-bed catalysts." Journal of Analytical and Applied Pyrolysis **100**(0): 207-212.

Ciacci, T., A. Galgano and C. Di Blasi (2010). "Numerical simulation of the electromagnetic field and the heat and mass transfer processes during microwave-induced pyrolysis of a wood block." Chemical Engineering Science **65**(14): 4117-4133.

Clark, D. E., D. C. Folz and J. K. West (2000). "Processing materials with microwave energy." Materials Science and Engineering A **287**(2): 153-158.

Cuccurullo, G., P. G. Berardi, R. Carfagna and V. Pierro (2002). "IR temperature measurements in microwave heating." Infrared Physics & Technology **43**(3-5): 145-150.

D.E. Clark, D. C. F. (2005). What is microwave processing. Microwave Solutions for Ceramic Engineers. D. C. F. D.E. Clark, C.E. Folgar, M.M. Mahmoud. Westerville, OH The American Ceramics Society, Inc**:** 1–26.

Datta, A. K. and H. Ni (2002). "Infrared and hot-air-assisted microwave heating of foods for control of surface moisture." Journal of Food Engineering **51**(4): 355-364.

de Wild, P. J., W. J. J. Huijgen and H. J. Heeres (2012). "Pyrolysis of wheat straw-derived organosolv lignin." Journal of Analytical and Applied Pyrolysis **93**(0): 95-103.

Dogan, H. and N. D. Hilmioglu (2009). "Dissolution of cellulose with NMMO by microwave heating." Carbohydrate Polymers **75**(1): 90-94.

Domínguez, A., Y. Fernández, B. Fidalgo, J. J. Pis and J. A. Menéndez (2008). "Bio-syngas production with low concentrations of CO2 and CH4 from microwave-induced pyrolysis of wet and dried sewage sludge." Chemosphere **70**(3): 397-403.

Domínguez, A., J. A. Menéndez, M. Inguanzo and J. J. Pis (2005). "Investigations into the characteristics of oils produced from microwave pyrolysis of sewage sludge." Fuel Processing Technology **86**(9): 1007-1020.

Doucet, J., J.-P. Laviolette, S. Farag and J. Chaouki (2013). "Distributed Microwave Pyrolysis of Domestic Waste." Waste and Biomass Valorization: 1-10.

Durka, T., T. V. Gerven and A. Stankiewicz (2009). "Microwaves in Heterogeneous Gas-Phase Catalysis: Experimental and Numerical Approaches." Chemical Engineering & Technology **32**(9): 1301-1312.

Durka, T., T. Van Gerven and A. Stankiewicz (2009). "Microwaves in Heterogeneous Gas-Phase Catalysis: Experimental and Numerical Approaches." Chemical Engineering & Technology **32**(9): 1301-1312.

El harfi, K., A. Mokhlisse, M. B. Chanâa and A. Outzourhit (2000). "Pyrolysis of the Moroccan (Tarfaya) oil shales under microwave irradiation." Fuel **79**(7): 733-742.

Farag, S., A. Sobhy, C. Akyel, J. Doucet and J. Chaouki (2012). "Temperature profile prediction within selected materials heated by microwaves at 2.45GHz." Applied Thermal Engineering **36**(0): 360-369.

Farag., S. and J. Chaouki. (2013). "A Kinetic Investigation of Microwave Pyrolysis of Sawdust Using an Original Microwave –Thermogravimetric Analyzer." under revision

Farag., S., D. Fu., P. G. Jessop. and J. Chaouki. (2013). "A Detailed Compositional Analysis and Structural Investigation of a Bio-oil from Microwave Pyrolysis of Kraft Lignin."

Faravelli, T., A. Frassoldati, G. Migliavacca and E. Ranzi (2010). "Detailed kinetic modeling of the thermal degradation of lignins." Biomass and Bioenergy **34**(3): 290-301.

Ferdous, D., A. K. Dalai, S. K. Bej and R. W. Thring (2002). "Pyrolysis of Lignins: Experimental and Kinetics Studies." Energy & Fuels **16**(6): 1405-1412.

Fernández, Y., A. Arenillas, M. A. Díez, J. J. Pis and J. A. Menéndez (2009). "Pyrolysis of glycerol over activated carbons for syngas production." Journal of Analytical and Applied Pyrolysis **84**(2): 145-150.

Fu, D., S. Farag, J. Chaouki and P. G. Jessop (2014). "Extraction of phenols from lignin microwave-pyrolysis oil using a switchable hydrophilicity solvent." Bioresource Technology **154**(0): 101-108.

Fukushima, J., K. Kashimura, S. Takayama, M. Sato, S. Sano, Y. Hayashi and H. Takizawa (2013). "In-situ kinetic study on non-thermal reduction reaction of CuO during microwave heating." Materials Letters **91**(0): 252-254.

Geedipalli, S. S. R., V. Rakesh and A. K. Datta (2007). "Modeling the heating uniformity contributed by a rotating turntable in microwave ovens." Journal of Food Engineering **82**(3): 359-368.

Granata, A. and D. S. Argyropoulos (1995). "2-Chloro-4,4,5,5-tetramethyl-1,3,2-dioxaphospholane, a Reagent for the Accurate Determination of the Uncondensed and Condensed Phenolic Moieties in Lignins." Journal of Agricultural and Food Chemistry **43**(6): 1538-1544.

Gu, X., X. Ma, L. Li, C. Liu, K. Cheng and Z. Li (2013). "Pyrolysis of poplar wood sawdust by TG-FTIR and Py–GC/MS." Journal of Analytical and Applied Pyrolysis **102**(0): 16-23.

Guiotoku, M., C. R. Rambo, F. A. Hansel, W. L. E. Magalhães and D. Hotza (2009). "Microwave-assisted hydrothermal carbonization of lignocellulosic materials." Materials Letters **63**(30): 2707-2709.

Gunasekaran, S. and H.-W. Yang (2007). "Effect of experimental parameters on temperature distribution during continuous and pulsed microwave heating." Journal of Food Engineering **78**(4): 1452-1456.

Guo, W., S. Wang, G. Tiwari, J. A. Johnson and J. Tang (2010). "Temperature and moisture dependent dielectric properties of legume flour associated with dielectric heating." LWT - Food Science and Technology **43**(2): 193-201.

Imam, T. and S. Capareda (2012). "Characterization of bio-oil, syn-gas and bio-char from switchgrass pyrolysis at various temperatures." Journal of Analytical and Applied Pyrolysis **93**(0): 170-177.

Janković, B. (2011). "The comparative kinetic analysis of Acetocell and Lignoboost® lignin pyrolysis: The estimation of the distributed reactivity models." Bioresource Technology **102**(20): 9763-9771.

Jiang, G., D. J. Nowakowski and A. V. Bridgwater (2010). "Effect of the Temperature on the Composition of Lignin Pyrolysis Products." Energy & Fuels **24**(8): 4470-4475.

Jiang, G., D. J. Nowakowski and A. V. Bridgwater (2010). "A systematic study of the kinetics of lignin pyrolysis." Thermochimica Acta **498**(1-2): 61-66.

Jones, D. A., T. P. Lelyveld, S. D. Mavrofidis, S. W. Kingman and N. J. Miles (2002). "Microwave heating applications in environmental engineering--a review." Resources, Conservation and Recycling **34**(2): 75-90.

Karaduman, A. (2002). "Pyrolysis of Polystyrene Plastic Wastes with Some Organic Compounds for Enhancing Styrene Yield." Energy Sources **24**(7): 667-674.

Karthikeyan, S., R. Balasubramanian and S. W. See (2006). "Optimization and validation of a low temperature microwave-assisted extraction method for analysis of polycyclic aromatic hydrocarbons in airborne particulate matter." Talanta **69**(1): 79-86.

Kibet, J., L. Khachatryan and B. Dellinger (2012). "Molecular Products and Radicals from Pyrolysis of Lignin." Environmental Science & Technology **46**(23): 12994-13001.

Klinbun, W. and P. Rattanadecho "Analysis of microwave induced natural convection in a single mode cavity (Influence of sample volume, placement, and microwave power level)." Applied Mathematical Modelling(0).

Kol, H. Ş. (2009). "THERMAL AND DIELECTRIC PROPERTIES OF PINE WOOD IN THE TRANSVERSE DIRECTION." BioResources **Vol 4, No 4**

Krzan, A. and E. Zagar (2009). "Microwave driven wood liquefaction with glycols." Bioresource Technology **100**(12): 3143-3146.

Ledesma, E. B., N. D. Marsh, A. K. Sandrowitz and M. J. Wornat (2002). "An experimental study on the thermal decomposition of catechol." Proceedings of the Combustion Institute **29**(2): 2299-2306.

Li, D., Y. Zhang, X. Quan and Y. Zhao (2009). "Microwave thermal remediation of crude oil contaminated soil enhanced by carbon fiber." Journal of Environmental Sciences **21**(9): 1290-1295.

Li, Z., L. Han and W. Xiao (2013). "Influence of microwave heating on the liquefaction kinetics of corn stover in ethylene glycol." BioResources **8**(3): 3453-3460.

Lidström, P., J. Tierney, B. Wathey and J. Westman (2001). "Microwave assisted organic synthesis--a review." Tetrahedron **57**(45): 9225-9283.

Lou, R. and S.-b. Wu (2011). "Products properties from fast pyrolysis of enzymatic/mild acidolysis lignin." Applied Energy **88**(1): 316-322.

Lou, R., S.-b. Wu and G.-j. Lv (2010). "Effect of conditions on fast pyrolysis of bamboo lignin." Journal of Analytical and Applied Pyrolysis **89**(2): 191-196.

Lucchesi, M. E., F. Chemat and J. Smadja (2004). "Solvent-free microwave extraction of essential oil from aromatic herbs: comparison with conventional hydro-distillation." Journal of Chromatography A **1043**(2): 323-327.

Luo, Z., S. Wang and X. Guo (2012). "Selective pyrolysis of Organosolv lignin over zeolites with product analysis by TG-FTIR." Journal of Analytical and Applied Pyrolysis **95**(0): 112-117.

Luque, R., J. A. Menendez, A. Arenillas and J. Cot (2012). "Microwave-assisted pyrolysis of biomass feedstocks: the way forward?" Energy & Environmental Science **5**(2): 5481-5488.

Ma, H., W.-W. Liu, X. Chen, Y.-J. Wu and Z.-L. Yu (2009). "Enhanced enzymatic saccharification of rice straw by microwave pretreatment." Bioresource Technology **100**(3): 1279-1284.

Ma, S. J., et al. (2009). " A new practical method to determine the microwave energy absorption." Minerals Engineering **22(13)**: 1154-1159.

Mani, T., P. Murugan and N. Mahinpey (2008). "Determination of Distributed Activation Energy Model Kinetic Parameters Using Simulated Annealing Optimization Method for Nonisothermal Pyrolysis of Lignin." Industrial & Engineering Chemistry Research **48**(3): 1464-1467.

Manoj Gupta, E. W. W. L., Wai Leong Wong (2007). Microwaves and metals, John Wiley & sons (Asia) Pte Ltd

Mazo, P., D. Estenoz, M. Sponton and L. Rios (2012). "Kinetics of the Transesterification of Castor Oil with Maleic Anhydride Using Conventional and Microwave Heating." Journal of the American Oil Chemists' Society **89**(7): 1355-1361.

Menéndez, J. A., A. Domínguez, M. Inguanzo and J. J. Pis (2004). "Microwave pyrolysis of sewage sludge: analysis of the gas fraction." Journal of Analytical and Applied Pyrolysis **71**(2): 657-667.

Menéndez, J. A., M. Inguanzo and J. J. Pis (2002). "Microwave-induced pyrolysis of sewage sludge." Water Research **36**(13): 3261-3264.

Miura, M., H. Kaga, A. Sakurai, T. Kakuchi and K. Takahashi (2004). "Rapid pyrolysis of wood block by microwave heating." Journal of Analytical and Applied Pyrolysis **71**(1): 187-199.

Monsef-Mirzai, P., M. Ravindran, W. R. McWhinnie and P. Burchill (1995). "Rapid microwave pyrolysis of coal : Methodology and examination of the residual and volatile phases." Fuel **74**(1): 20-27.

Montané, D., V. Torné-Fernández and V. Fierro (2005). "Activated carbons from lignin: kinetic modeling of the pyrolysis of Kraft lignin activated with phosphoric acid." Chemical Engineering Journal **106**(1): 1-12.

Motasemi, F. and M. T. Afzal (2013). "A review on the microwave-assisted pyrolysis technique." Renewable and Sustainable Energy Reviews **28**(0): 317-330.

Mu, W., H. Ben, A. Ragauskas and Y. Deng (2013). "Lignin Pyrolysis Components and Upgrading—Technology Review." BioEnergy Research: 1-22.

Mullen, C. A. and A. A. Boateng (2010). "Catalytic pyrolysis-GC/MS of lignin from several sources." Fuel Processing Technology **91**(11): 1446-1458.

Mutyala, S., C. Fairbridge, J. R. J. Paré, J. M. R. Bélanger, S. Ng and R. Hawkins (2010). "Microwave applications to oil sands and petroleum: A review." Fuel Processing Technology **91**(2): 127-135.

Oloyede, A. and P. Groombridge (2000). "The influence of microwave heating on the mechanical properties of wood." Journal of Materials Processing Technology **100**(1-3): 67-73.

Orozco, A., M. Ahmad, D. Rooney and G. Walker (2007). "Dilute Acid Hydrolysis of Cellulose and Cellulosic Bio-Waste Using a Microwave Reactor System." Process Safety and Environmental Protection **85**(5): 446-449.

Paixão, V., R. Monteiro, M. Andrade, A. Fernandes, J. Rocha, A. P. Carvalho and A. Martins (2011). "Desilication of MOR zeolite: Conventional versus microwave assisted heating." Applied Catalysis A: General **402**(1–2): 59-68.

Pan, R., Y. Wu, Q. Wang and Y. Hong (2009). "Preparation and catalytic properties of platinum dioxide nanoparticles: A comparison between conventional heating and microwave-assisted method." Chemical Engineering Journal **153**(1–3): 206-210.

Pandit, R. B. and S. Prasad (2003). "Finite element analysis of microwave heating of potato--transient temperature profiles." Journal of Food Engineering **60**(2): 193-202.

Patil, P., V. G. Gude, S. Pinappu and S. Deng (2011). "Transesterification kinetics of Camelina sativa oil on metal oxide catalysts under conventional and microwave heating conditions." Chemical Engineering Journal **168**(3): 1296-1300.

Radmanesh, R., Y. Courbariaux, J. Chaouki and C. Guy (2006). "A unified lumped approach in kinetic modeling of biomass pyrolysis." Fuel **85**(9): 1211-1220.

Ramasamy, S. and B. Moghtaderi (2010). "Dielectric Properties of Typical Australian Wood-Based Biomass Materials at Microwave Frequency." Energy & Fuels **24**(8): 4534-4548.

Rattanadecho, P. (2006). "The simulation of microwave heating of wood using a rectangular wave guide: Influence of frequency and sample size." Chemical Engineering Science **61**(14): 4798-4811.

Ren, S., H. Lei, L. Wang, Q. Bu, S. Chen, J. Wu, J. Julson and R. Ruan (2012). "Biofuel production and kinetics analysis for microwave pyrolysis of Douglas fir sawdust pellet." Journal of Analytical and Applied Pyrolysis **94**(0): 163-169.

Robinson, J. P., S. W. Kingman, R. Barranco, C. E. Snape and H. Al-Sayegh (2009). "Microwave Pyrolysis of Wood Pellets." Industrial & Engineering Chemistry Research **49**(2): 459-463.

Rutkowski, P. (2011). "Pyrolysis of cellulose, xylan and lignin with the K2CO3 and ZnCl2 addition for bio-oil production." Fuel Processing Technology **92**(3): 517-522.

Salmoria, G. V., E. Dall'Oglio and C. Zucco (1998). "Aromatic nucleophilic substitutions under microwave irradiation." Tetrahedron Letters **39**(17): 2471-2474.

Sithambaram, S., E. K. Nyutu and S. L. Suib (2008). "OMS-2 catalyzed oxidation of tetralin: A comparative study of microwave and conventional heating under open vessel conditions." Applied Catalysis A: General **348**(2): 214-220.

Stuerga, D. and P. Gaillard (1996). "Microwave heating as a new way to induce localized enhancements of reaction rate. Non-isothermal and heterogeneous kinetics." Tetrahedron **52**(15): 5505-5510.

Sun, J., W. Wang, Z. Liu, Q. Ma, C. Zhao and C. Ma (2012). "Kinetic Study of the Pyrolysis of Waste Printed Circuit Boards Subject to Conventional and Microwave Heating." Energies **5**(9): 3295-3306.

Tang, S.-Y., Z.-N. Xia, Y.-J. Fu and Q. Gou (2008). "Advances and Applications of Microwave Spectroscopy." Chinese Journal of Analytical Chemistry **36**(8): 1145-1151.

Temur Ergan, B. a. and M . Bayramoğlu (2011). "Kinetic Approach for Investigating the "Microwave Effect": Decomposition of Aqueous Potassium Persulfate." Industrial & Engineering Chemistry Research **50**(11): 6629-6637.

Thostenson, E. T. and T. W. Chou (1999). "Microwave processing: fundamentals and applications." Composites Part A: Applied Science and Manufacturing **30**(9): 1055-1071.

Vos, B., J. Mosman, Y. Zhang, E. Poels and A. Bliek (2003). "Impregnated carbon as a susceptor material for low loss oxides in dielectric heating." Journal of Materials Science **38**(1): 173-182.

Wan, Y., P. Chen, B. Zhang, C. Yang, Y. Liu, X. Lin and R. Ruan (2009). "Microwave-assisted pyrolysis of biomass: Catalysts to improve product selectivity." Journal of Analytical and Applied Pyrolysis **86**(1): 161-167.

Will, H., P. Scholz, B. Ondruschka and W. Burckhardt (2003). "Multimode Microwave Reactor for Heterogeneous Gas-Phase Catalysis." Chemical Engineering & Technology **26**(11): 1146-1149.

Xu, F., J.-X. Jiang, R.-C. Sun, D. She, B. Peng, J.-X. Sun and J. F. Kennedy (2008). "Rapid esterification of wheat straw hemicelluloses induced by microwave irradiation." Carbohydrate Polymers **73**(4): 612-620.

Yadav, G. D. and I. V. Borkar (2006). "Kinetic modeling of microwave-assisted chemoenzymatic epoxidation of styrene." AIChE Journal **52**(3): 1235-1247.

Yan, W., X. Hu, G. Zhang, M. Deng, C. Yi and Z. Xu (2012). "Microwave assisted preparation of monodisperse polymeric microspheres and its morphologies and kinetics." Journal of Wuhan University of Technology-Mater. Sci. Ed. **27**(6): 1100-1104.

Yang, H., R. Yan, H. Chen, D. H. Lee and C. Zheng (2007). "Characteristics of hemicellulose, cellulose and lignin pyrolysis." Fuel **86**(12–13): 1781-1788.

Yang, H. W. and S. Gunasekaran (2001). "Temperature Profiles in a Cylindrical Model Food During Pulsed Microwave Heating." Journal of Food Science **66**(7): 998-1004.

Zakzeski, J., P. C. Bruijnincx, A. L. Jongerius and B. M. Weckhuysen (2010). "The catalytic valorization of lignin for the production of renewable chemicals." Chemical Reviews **110**(6): 3552.

Zakzeski, J., P. C. A. Bruijnincx, A. L. Jongerius and B. M. Weckhuysen (2010). "The Catalytic Valorization of Lignin for the Production of Renewable Chemicals." Chemical Reviews **110**(6): 3552-3599.

Zhang, M., F. L. P. Resende, A. Moutsoglou and D. E. Raynie (2012). "Pyrolysis of lignin extracted from prairie cordgrass, aspen, and Kraft lignin by Py-GC/MS and TGA/FTIR." Journal of Analytical and Applied Pyrolysis **98**(0): 65-71.

Zhang, X., D. O. Hayward and D. M. P. Mingos (2003). "Effects of Microwave Dielectric Heating on Heterogeneous Catalysis." Catalysis Letters **88**(1): 33-38.

Zhang, Z. and Z. K. Zhao (2010). "Microwave-assisted conversion of lignocellulosic biomass into furans in ionic liquid." Bioresource Technology **101**(3): 1111-1114.

Zheng, Y., D. Chen and X. Zhu "Aromatic Hydrocarbon Production by the Online Catalytic Cracking of Lignin Fast Pyrolysis Vapors using Mo2N/γ-Al2O3." Journal of Analytical and Applied Pyrolysis(0).

Zheng, Y., D. Chen and X. Zhu (2013). "Aromatic hydrocarbon production by the online catalytic cracking of lignin fast pyrolysis vapors using Mo2N/γ-Al2O3." Journal of Analytical and Applied Pyrolysis(0).

Zhou, L., V. M. Puri, R. C. Anantheswaran and G. Yeh (1995). "Finite element modeling of heat and mass transfer in food materials during microwave heating -- Model development and validation." Journal of Food Engineering **25**(4): 509-529.

Zhou, R., S. Zhong, X. Lin and N. Xu (2009). "Synthesis of zeolite T by microwave and conventional heating." Microporous and Mesoporous Materials **124**(1–3): 117-122.

Zhu, S., Y. Wu, Z. Yu, Q. Chen, G. Wu, F. Yu, C. Wang and S. Jin (2006). "Microwave-assisted Alkali Pre-treatment of Wheat Straw and its Enzymatic Hydrolysis." Biosystems Engineering **94**(3): 437-442.

Zhu, S., Y. Wu, Z. Yu, J. Liao and Y. Zhang (2005). "Pretreatment by microwave/alkali of rice straw and its enzymic hydrolysis." Process Biochemistry **40**(9): 3082-3086.